SYNTHESIS OF LACTIC ACID AND 3-HYDROXYPROPIONIC ACID VIA 1,3- AND 1,4-HYDRATION OF ACETYLENECARBOXYLIC ACID

Ву

Katie Lynn Kwiatkowski

A DISSERTATION

Submitted to
Michigan State University
in partial fulfillment of the requirements
for the degree of

Chemistry—Doctor of Philosophy

2023

ABSTRACT

Fossil fuel use remains prevalent for the production of chemicals, but with increasing environmental concern and limited availability, alternative sustainable methods are being developed. Starch-derived feedstocks like glucose have been used to produce chemicals such as lactic acid, but this method requires expensive downstream processing and puts the food industry in competition with the chemical industry. Non-edible lignocellulosic feedstock has a more complex composition and requires expensive pretreatment. With abundant quantities, methane and carbon dioxide can serve as an alternative feedstock. Dehydrodimerization of methane affords acetylene, a high energy gas that is difficult to transport. Subsequent carboxylation provides acetylenecarboxylic acid (ACA), a stable easy-to-handle liquid. The RuCl₃-catalyzed 1,3hydration of ACA results in pyruvic acid, while the 1,4-hydration to malonic semialdehyde is catalyzed by tautomerase enzyme Cg10062(E114N). Subsequent stereoselective enzymatic reduction of pyruvic acid using L- and D-lactate dehydrogenase (LDH) results in L- and D-lactic acids respectively. Hydrogen gas is utilized to enzymatically drive the recycling of NAD+ as cofactor to NADH using O₂-tolerant and soluble NAD+-reducing hydrogenase (SH) from Ralstonia eutropha, allowing the possibility of using H₂ formed during the dehydrodimerization of methane. The subsequent reduction of malonic semialdehyde to 3-HP can be achieved using NADHdependent 3-hydroxyisobutyrate dehydrogenase (MmsB) from Pseudomonas putida. This system is also coupled with soluble hydrogenase for cofactor recycling. A separate system is compared using phosphite dehydrogenase (PTDH) to recycle cofactor.

This dissertation is dedicated to my family and friends. I wouldn't be where I am today without your love, support, and encouragement. Thank you!

ACKNOWLEDGMENTS

I am incredibly grateful to my research advisor, Dr. Karen Draths. You have guided me through the most challenging academic journey and I wouldn't have made it to the end without you. I appreciate all of your patience and support, especially when I had days where I didn't think I could finish this journey. You have taught me valuable lessons and toughened me up. Thank you for developing me as a scientist and giving me opportunities to better prepare for a career in academia.

Thank you also to my committee, Dr. Xuefei Huang, Dr. Kevin Walker, and Dr. William Wulff for your guidance through this program. Dr. Daniel Holmes and Dr. Li Xie, thank you for all of your valuable help with NMR and for always being a friendly listening ear. I am grateful to Dr. Melanie Cooper and Dr. Brittany Busby. Thank you for supporting me in my journey and for helping me to become a better educator. I am also very appreciative of Nancy Lavrik and Chantal McWillie. Thank you for always being a ray of sunshine to brighten up my day.

I am so grateful to my teachers and professors who have inspired me through this long journey. Thank you, Mrs. Schafer, for helping me to find my passion for chemistry back in 11th grade. Your enthusiasm is where this whole journey began for me. Dr. Jennifer Chaytor, Dr. Kyle Cissell, and Dr. David Karpovich, you taught me so much during my time at SVSU and provided me so many opportunities to grow as a scientist and I am very grateful.

I would like to express my gratitude to Dr. Van Nguyen. Thank you for your friendship and guidance in my early days of graduate school. A special thank you goes to my friends and colleagues Allison Vanecek, Katelyn Silva, Bismarck Amaniampong, Dr. Amaya Mathes Hewage, Megan Gruenberg, and Esther Lee. You have become family and I'm so grateful to have gotten to know you all. Thank you also to Dr. Hansamali Sirinimal, Dr. Yasheen Jadidi, Eric Firestone, Austin King, Austin Jones, and my friends in the Cooper group for your friendship, support, and fruitful conversations throughout grad school.

My best friends from back home, Ashley, Nicole, Paige, Ana, and Courtney, your friendship means the world to me. You have always had faith in me through my years of schooling, and you're my best cheerleaders. I am also so grateful to my church family. You have provided me a home away from home, helped me to remember what is most important, checked in on me, and showed me so much love.

Last, but not least, I owe so much thanks to my family. Mom, thank you for always being so selfless and making sure I had everything I needed to achieve my goals. You have taught me kindness, humility, compassion, and so many other things. Your love has been a driving force in my success. Dad, you have always believed in me even when I didn't always believe in myself. You have always challenged me to push my limits and strive for excellence in everything I do. Thank you for your endless love, support, and sacrifice. To my wonderful grandparents, Ron, Sandi, Jim, Linda, Fabe, and Barb, thank you for sharing your valuable wisdom with me and for helping me to grow in my faith. You have shaped me into the person I am today and I am so grateful for your constant love and nurturing spirits. Ryan, you're the best little brother I could ask for. You inspire me to be the best role model. To the rest of my family, you each hold a special place in my heart and I appreciate your love and encouragement.

Proverbs 3:5-6

Philippians 4:13

TABLE OF CONTENTS

LIST OF ABBREVIATIONS	viii
Chapter One: Methane and Carbon Dioxide as Alternate Feedstocks for the Production of Commodity Chemicals	1
1.1 Feedstocks	
1.1.1 Petroleum Feedstocks	
1.1.2 Biomass Feedstocks	
1.1.3 Methane and Carbon Dioxide as Feedstocks	
1.1.4 Use of Methane and Carbon Dioxide for Chemical Production	
1.1.5 Methane to Olefin Synthesis	
1.2 A Modest Proposal	
1.2.1 Methane Dehydrodimerization and Carboxylation of Acetylene	
1.3 1,3- Versus 1,4-Hydration	
REFERENCES	26
Chapter Two: Stereospecific Synthesis of Lactic Acid from Methane and Carbon Dioxide	32
2.1 Introduction	
2.1.1 Chemical and Enzymatic Production of Lactic Acid	
2.1.2 Pyruvic Acid as an Intermediate	
2.2 Optimization of RuCl ₃ -Catalyzed ACA Hydration to Pyruvic Acid	
2.2.1 Assessing Reactions Using NMR	
2.2.2 Hydration of ACA in Various Solvents	
2.2.3 Optimization of the Hydration of ACA in Water	
2.2.4 Exploration of Metal Catalysts for the Hydration of ACA	
2.3 Pyruvic Acid Extraction and Removal of Ruthenium	
2.4 Proposed Mechanism for the Hydration of ACA	54
2.5 Production of Lactic Acid	
2.5.1 Purification and Characterization of Enzymes	
2.5.2 Preparation for Using Crude Hydration Mixture to Produce Lactic Acid	
2.5.3 Production of Lactic Acid with Cofactor Recycling	
2.6 Conclusion	
REFERENCES	
NEI ENEROLO	00
Chapter Three: The Enzymatic Production of 3-Hydroxypropionic Acid from	
Acetylenecarboxylic Acid	
3.1 Introduction	73
3.1.1 Production of 3-HP from Glucose and Glycerol	75
3.1.2 Enzymatic Conversion of ACA to 3-HP	81
3.2 Creation of a Plasmid for MmsB Production	
3.3 Purification and Characterization of Enzymes	88
3.3.1 MmsB Kinetics	
3.4 Enzymatic Synthesis of 3-HP	96
3.4.1 Buffer dependence of Cg10062(E114N), MmsB, and SH	96
3.4.2 Hydrogen Delivery to Reaction	
3.4.3 Production of 3-HP Using Cg10062(E114N), MmsB, and SH	
3.4.4 Kinetics of PTDH with NAD+ and NADP+	
3.4.5 Production of 3-HP Using Cg10062(E114N), MmsB, and PTDH	
3.5 Conclusion.	
REFERENCES	

Chapter Four: Experimental	126
4.1 General	126
4.1.1 Materials	126
4.1.2 Instrumentation	127
4.1.3 Culture Media and Stock Solutions	127
4.1.4 Preparation and Transformation of Electrocompetent E. coli	129
4.1.5 Preparation and Transformation of Chemical Competent E. coli	130
4.1.6 Isolation of Plasmid DNA	
4.1.7 Restriction Digestion of DNA	131
4.1.8 DNA Gel Electrophoresis	132
4.1.9 Protein Expression	133
4.1.10 Protein Purification	133
4.1.11 Protein Quantification	134
4.2 Chapter Two: Stereospecific Synthesis of Lactic Acid from Methane an	ıd
Carbon Dioxide	
4.2.1 Vacuum Distillation of ACA and pyruvic acid	136
4.2.2 Standard Hydration Reaction	
4.2.3 Calculating Concentrations via NMR	137
4.2.4 Extraction Methods for Ruthenium Removal	
4.2.5 ICP-OES	
4.2.6 Expression of SH	140
4.2.7 Purification of SH	
4.2.8 Calculation of Enzyme Specific Activity	
4.2.9 Enzyme Assays	
4.2.10 Production of Lactic Acid	
4.3 Chapter Three: The Enzymatic Production of 3-Hydroxypropionic Acid	
Acetylenecarboxylic Acid	
4.3.1 Bacterial Strains, Genes, Plasmids, and Primers	145
4.3.2 Isolation of Genomic DNA	
4.3.3 PCR Amplification of MmsB from P. putida	
4.3.4 Creation of pKK1.1025	
4.3.5 Enzyme Assays	
4.3.6 Kinetics of MmsB	
4.3.7 PTDH Kinetics	
4.3.8 Buffer Dependence Assays	
4.3.9 Production of 3-HP	152
REFERENCES	155

LIST OF ABBREVIATIONS

3-HP 3-hydroxypropionic acid/3-hydroxypropionate

ACA acetylenecarboxylic acid/acetylenecarboxylate

ADCA acetylenedicarboxylic acid/acetylenedicarboxylate

ADH alcohol dehydrogenase

Ap ampicillin

cis-Caa cis-3-chloroacrylic acid/cis-3-chloroacrylate

cis-CaaD cis-3-chloroacrylate dehydrogenase

CPS counts per second

CV column volumes

DNA deoxyribonucleic acid

DOE department of energy

DTT dithiothreitol

EDTA ethylenediaminetatraacetic acid

glu glucose

h hour(s)

HPLC high-performance liquid chromtography

ICP-OES inductively coupled plasma- optical emmission spectrometry

IPTG isopropyl-β-D-1-thiogalactopyranoside

kb kilobase

kDa kilo Dalton

LB Luria-Bertani

LDH lactate dehydrogenase

M molar

MCTO methyl chloride to olefins

mg milligram

min minute(s)

mL milliliter

mM millimolar

MSA malonic/malonate semialdehyde

MSAD malonate semialdehyde decarboxylase

MTBE methyl tert-butyl ether

MTO methanol to olefins

MTP methanol to propylene

NAD+ nicotinamide adenine dinucleotide, oxidized form

NADH nicotinamide adenine dinucleotide, reduced form

NADP⁺ nicotinamide adenine dinucleotide phosphate, oxidized form

NADPH nicotinamide adenine dinucleotide phosphate, reduced form

NMR nuclear magnetic resonance

NREL national renewable energy laboratory

OCM oxidative coupling of methane

OD optical density

PAH polycyclic aromatic hydrocarbon

PCR polymerase chain reaction

PET polyethylene terephthalate

PHB polyhydroxybutyrate

RID refractive index detector

s second(s)

SDS-PAGE sodium dodecyl sulfate polyacrylamide gel electrophoresis

SH soluble hydrogenase

TAE tris-acetate EDTA

Tc tetracycline

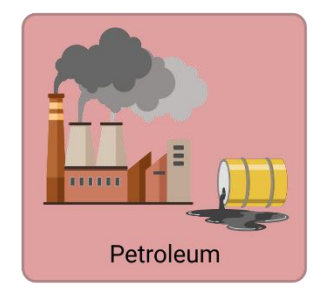
U unit; μmol min⁻¹

UV-vis ultraviolet-visible

Chapter One: Methane and Carbon Dioxide as Alternate Feedstocks for the Production of Commodity Chemicals

1.1 Feedstocks

A chemical feedstock is defined as a raw material used in the production of chemical products. Today's modern society is very dependent on chemical products, from clothing, to electronics, to packaging, to pharmaceuticals, and too many others to name. Chemical products increase our standard of living. For example, to keep up with the crop output necessary, fertilizer and other agrochemicals are needed. Fertilizer supplies nutrients to plants to increase yield and reliability of the crop. As modern insulation is developed, it reduces the cooling and heating needs in buildings. The largest output by the chemical industry is plastic, with production increasing by more than tenfold since 1970. Plastic has a multitude of applications, ranging from packaging, to automobile parts, to toys and utensils. Petroleum has served as the main feedstock for chemical production. Due to concerns with renewability and rising atmospheric carbon dioxide levels, alternate feedstocks are being explored including renewable sugars and lignocellulose, and methane and carbon dioxide.²





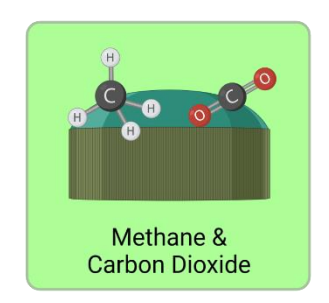


Figure 1.1. Feedstocks for chemical production.

1.1.1 Petroleum Feedstocks

Fossil fuels, including petroleum, natural gas, and coal, are a major carbon source used in the production of chemicals, polymers, and organic fuels.³ Petrochemicals have become fundamental to modern society with plastics and synthetic fertilizers accounting for the two largest groups of products. Approximately 22% of the world's oil and gas are used for the production of petrochemicals.² Fossil fuels are also important for the production of electricity, fuel, and heat. In 2014, fossil fuels accounted for 82% of the world's primary energy supply with the global energy consumption expected to increase by 28% by 2040.⁴

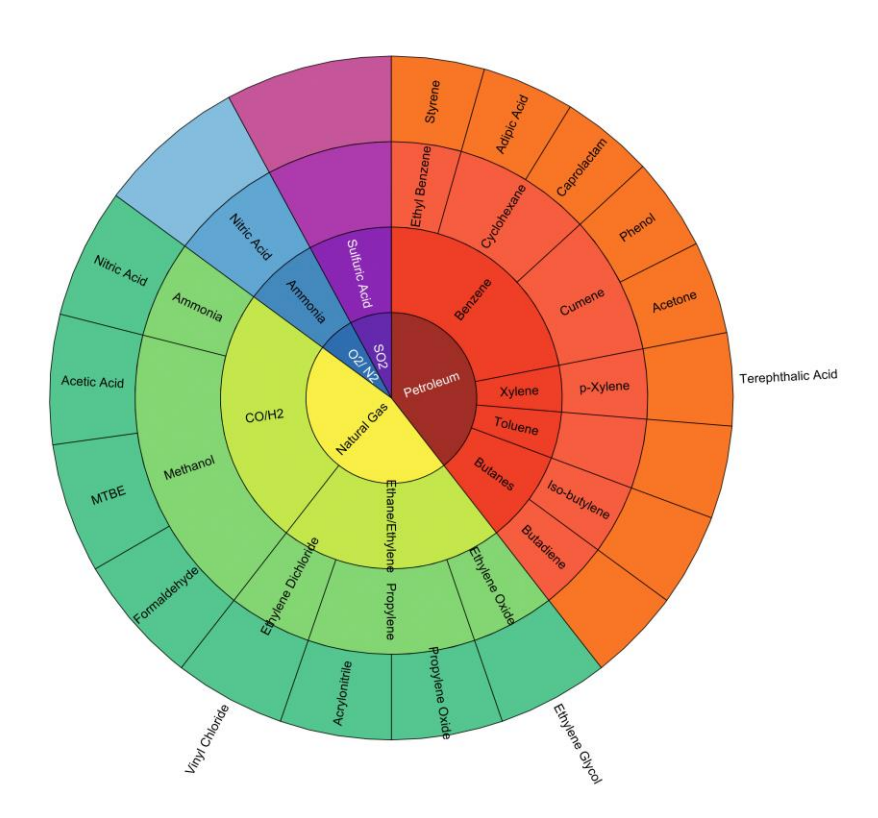


Figure 1.2. Chemicals produced from petroleum, natural gas, O_2/N_2 , and SO_2 .

The primary feedstocks for plastic production are oil, gas, and coal. In the distillation of crude oils, naphtha, a mixture of heavy flammable hydrocarbons, is produced and serves as the key petrochemical for plastic production. There is also a reliance on fossil fuel-based energy for

processing. Polyethylene is the most widely produced plastic, accounting for almost 30% of the global plastic production in 2019.⁵ Polyethylene is produced from the polymerization of ethylene, which is often produced from the cracking of ethane. Ethane is produced when distilling petroleum, and is also a minor component of natural gas. Polyethylene is produced in low density and high density forms. Low density polyethylene (LDPE) forms chains with long and short branches which keeps the chains from packing tightly. It is therefore used in applications where the polymer doesn't need to be very rigid, including trash and grocery bags, and packaging film. High density polyethylene (HDPE) is much more rigid due to the creation of linear chains that can pack tightly and form a stiff, highly crystalline material. This can be used for blow-molded bottles, among other products.⁶ Polyethylene terephthalate (PET) is another widely produced plastic that relies on petroleum. PET is often used in blow-molded bottles for carbonated beverages due to its excellent gas-barrier properties. A staggering 11 billion pounds of PET is consumed in the US each year,8 and it is the most widely recycled plastic although only 20% of PET is recycled.9 PET is synthesized using ethylene glycol and terephthalic acid. Almost all terephthalic acid is produced using the Amoco-MidCentury oxidation of p-xylene¹⁰ which is produced from the catalytic reforming of petroleum.8 Bio-based ethylene glycol is commercially available, but bio-based terephthalic acid is not.¹⁰

Fertilizer is another important product that is produced from petrochemicals. With a growing population and an increase in food demand, synthetic fertilizer was developed to increase crop output. Plants require 17 essential elements for growth, but the three main nutrients found in commercial fertilizer are nitrogen, phosphorus, and potassium. Atmospheric nitrogen is not very useful on its own, so Fritz Haber and Carl Bosch developed a method to use it for the synthesis of ammonia. In their Noble Prize-winning technology, the Haber-Bosch process involves the reaction of nitrogen and hydrogen over an iron catalyst at around 500 °C and a pressure between 150 – 200 atm (reaction 1).

$$N_2 + 3 H_2 \xrightarrow{\text{Fe cat.}} 2 \text{ NH}_3$$
 (1)
 $500 \, ^{\circ}\text{C}$
 $150\text{-}200 \text{ atm}$

Approximately 50% of the nitrogen in our bodies comes from ammonia that was produced using the Haber-Bosch process. The majority of hydrogen used for this process comes from natural gas. ¹¹ Hydrogen is produced from natural gas through the process of steam reforming. This is an endothermic process that uses Ni-based catalysts, temperatures up to 900 °C, and pressures above 30 atm (reactions 2 & 3). For every molecule of methane used to produce three hydrogen molecules, a molecule of carbon dioxide is produced. ¹²

CH₄ + H₂O
$$\stackrel{\text{Ni cat.}}{=}$$
 CO + 3 H₂ (2)
900 °C
> 30 atm

CO +
$$H_2O$$
 Ni cat.
900 °C
> 30 atm

There are many drawbacks to relying on fossil fuels for the production of chemicals including pollution and long-term climate effects, health effects, and non-renewability. The petrochemical industry generates 1.5 Gt of carbon dioxide annually. Increases in greenhouse gases including carbon dioxide can lead to global climate change which would have serious effects. Average global temperatures are rising by 0.2 °C per decade. An average global increase of only 1.5 °C compared to pre-industrial temperatures can lead to extreme weather patterns, changes in precipitation, rising sea levels, ocean acidification, etcetera. These changes will have negative impacts on ecosystems, biodiversity, and food security. Burning fossil fuels also releases pollutants like nitrogen oxides, sulfur dioxide, particulate matter, and other heavy metals. Nitrogen oxides can form smog and acid rain which can cause lung damage and other respiratory

problems. Sulfur dioxide can also cause respiratory problems, asthma, and nasal congestion. Particulate matter has been linked to elevated occurrence of premature death. When burning coal, it releases mercury and other heavy metals. These metals will end up in the environment and eventually end up in the food chain. This can cause neurological problems in infants.⁴ Fossil fuels take millions of years to form. Since they cannot be replenished within a short period of time, they are considered non-renewable. According to a modified Klass model, it is estimated that the oil and gas reserves will be depleted by 2042, and the coal reserves will be depleted by 2112.15 In addition to these concerns, the transportation industry and chemical industry have direct ties in their reliance on the petroleum industry. In 2022, approximately 10% of vehicle sales were electric vehicles. Globally, this is a 68% increase from electric vehicle sales in 2021. 16 With the transition to electric vehicles, and improved fuel economies, there will be less reliance on gasoline. Many chemical processes rely on by-products from the distillation of crude oil in the production of gasoline. These products, often referred to as "top of the barrel", include naphtha, ethane, and liquified petroleum gas. Although alternative feedstocks are being explored, the demand for oil as a chemical feedstock is expected to rise from 6 million barrels per day to 18 million barrels per day by 2050.2 Without this reliance on the transportation industry, petroleum-based starting materials will likely be more expensive for chemical production.

1.1.2 Biomass Feedstocks

Figure 1.3. Lactic acid 2, succinic acid 3, sorbitol 4, and muconic acid 5 are all examples of molecules that can be produced from glucose 1.

With the environmental concerns and non-renewability of using fossil fuels for chemical production, a significant focus has been placed on using biomass, relying on fermentation technology and bio-based production.¹⁷ Biomass can be categorized as first or second-generation. First-generation biomass is considered to be edible and includes crops such as corn, sugarcane, whey, and barley. Second-generation biomass is non-edible and includes lignocellulosic materials such as corn stover and agricultural/ forest residue as well as other solid municipal waste. ¹⁸ There are many molecules that are produced industrially using first-generation biomass. Lactic acid **2** is a C3 alpha-hydroxy acid with applications for food and beverages, personal care, solvents, and polymers. ¹⁹ Currently, more than 90% of lactic acid **2** is produced using microbial fermentation of biomass, ²⁰ and about 90% relies on carbohydrates from edible feedstocks like corn. ²¹ Succinic acid **3** is a C4 dicarboxylic acid and is a building block for solvents, fibers, and water-soluble polymers. It is produced by companies such as BASF and BioAmber

using glucose 1 and engineered strains including *Escherichia coli* and *Anaerobiospirillum succiniciproducens*. Sorbitol 4 is a polyol and is a naturally occurring sweetener. It can also serve as a building block for PET equivalent polymers and antifreeze. It is produced through the hydrogenation of glucose 1 and has a production volume of approximately 200 million pounds annually.²² The Draths Corporation developed a synthesis for muconic acid 5 from glucose 1, a synthesis that typically relies on petroleum-derived benzene. They used engineered *E. coli* to achieve a yield of 60 g L⁻¹.^{23,24} Using first-generation biomass as a feedstock puts the chemical and food industries in direct competition. The world's population is increasing, with the expectation that it will increase by 2 billion people within the next 30 years.²⁵ Considering the food available in 2006, and the food likely needed in 2050, the world would need to close a food gap of 6,500 trillion kilocalories per year. Not only is corn used for chemical production, but approximately one third of all of the corn produced in the United States is used to make ethanol for fuel.²⁶ Even with this large use of corn, it only offsets domestic gasoline use by 6%. In addition to crops being used directly for chemical production instead of food, there is also competition for land. Any land dedicated to the production of chemicals or biofuels cannot be used to produce food.²⁷

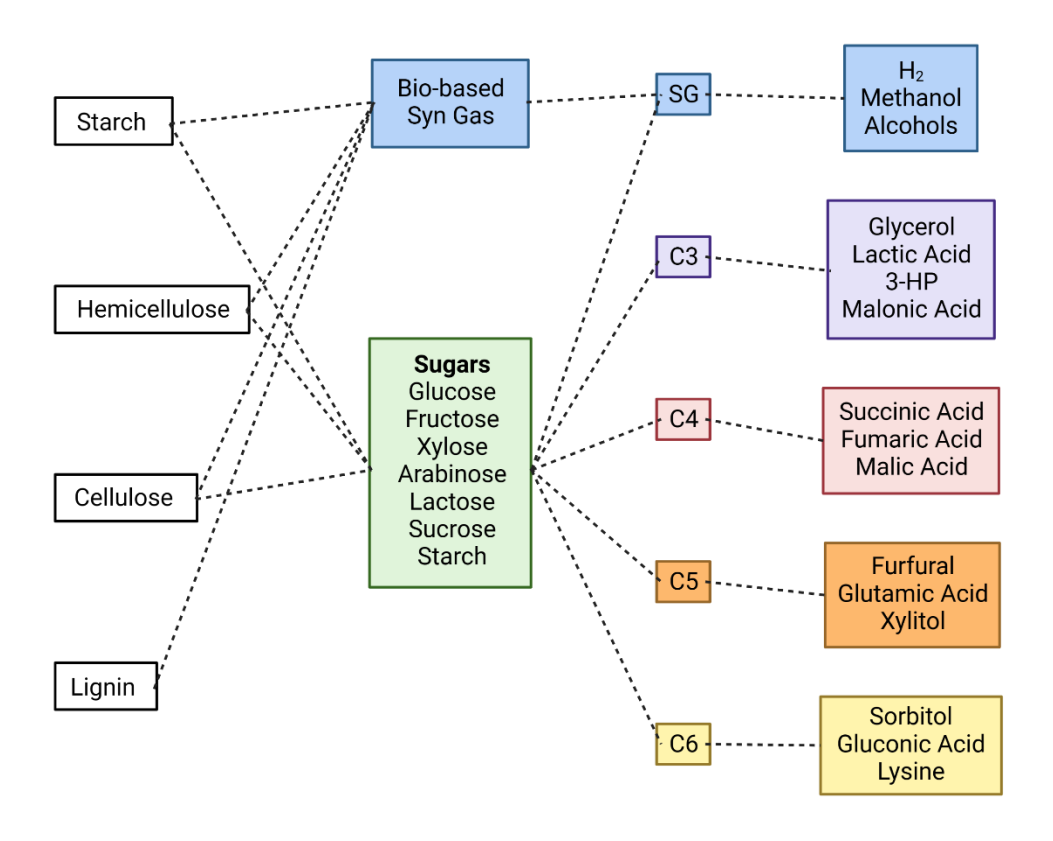


Figure 1.4. Products produced from starch, hemicellulose, cellulose, and lignin.

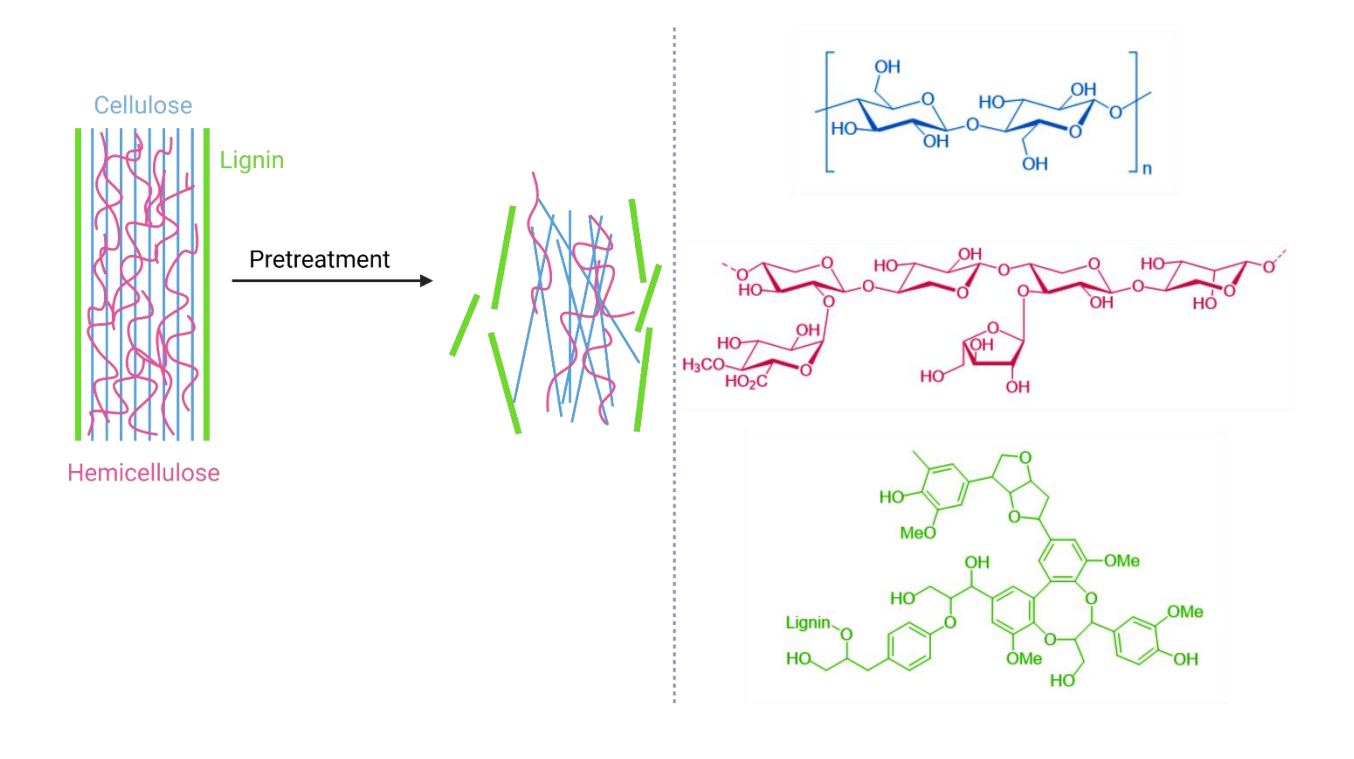


Figure 1.5. Lignocellulose is composed of cellulose, lignin, and hemicellulose, and requires pretreatment prior to use as a feedstock.

Although using lignocellulose as a feedstock would avoid competition with the food industry, it has a more complex composition and requires pretreatment. Lignocellulosic feedstocks are composed of cellulose, hemicellulose, and lignin (Figure 1.5). Cellulose is a polymer of glucose 1 that is linked via β-1,4 glycosidic bonds. Hemicellulose is a highly branched polymer with varying composition, but can contain a mixture of arabinose, xylose, glucose 1, galactose, and mannose. Lignin is a complex phenolic polymer that is not useful in the fermentation process.²⁸ In lignocellulosic biomass, bundles of cellulose chains form tightly packed microfibrils. The cellulose is so tightly packed that it is not water soluble or susceptible to enzymatic attack. Because of this, lignocellulose must undergo pretreatment to separate its components and allow solubilization prior to fermentation. There are various methods for

pretreatment including biological, chemical, and mechanical methods, each having advantages and disadvantages depending on the feedstock.²⁹ Chemical pretreatment techniques are the most studied and include acid, alkali, organic acids, and ionic liquids. Acid pretreatment using dilute sulfuric acid has been studied using corn stover, switchgrass, spruce, and poplar. This method requires constant mixing of the lignocellulosic material with dilute acid at temperatures between 130 °C and 210 °C, resulting in hydrolysis of the hemicellulose.²⁹ An important physio-chemical process of pretreatment is steam explosion. In this technique, the biomass is heated to temperatures between 160-260 °C and corresponding pressures up to 5 MPa. The material is then quickly exposed to atmospheric pressure. This explosive decompression results in hemicellulose degradation, lignin transformation, and an increased potential for cellulose hydrolysis. Due to the added cost of pretreatment, lignocellulose as a feedstock is limited at industrial scale.²⁹

1.1.3 Methane and Carbon Dioxide as Feedstocks

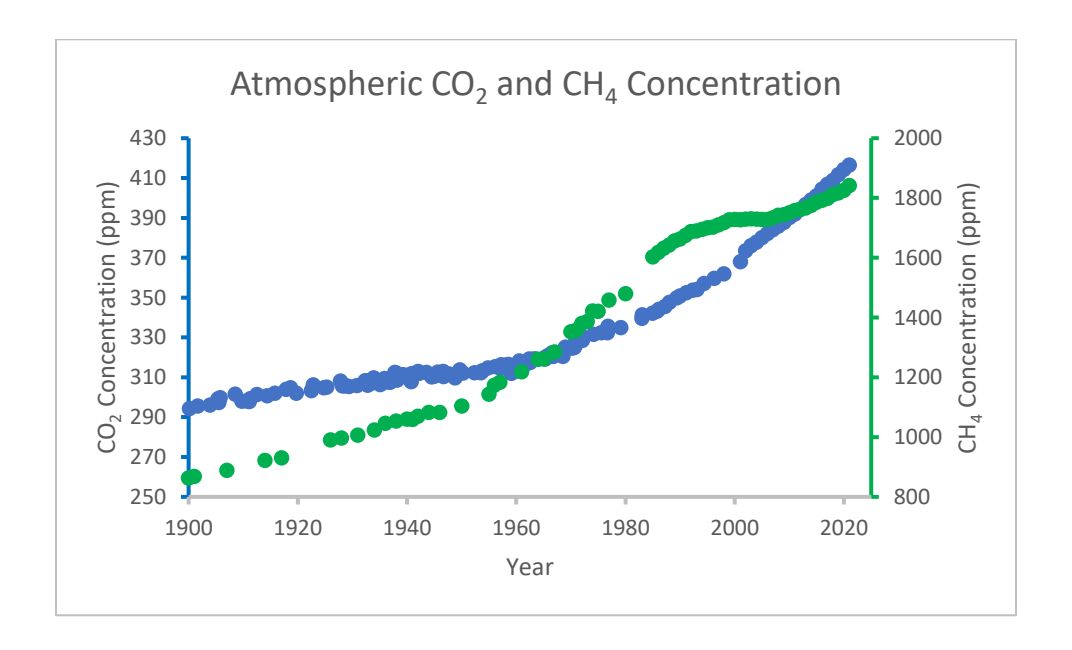


Figure 1.6. Atmospheric CO₂ and CH₄ concentration from 1900 to 2021.³⁰

Methane and carbon dioxide can serve as an alternate starting material for the production of commodity chemicals. The U.S. has abundant amounts of methane and carbon dioxide, both

of which are greenhouse gases, that trap heat and cause global change in climate. Carbon dioxide is produced from natural processes as well as sectors of the economy including transportation and industry. In 2018, 93% of CO₂ emissions were due to combustion of fossil fuels.³¹ As of June 2021, atmospheric CO₂ levels were at a concentration of 417 ppm, an increase of 48% from preindustrial levels.³² Methane traps atmospheric heat 25-fold more than CO₂. Some of the largest sources of CH₄ come from livestock, landfills, and petroleum systems.³¹ In 2017, the U.S. had an estimated 70 x 10¹² m³ of CH₄ reserves.³³ In the last 250 years, atmospheric methane concentrations have increased by 167%.³⁴

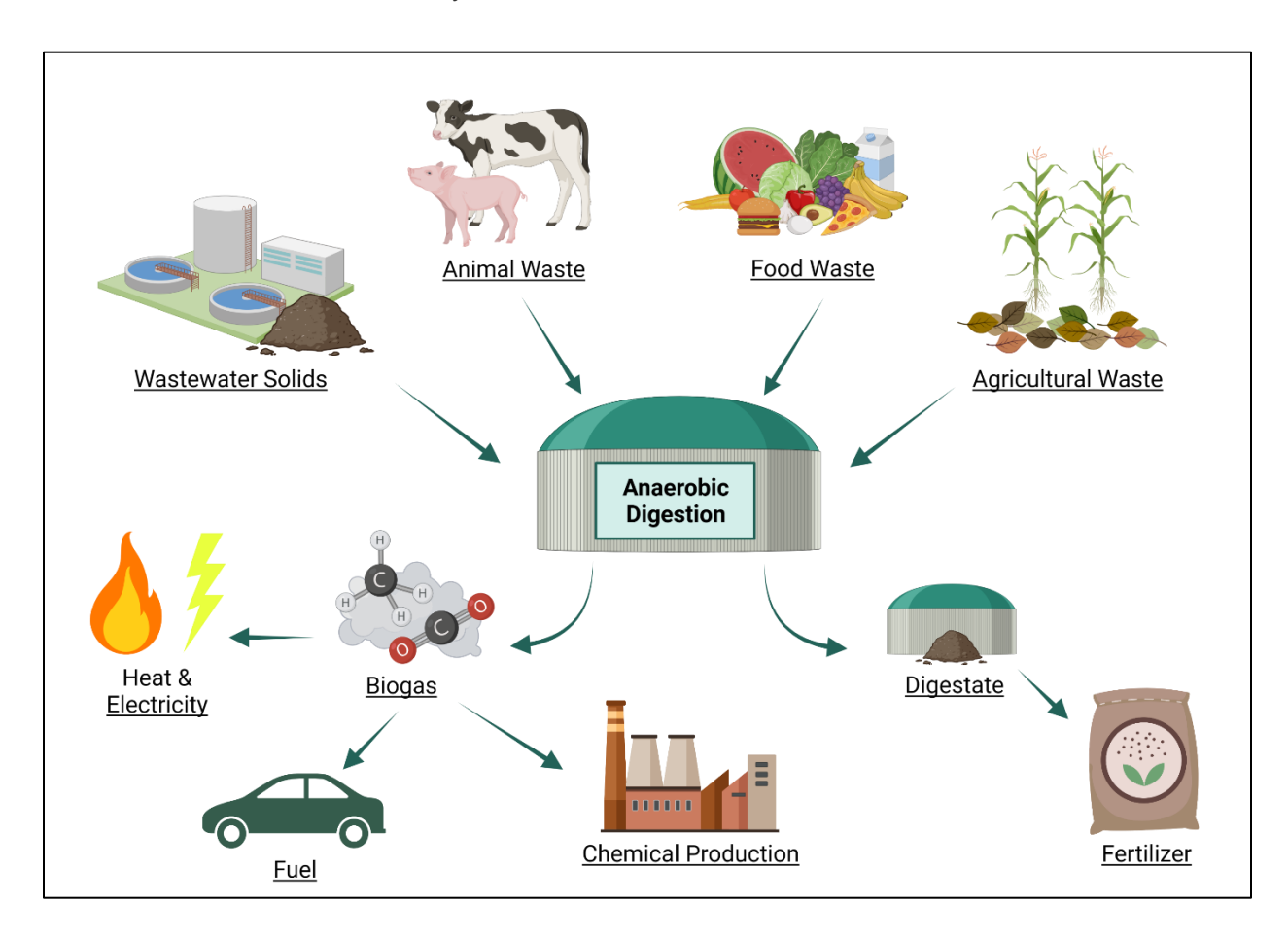


Figure 1.7. Production of biogas from the anaerobic digestion of organic waste.

Another important source of methane and carbon dioxide is from biogas. Biogas produced from the anaerobic digestion of organic material is typically composed of 50-70% methane and 30-40% carbon dioxide. Each year, millions of tons of organic waste is produced from industrial,

agricultural, and municipal sources. The decomposition of this waste can lead to pollution. Utilizing this waste for biogas production can help to reduce the amount of waste accumulating in the environment. Along with biogas formation, this process creates a nutrient-rich digestate that can be used as fertilizer.³⁵ The anaerobic digestion of organic waste has three steps. First, the waste is hydrolyzed into smaller molecules using fermentative bacteria.³⁶ This bacteria secretes hydrolytic enzymes including proteases, cellulases, lipases, and amylases. This step is generally considered the rate limiting step.³⁷ Second, is acidogenesis, where the products of the first step are transformed into smaller organic molecules including acetic acid 14, propionic acid, and butyric acid. The bacteria responsible for this step includes *Lactobacillus, Actinomyces, Clostridium,*, and others. The third step is methanogenesis where methanogens convert acetic acid 14 and carbon dioxide into methane.³⁷ Utilizing anaerobic digestion allows for easier capture of methane and carbon dioxide and reduces the amount that is released into the atmosphere from natural decomposition. The United States operates over 2,000 biogas systems and has the potential to add over 13,000 more.³⁸ Biogas is a sustainable methane and carbon dioxide source that can be readily stored and is produced from waste.³⁸

1.1.4 Use of Methane and Carbon Dioxide for Chemical Production

There have been significant efforts to produce chemicals from methane and carbon dioxide. Much research has focused on microbial transformation due to its mild operating conditions and lack of toxic by-product formation.³⁹ Gas-fermenting microbes including autotrophic acetogenic (produces acetate), carboxydotrophic (oxidizes CO) and methanotrophic (metabolizes methane) bacteria are able to grow on carbon dioxide and methane. Six pathways have been identified for microbial carbon dioxide fixation including the Wood-Ljungdahl pathway (Figure 1.8), the Calvin cycle, the 3-hydroxypropionate/4-hydroxybutyrate cycle, the reductive citrate cycle, the 3-hydroxypropionate bi-cycle, and the dicarboxylate/4-hydroxybutyrate cycle.^{40,41} Acetogenic bacteria typically produce acetate **14** which has a global

demand of more than 10 million tons per year and current production relies on petrochemicals.⁴⁰ Dürre and coworkers produced acetate 14 in a batch process with Acetobacterium woodii that was fed with carbon dioxide and hydrogen gas. They selectively overexpressed groups of genes that increased carbon flow through the Wood-Ljungdahl pathway. 42 Ralstonia eutropha is a facultative chemolithoautotrophic bacterium (obtains energy by oxidizing inorganic compounds)⁴³ that uses the reductive pentose phosphate cycle for CO₂ fixation.⁴⁰ R. eutropha naturally produces polyhydroxybutyrate (PHB) from acetyl-CoA as a way of stockpiling organic carbon.⁴⁴ Bio-polyester made of PHB is biodegradable and biocompatible, and therefore has applications in industry and the medical field. R. eutropha can grow chemoautotrophically on compounds such as succinate and pyruvate, or lithoautotrophically (growth on inorganic substrates) on dihydrogen and carbon dioxide. Friedrich and coworkers found that R. eutropha produces more of the enzymes responsible for PHB synthesis when grown lithoautotrophically. 45 Another study was conducted by Michael and coworkers, where they transferred the ability for carbon fixation to a heterotrophic organism. Pyrococcus furiosus is an archaeon that grows on carbohydrates at 100 °C. Five genes responsible for carbon fixation in archaeon Metallosphaera sedula were heterologously expressed in *Pyrococcus furiosus*. Whole cell and cell-free approaches resulted in the production of 3-hydroxypropionic acid (3-HP) 10 using carbon dioxide and dihydrogen.⁴⁶ Zhang and coworkers also developed a synthesis for 3-HP 10 from carbon dioxide. They constructed a biosynthetic pathway for 3-HP 10 in cyanobacterium Synechocystis sp. PCC 6803. Via acetyl-CoA and malonyl-CoA intermediates, 3-HP 10 was produced from carbon dioxide at a vield of 837 mg L⁻¹.47

Figure 1.8. Wood-Ljungdahl pathway for microbial carbon dioxide fixation.⁴⁸

Methanotrophs are a subgroup of methylotrophic bacteria that rely mainly on aerobic growth and utilize the ribulose monophosphate and/or the serine pathway for carbon fixation (Figure 1.9). Methane monooxygenase (MMO) is a key enzyme as it adds oxygen to methane to produce methanol. The production of methanol from methane has been studied in *Methylosinus trichosporium* and *Methylotrophus capsulatus*. This synthesis requires inhibition of methanol dehydrogenase (MDH) to prevent oxidation of methanol to formaldehyde.⁴⁰ The addition of MDH inhibitors results in the depletion of NADH, and MMO is NADH-dependent. Formate is therefore added to the culture media to enable cofactor regeneration, adding to the cost of the process.

The conversion of methane to methanol is limited by low production and slow growth rate.³⁹ Methanotrophic bacteria have also been shown to produce PHB from methane, although this process is not currently economically viable.⁴⁰ Lactate **2** production from methane was demonstrated by Henard and coworkers. They cultivated *Methylomicrobium alcaliphilum* 20Z^R on pure methane as well as AD-derived biogas containing 20% methane and 13% carbon dioxide. They observed productivity up to 0.027 g lactate/gDCW/h.⁴⁹ Guarnieri and coworkers developed a synthesis for muconic acid **5** from methane using Methylotuvimicrobium buryatense. They knocked out genes leading to aromatic amino acid synthesis to allow for the accumulation of muconic acid **5** up to 12 mg L⁻¹.⁵⁰ This is compared to the 60 g L⁻¹ muconic acid **5** produced by the Draths Corporation using glucose **1** and engineered *E. coli* (Figure 1.10).^{23,24}

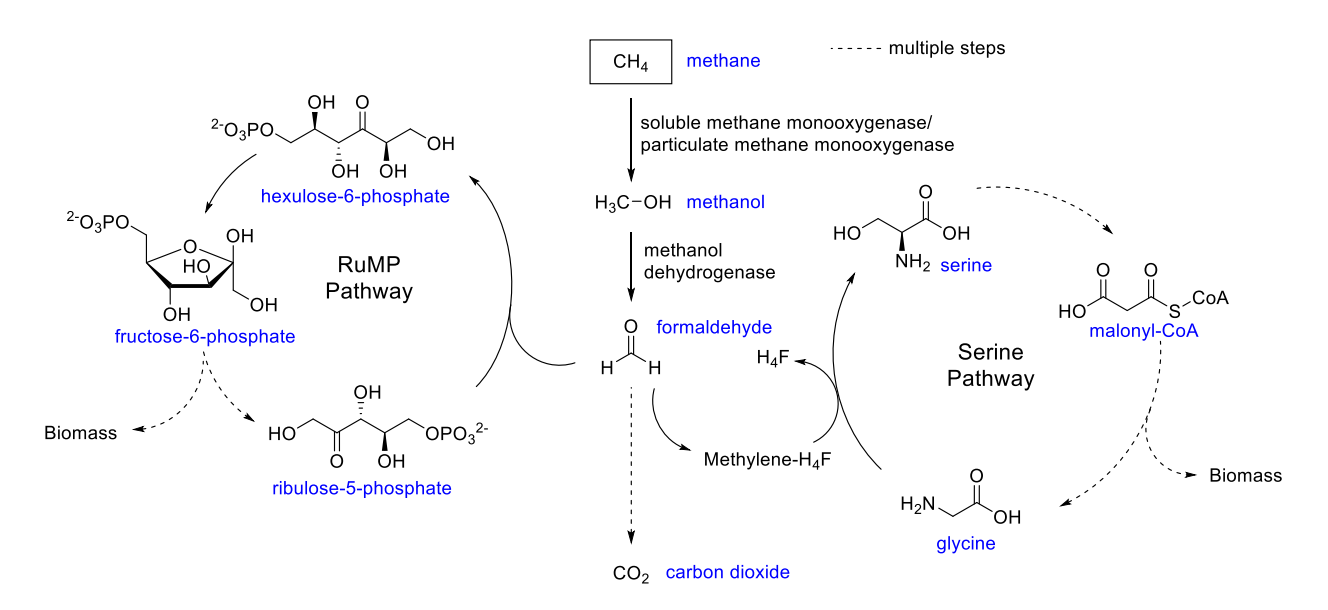


Figure 1.9. Methanotrophs fix carbon via the ribulose monophosphate or serine pathway. Methylene-H₄F: methylenetetrahydrofolate, H₄F: tetrahydrofolate.⁵¹

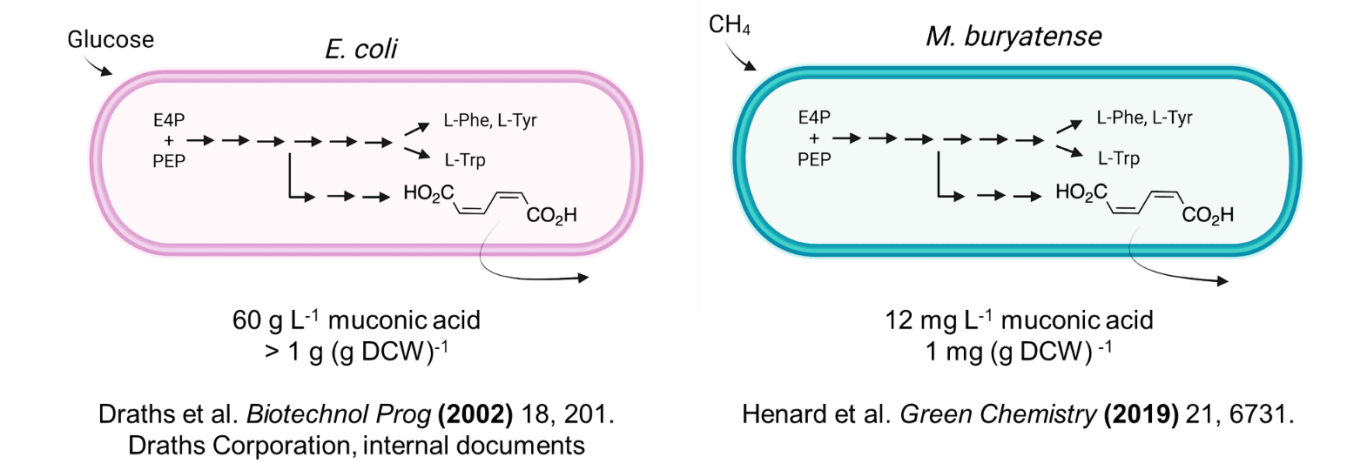


Figure 1.10. Comparison of muconic acid 5 production from glucose 1 and methane.

Direct microbial transformation of methane and carbon dioxide to chemicals presents challenges. Gas-to-liquid mass transfer limitations remains a significant problem. Since many syntheses rely on gas fermentation, the low solubility of the gaseous substrates will result in low productivity. Significant process engineering is needed to overcome this limitation.³⁹ Although the microbial conversion of carbon dioxide to a variety of chemicals seems promising, there are still shortcomings that need to be addressed. A technoeconomic analysis shows that the process is costly and requires optimization to obtain higher purity product. The scale-up process is also challenging as the transformation of carbon dioxide to chemicals is low.⁵² The conversion of methane to chemicals by methanotrophic bacteria requires metabolic engineering to optimize the process, but the genetic toolbox is small.⁴⁰

1.1.5 Methane to Olefin Synthesis

Chemical conversion of methane to olefins (propylene, ethylene, butenes) has been implemented in industry. Olefins have historically been made from the pyrolysis of naphtha, a product of petroleum distillation, and are important for polymer production and as building blocks of other industrially relevant chemicals. Due to the price and limited availability of petroleum, natural gas has been increasingly utilized for olefin synthesis, accounting for more than 40% of

olefin production in the US. When using natural gas, the propane component is used, while the methane component, accounting for 55-99% of the natural gas, is left untouched. This led to the development of four major methods for the conversion of methane to olefins.⁵³

MTO & MTP

$$CH_4 + H_2O \longrightarrow CO + 3H_2$$
 (4)

$$CH_4 + 1/2 O_2 \longrightarrow CO + 2 H_2$$
 (5)

$$CH_4 + CO_2 \longrightarrow 2CO + 2H_2$$
 (6)

$$CO + 2 H_2 \longrightarrow CH_3OH$$
 (7)

$$5 \text{ CH}_3 \text{OH} \longrightarrow \text{C}_2 \text{H}_4 + \text{C}_3 \text{H}_6 + 5 \text{H}_2 \text{O}$$
 (8)

$$2 CH3OH \longrightarrow (CH3)2O + H2O$$
 (9)

$$4 (CH_3)_2O \longrightarrow C_2H_4 + 2 C_3H_6 + 4 H_2O$$
 (10)

One technique involves methane reforming to syngas, and conversion of syngas to olefins. Syngas is composed of a mixture of carbon monoxide and hydrogen gas. Methane is converted to syngas using methane reforming via steam, oxidative, or dry methods (reactions 4-6). These reactions use nickel oxide catalysts at temperatures between 750-950 °C. Steam reforming of methane is the most commonly used process. Syngas is converted to methanol in a widely used industrial process using a Cu/ZnO/Al₂O₃ catalyst at temperatures between 270-300 °C and pressures between 5-10 MPa (reaction 7). The two main processes for converting methanol to olefins are the MTO (methanol to olefins) and MTP (methanol to propylene) methods. MTO is the direct conversion of methanol to ethylene and propylene using a silicoaluminophosphate (SAPO-34) catalyst at temperatures between 450-550 °C (reaction 8). SAPO-34 is a molecular sieve with high selectivity towards lower olefins due to its pore size. MTO results in 95% conversion. MTP involves the dehydration of methanol to dimethyl ether (reaction 9). A mixture of methanol and dimethyl ether are then reacted on ZSM-5 zeolites (a porous framework) at temperatures between

430-550 °C (reactions 8 & 10). MTP results in greater than 99% conversion. These processes are widely applied by companies including Honeywell, Mobil Oil Corporation, Exxon Mobil, and etc. Annually, methane is used to produce approximately 6 million tons of ethylene and 9 million tons of propylene.⁵³

OCM

$$2 CH_4 + 1/2 O_2 \longrightarrow C_2H_6 + H_2O$$
 (11)

$$C_2H_6 + 1/2 O_2 \longrightarrow C_2H_4 + H_2O$$
 (12)

The second method is the oxidative coupling of methane (OCM). In this technique, methane is reacted with oxygen to form ethane (reaction 11), which undergoes oxidative dehydrogenation to form ethylene (reaction 12). These reactions can proceed without a catalyst at temperatures above 600 °C, or with a catalyst like manganese oxide at lower temperatures. The production of ethane and ethylene using OCM results in their oxidation to carbon oxides, resulting in a maximum ethylene production of only about 18%.⁵³ This process has a high carbon footprint and costly product separation.⁵⁵ Strategies are underway to solve these limitations, but this causes OCM to be industrially unattractive.⁵³

non-OCM

$$2 CH_4 \longrightarrow C_2H_4 + 2 H_2$$
 (13)

The third method is the non-oxidative coupling of methane (non-OCM). Non-OCM allows for the direct conversion of methane to ethylene (reaction 13) without the formation of carbon oxides, but it requires higher temperatures and the selectivity is hard to control. The most common catalyst is molybdenum carbide supported on zeolites, and temperatures above 900 °C are necessary. Vazhnova and Lukyanov however, were able to achieve non-OCM using a platinum-containing zeolite at only 370 °C, but with low conversion of less than 1%. Low selectivity of Non-OCM is due to the rapid condensation of ethylene, leading to the production of aromatic hydrocarbons.

мсто

$$CH_4 + HCI + 1/2 O_2 \longrightarrow CH_3CI + H_2O$$
 (14)

$$CH_4 + CI_2 \longrightarrow CH_3CI + HCI$$
 (15)

$$CH_3CI \longrightarrow HCI + C_2H_4 + C_3H_6 + C_4H_8$$
 (16)

The fourth method is methyl chloride to olefins (MCTO). In this method, methane is first converted to methyl chloride using either an oxidative halogenation (reaction 14) or a halogenation reaction (equation 15) approach. These reactions use metal chloride catalysts on a porous support, with temperatures between 300-400 °C. Following the production of methyl chloride, it is converted to olefins using a SAPO-34 catalyst (reaction 16). Temperatures from 425-450 °C and pressures between 0.2-0.5 MPa are used. These reactions are all conducted in fluidized-bed reactors. The comparatively mild operating conditions of these reactions are favorable however, the products contain organochlorine impurities including dichloromethane, methyl chloride, and carbon tetrachloride. The products from MCTO are used for the production of chlorine-containing chemicals, but are not suitable for the production of other chemicals. Of the methods presented, the MTO and MTP processes are the only ones that have been industrialized.⁵³

Conversion of methane and carbon dioxide into chemicals is unlikely to reduce atmospheric concentrations by itself. In 2017, human activities generated 40 gigatons of carbon dioxide, but only 0.35 billion tons of plastic were made.⁵⁷ However, a combination of lessened reliance on petroleum and use of methane and carbon dioxide as a chemical feedstock can result in a greater reduction in emissions. The chemical industry may be reluctant to transition an existing synthesis to using methane or carbon dioxide due to the economic ties between syntheses. For example, acrylonitrile **18** is produced from propylene and acetonitrile is produced as a byproduct. If acrylonitrile **18** is instead produced from carbon dioxide, it will have an impact on the production of acetonitrile.⁵⁷ Therefore, the conversion of using methane and carbon dioxide as feedstock will require great work to changing existing processes.

1.2 A Modest Proposal

Figure 1.11. Oxidation of propargyl alcohol to form ACA 6.

Acetylenecarboxylic acid (ACA) **6** can function as a bridge between methane and carbon dioxide and commodity chemicals. To produce ACA **6** from methane and carbon dioxide in proof of concept, methane can first be dehydrodimerized to from acetylene. Acetylene can then be carboxylated to form ACA **6**. Direct use of methane and carbon dioxide as a carbon feedstock for biological syntheses presents the challenge of incorporating a gas into microbial metabolism or into an in-vitro system, so using ACA **6** allows for the simple addition of a liquid. The industrial synthesis of ACA **6** relies on the oxidation of propargyl alcohol using a PbO₂ anode, aqueous sulfuric acid, and a compartmented cell (Figure 1.11).^{58,59} The work presented here will rely on commercially purchased ACA **6**.

Figure 1.12. a) Dehydrodimerization of methane to acetylene and b) subsequent carboxylation of acetylene can be used to form acetylenecarboxylic acid **6** and acetylenedicarboxylic acid **7**.

1.2.1 Methane Dehydrodimerization and Carboxylation of Acetylene

To be used as starting material in a bio-based synthesis without incorporation of a gas into microbial metabolism, methane can first be dehydrodimerized to form acetylene. Plasma approaches are the most common method for this conversion because the process of converting methane to acetylene is very endothermic, and thus, large amounts of energy are needed. In one approach, a stream of CH₄ can be fed at supersonic speeds through an externally heated copper reactor at temperatures above 1500 °C.60-62 This relies on the conversion of kinetic energy to heat. The earliest versions of this technology were developed by Chemische Werke Huels and DuPont. The Huels plant originally used the low boiling components of motor fuel, although a range of hydrocarbons could be used, including methane. The DuPont process relied on liquid hydrocarbon, but a pilot-scale version was built to utilize methane as a feedstock.⁶² Some of these reactors have shock waves that form when a restriction of flow creates back pressure and causes a shock wave. This increases temperature by converting kinetic energy to heat. This method does have drawbacks, however. Some systems require temperatures up to 3000 °C and the severe operating conditions can damage the supersonic flow reactor, as well as other equipment. 60 A quench is often needed as benzene rings and other aromatics are formed from acetylene. These polycyclic aromatic hydrocarbons (PAHs) interact with acetylene and become hydrogen deficient due to hydrogen abstraction. Acetylene will continue to decompose on their surface which leads to the formation of soot. An early quench will stop soot formation.⁶² A second approach for converting methane to acetylene involves using a rotating arc reactor with AC power. This has a lower energy cost than other plasma approaches and greater than 70% methane conversion. This process has a specific energy requirement of 10.2 kW h kg⁻¹ C₂H₂ which is compared to 12.1 kW h kg⁻¹ C₂H₂ from the Huels process. Using AC power rather than DC power results in greater arc stability as well as less conductive heat loss to the reactor body. This enhances heat transfer to the feed gas and results in lower energy cost. Less soot formation was also observed by using hydrogen as the discharge gas.⁶³

Acetylene is produced on a large scale industrially. One method involves the reaction of calcium carbide and water. Care must be taken as an excess amount of heat is produced in this process which can cause accidental explosion of the acetylene gas. Acetylene can also be produced from the thermal cracking of hydrocarbons where temperatures around 1500 °C are used to break covalent bonds, resulting in smaller molecules that can re-bond to form other molecules. The storage and transport of acetylene is difficult due to it being unstable in its pure form. It must be kept at low pressures and only transported short distances. To be used for welding, specialty tanks are used that often contain an absorbent material like diatomaceous earth and acetone. Once dissolved, acetylene loses its explosive nature.⁶⁴ BASF is a major industrial producer of acetylene.⁶⁵

H = H
$$\frac{\text{CO}_2 (12 \text{ bar})}{50 \text{ °C, DMAc, } 18 \text{ h}}$$
 6 $\frac{\text{H}_2, \text{Pd/C}}{\text{MeOH}}$ 49% $\frac{\text{CO}_2 (12 \text{ bar})}{100 \text{ °C, DMAc, } 42 \text{ h}}$ HO 7 $\frac{\text{H}_2, \text{Pd/C}}{\text{MeOH}}$ HO 94%

Figure 1.13. Mono- and dicarboxylation of acetylene yielding ACA 6 and ADCA 7, respectively.

For easier handling, acetylene can be monocarboxylated with CO₂ to form acetylenecarboxylic acid (ACA) **6** or dicarboxylated to form acetylenedicarboxylic acid (ADCA) **7**

which are both stable molecules in liquid and solid forms, respectively (Figure 1.13). Since acetylene is difficult to work with, many carboxylation studies have been performed using phenylacetylene. The two most commonly studied methods are metal catalysis using copper or silver and base-mediated carboxylation. Lange and coworkers carboxylated phenylacetylene in up to 99% yield using varying phenanthroline phosphine Cu(I) nitrate complexes, cesium carbonate, and dimethyl formamide (DMF) at 35 °C.66 Han and coworkers demonstrated the carboxylation of phenylacetylene in 95% vield using copper iodide diazabicyclo[5.4.0]undec-7-ene (DBU) at 8 MPa of pressure and 50 °C. This same conversion was also shown without the presence of copper iodide. It is proposed that a DBU-CO₂ adduct forms followed by nucleophilic addition to form a DBU-propiolate salt. DBU can act as a nucleophile and a base in the carboxylation process (Figure 1.14). The mechanism is not known when copper is not present.⁶⁷ Monocarboxylation of acetylene can be achieved via a DBUmediated mechanism in N,N-dimethylacetamide (DMAc) as the solvent at 50 °C and 12 bar CO₂ and dicarboxylation can be achieved via a 1,5,7-triazabicyclo[4.4.0]dec-5-ene (TBD)-mediated mechanism in DMAc as the solvent at 100 °C and 12 bar CO2.68 Acetylene can also be monocarboxylated with a silver bis N-heterocyclic carbene complex and cesium carbonate in dimethyl sulfoxide (DMSO) at room temperature.⁶⁹

Figure 1.14. Proposed mechanism for the DBU-mediated carboxylation of a terminal alkyne.

1.3 1,3- Versus 1,4-Hydration

ACA 6 can undergo 1,3-hydration to form pyruvic acid, or 1,4-hydration to form malonic semialdehyde 9. In 1961, Halpern and coworkers reported the production of a 1,4-addition product via the RuCl₃-catalyzed hydration of phenylacetylenecarboxylic acid.⁷⁰ However, a 2012 patent showed the RuCl₃-catalyzed hydration of ACA 6 yielded pyruvic acid, the 1,3-addition product.⁷¹ To achieve selective 1,4-hydration of ACA 6, it can be reacted with tautomerase enzyme Cg10062. Mutants of Cg10062 yield malonic semialdehyde 9 as the sole product.^{72,73} Chapter 2 discusses the RuCl₃-catalyzed 1,3-hydration of ACA 6 to form pyruvic acid, followed by reduction to lactic acid 2 using lactate dehydrogenase (LDH). Chapter 3 discusses the 1,4-hydration of ACA 6 using Cg10062(E114N) to form malonic semialdehyde 9, which is reduced to 3-hydroxypropionic acid 10 using 3-hydroxyisobutyrate dehydrogenase (MmsB). Both systems employ coupled enzyme methods for cofactor regeneration to allow for sub-stoichiometric use of cofactor (Figure 1.15). Using ACA 6 as a bridge creates synthetic routes for the production of lactic acid 2 and 3-hydroxypropionic acid 10 from methane and carbon dioxide. Employing enzymatic methods results in high stereospecificity without the expensive downstream processing resulting from a fermentation method.

Figure 1.15. 1,3- and 1,4-hydration of acetylenecarboxylic acid **6** for the production of lactic acid **2** and 3-hydroxypropionic acid **10**, respectively. Chemical and enzymatic methods are applied.

REFERENCES

- (1) What Is A Chemical Feedstock? | The Science Blog. https://www.reagent.co.uk/blog/what-is-a-chemical-feedstock/ (accessed 2023-03-08).
- (2) *The Future of Petrochemicals*; International Energy Agency, 2018. https://www.iea.org/reports/the-future-of-petrochemicals (accessed 2023-03-07).
- (3) Yadav, V. G.; Yadav, G. D.; Patankar, S. C. The Production of Fuels and Chemicals in the New World: Critical Analysis of the Choice between Crude Oil and Biomass Vis-à-Vis Sustainability and the Environment. *Clean Technol. Environ. Policy* **2020**, *22* (9), 1757–1774.
- (4) Doelle, K.; Hughes, T.; Kurzmann, D. From Fossil Fuels to Renewable Biogas Production from Biomass Based Feedstock A Review of Anaerobic Digester Systems. *J. Energy Res. Rev.* **2020**, 1–37.
- (5) Singh, N.; Ogunseitan, O. A.; Wong, M. H.; Tang, Y. Sustainable Materials Alternative to Petrochemical Plastics Pollution: A Review Analysis. *Sustain. Horiz.* **2022**, *2*, 100016.
- (6) Polyethylene | Properties, Structures, Uses, & Facts | Britannica. https://www.britannica.com/science/polyethylene (accessed 2023-03-07).
- (7) Venkatachalam, S.; Nayak, S. G.; Labde, J. V.; Gharal, P. R.; Rao, K.; Kelkar, A. K. Degradation and Recyclability of Poly (Ethylene Terephthalate). *Polyester* **2012**.
- (8) Lyons, T. W.; Guironnet, D.; Findlater, M.; Brookhart, M. Synthesis of P-Xylene from Ethylene. *JACS*. **2012**, *134* (38), 15708–15711.
- (9) Polyethylene terephthalate | Structure, Properties, & Uses | Britannica. https://www.britannica.com/science/polyethylene-terephthalate (accessed 2023-03-07).
- (10) Zhang, P.; Nguyen, V.; Frost, J. W. Synthesis of Terephthalic Acid from Methane. *ACS Sustainable Chem. Eng.* **2016**, *4* (11), 5998–6001.
- (11) Chen, S.; Perathoner, S.; Ampelli, C.; Centi, G. Chapter 2 Electrochemical Dinitrogen Activation: To Find a Sustainable Way to Produce Ammonia. In *Studies in Surface Science and Catalysis*; Albonetti, S., Perathoner, S., Quadrelli, E. A., Eds.; Horizons in Sustainable Industrial Chemistry and Catalysis; Elsevier, 2019; Vol. 178, pp 31–46.
- (12) Schneider, S.; Bajohr, S.; Graf, F.; Kolb, T. State of the Art of Hydrogen Production via Pyrolysis of Natural Gas. *ChemBioEng Rev.* **2020**, *7* (5), 150–158.
- (13) Tickner, J.; Geiser, K.; Baima, S. Transitioning the Chemical Industry: The Case for Addressing the Climate, Toxics, and Plastics Crises. *Environ. Sci. Policy Sustainable Dev.* **2021**, *6*3 (6), 4–15.
- (14) Global Warming of 1.5 °C. https://www.ipcc.ch/sr15/ (accessed 2023-03-09).
- (15) Shafiee, S.; Topal, E. When Will Fossil Fuel Reserves Be Diminished? *Energy Policy* **2009**, 37 (1), 181–189.

- (16) Boston, W. EVs Made Up 10% of All New Cars Sold Last Year. *Wall Street Journal*. January 16, 2023. https://www.wsj.com/articles/evs-made-up-10-of-all-new-cars-sold-last-year-11673818385 (accessed 2023-04-06).
- (17) Chemicals and Fuels from Bio-Based Building Blocks, 1st ed.; John Wiley & Sons, Ltd, 2016.
- (18) Lee, R. A.; Lavoie, J.-M. From First- to Third-Generation Biofuels: Challenges of Producing a Commodity from a Biomass of Increasing Complexity. *Anim. Front.* **2013**, *3* (2), 6–11.
- (19) Komesu, A.; Oliveira, J. A. R. de; Martins, L. H. da S.; Maciel, M. R. W.; Maciel Filho, R. Lactic Acid Production to Purification: A Review. *BioResources* **2017**, *12* (2), 4364–4383.
- (20) Jantasee, S.; Kienberger, M.; Mungma, N.; Siebenhofer, M. Potential and Assessment of Lactic Acid Production and Isolation a Review. *J. Chem. Technol. Biotechnol.* **2017**, *92* (12), 2885–2893.
- (21) Wang, Y.; Meng, H.; Cai, D.; Wang, B.; Qin, P.; Wang, Z.; Tan, T. Improvement of L-Lactic Acid Productivity from Sweet Sorghum Juice by Repeated Batch Fermentation Coupled with Membrane Separation. *Bioresour. Technol.* **2016**, *211*, 291–297.
- (22) Sengupta, D.; Pike, R. W. Chemicals from Biomass. In *Handbook of Climate Change Mitigation and Adaptation*; Chen, W.-Y., Suzuki, T., Lackner, M., Eds.; Springer: New York, NY, 2014; pp 1–38.
- (23) Draths Corporation. Internal Documents.
- (24) Niu, W.; Draths, K. M.; Frost, J. W. Benzene-Free Synthesis of Adipic Acid. *Biotechnol. Prog.* **2002**, *18* (2), 201–211.
- (25) Nations, U. *Population*. United Nations. https://www.un.org/en/global-issues/population (accessed 2023-03-10).
- (26) Hill, J. The Sobering Truth about Corn Ethanol. *Proc. Natl. Acad. Sci.* **2022**, *119* (11), e2200997119.
- (27) Searchinger, T.; Heimlich, R. Avoiding Bioenergy Competition for Food Crops and Land. **2015**.
- (28) Speight, J. G. Chapter 1 Feedstocks. In *The Refinery of the Future*; Speight, J. G., Ed.; William Andrew Publishing: Boston, 2011; pp 1–37.
- (29) Menon, V.; Rao, M. Trends in Bioconversion of Lignocellulose: Biofuels, Platform Chemicals & Biorefinery Concept. *Prog. Energy Combust. Sci.* **2012**, *38* (4), 522–550.
- (30) US EPA, O. *Climate Change Indicators: Atmospheric Concentrations of Greenhouse Gases.* https://www.epa.gov/climate-indicators/climate-change-indicators-atmospheric-concentrations-greenhouse-gases (accessed 2023-04-01).

- (31) *Inventory of U.S. Greenhouse Gas Emissions and Sinks*. US EPA. https://www.epa.gov/ghgemissions/inventory-us-greenhouse-gas-emissions-and-sinks (accessed 2020-04-23).
- (32) *Carbon Dioxide Concentration*. NASA Global Climate Change: Vital Signs of the Planet. https://climate.nasa.gov/vital-signs/carbon-dioxide (accessed 2021-07-15).
- (33) How much natural gas does the United States have, and how long will it last? FAQ U.S. Energy Information Administration (EIA). https://www.eia.gov/tools/faqs/faq.php?id=58&t=8 (accessed 2019-09-25).
- (34) *Inventory of U.S. Greenhouse Gas Emissions and Sinks: 1990-2019.* US EPA. https://www.epa.gov/ghgemissions/inventory-us-greenhouse-gas-emissions-and-sinks-1990-2019 (accessed 2021-07-15).
- (35) Muhammad Nasir, I.; Mohd Ghazi, T. I.; Omar, R. Production of Biogas from Solid Organic Wastes through Anaerobic Digestion: A Review. *Appl. Microbiol. Biotechnol.* **2012**, *95* (2), 321–329.
- (36) Zhang, C.; Su, H.; Baeyens, J.; Tan, T. Reviewing the Anaerobic Digestion of Food Waste for Biogas Production. *Renew. Sustainable Energy Rev.* **2014**, *38*, 383–392.
- (37) Molino, A.; Nanna, F.; Ding, Y.; Bikson, B.; Braccio, G. Biomethane Production by Anaerobic Digestion of Organic Waste. *Fuel* **2013**, *103*, 1003–1009.
- (38) *Biogas: Converting Waste to Energy*. https://www.eesi.org/papers/view/fact-sheet-biogasconverting-waste-to-energy (accessed 2021-06-01).
- (39) Sahoo, K. K.; Goswami, G.; Das, D. Biotransformation of Methane and Carbon Dioxide Into High-Value Products by Methanotrophs: Current State of Art and Future Prospects. *Front. Microbiol.* **2021**, *12*.
- (40) Dürre, P.; Eikmanns, B. J. C1-Carbon Sources for Chemical and Fuel Production by Microbial Gas Fermentation. *Curr. Opin. Biotechnol.* **2015**, *35*, 63–72.
- (41) Fuchs, G. Alternative Pathways of Carbon Dioxide Fixation: Insights into the Early Evolution of Life? *Annu. Rev. Microbiol.* **2011**, *65* (1), 631–658.
- (42) Straub, M.; Demler, M.; Weuster-Botz, D.; Dürre, P. Selective Enhancement of Autotrophic Acetate Production with Genetically Modified Acetobacterium Woodii. *J. Biotechnol.* **2014**, *178*, 67–72.
- (43) Amils, R. Chemolithoautotroph. In *Encyclopedia of Astrobiology*; Gargaud, M., Amils, R., Quintanilla, J. C., Cleaves, H. J. (Jim), Irvine, W. M., Pinti, D. L., Viso, M., Eds.; Springer: Berlin, Heidelberg, 2011; pp 289–289.
- (44) Pohlmann, A.; Fricke, W. F.; Reinecke, F.; Kusian, B.; Liesegang, H.; Cramm, R.; Eitinger, T.; Ewering, C.; Pötter, M.; Schwartz, E.; Strittmatter, A.; Voß, I.; Gottschalk, G.; Steinbüchel, A.; Friedrich, B.; Bowien, B. Genome Sequence of the Bioplastic-Producing "Knallgas" Bacterium Ralstonia Eutropha H16. *Nat. Biotechnol.* **2006**, *24* (10), 1257–1262.

- (45) Kohlmann, Y.; Pohlmann, A.; Otto, A.; Becher, D.; Cramm, R.; Lütte, S.; Schwartz, E.; Hecker, M.; Friedrich, B. Analyses of Soluble and Membrane Proteomes of Ralstonia Eutropha H16 Reveal Major Changes in the Protein Complement in Adaptation to Lithoautotrophy. *J. Proteome Res.* **2011**, *10* (6), 2767–2776.
- (46) Keller, M. W.; Schut, G. J.; Lipscomb, G. L.; Menon, A. L.; Iwuchukwu, I. J.; Leuko, T. T.; Thorgersen, M. P.; Nixon, W. J.; Hawkins, A. S.; Kelly, R. M.; Adams, M. W. W. Exploiting Microbial Hyperthermophilicity to Produce an Industrial Chemical, Using Hydrogen and Carbon Dioxide. *Proc. Natl. Acad. Sci. U. S. A.* **2013**, *110* (15), 5840–5845.
- (47) Wang, Y.; Sun, T.; Gao, X.; Shi, M.; Wu, L.; Chen, L.; Zhang, W. Biosynthesis of Platform Chemical 3-Hydroxypropionic Acid (3-HP) Directly from CO2 in Cyanobacterium Synechocystis Sp. PCC 6803. *Metab. Eng.* **2016**, *34*, 60–70.
- (48) *The Acetyl-CoA Pathway*. Biology LibreTexts. https://bio.libretexts.org/Bookshelves/Microbiology/Microbiology_(Boundless)/05%3A_Microbial _Metabolism/5.12%3A_Biosynthesis/5.12G%3A_The_Acetyl-CoA_Pathway (accessed 2023-04-06).
- (49) Henard, C. A.; Franklin, T. G.; Youhenna, B.; But, S.; Alexander, D.; Kalyuzhnaya, M. G.; Guarnieri, M. T. Biogas Biocatalysis: Methanotrophic Bacterial Cultivation, Metabolite Profiling, and Bioconversion to Lactic Acid. *Front. Microbiol.* **2018**, *9*, 2610.
- (50) Henard, C. A.; Akberdin, I. R.; Kalyuzhnaya, M. G.; Guarnieri, M. T. Muconic Acid Production from Methane Using Rationally-Engineered Methanotrophic Biocatalysts. *Green Chem.* **2019**, *21* (24), 6731–6737.
- (51) Khider, M. L. K.; Brautaset, T.; Irla, M. Methane Monooxygenases: Central Enzymes in Methanotrophy with Promising Biotechnological Applications. *World J. Microbiol. Biotechnol.* **2021**, *37* (4), 72.
- (52) Irfan, M.; Bai, Y.; Zhou, L.; Kazmi, M.; Yuan, S.; Maurice Mbadinga, S.; Yang, S.-Z.; Liu, J. F.; Sand, W.; Gu, J.-D.; Mu, B.-Z. Direct Microbial Transformation of Carbon Dioxide to Value-Added Chemicals: A Comprehensive Analysis and Application Potentials. *Bioresour. Technol.* **2019**, *288*, 121401.
- (53) Kolesnichenko, N. V.; Ezhova, N. N.; Snatenkova, Y. M. Lower Olefins from Methane: Recent Advances. *Russ. Chem. Rev.* **2020**, *89* (2), 191.
- (54) Pashchenko, D. Numerical Study of Steam Methane Reforming over a Pre-Heated Ni-Based Catalyst with Detailed Fluid Dynamics. *Fuel* **2019**, *236*, 686–694.
- (55) Alturki, A. Techno-Economic Analysis of a Process to Convert Methane to Olefins, Featuring a Combined Reformer via the Methanol Intermediate Product. *Hydrogen* **2022**, *3* (1), 1–27.
- (56) Lukyanov, D. B.; Vazhnova, T. Transformation of Methane over Platinum Supported Catalysts at Moderate Temperature. *J. Mol. Catal. Chem.* **2011**, *342*–*343*, 1–5.
- (57) Burkart, M. D.; Hazari, N.; Tway, C. L.; Zeitler, E. L. Opportunities and Challenges for Catalysis in Carbon Dioxide Utilization. *ACS Catal.* **2019**, *9* (9), 7937–7956.

- (58) Steckhan, E. Electrochemistry, 3. Organic Electrochemistry. In *Ullmann's Encyclopedia of Industrial Chemistry*; John Wiley & Sons, Ltd, 2011.
- (59) Nohe, H.; Jaeger, P.; Aktiengesellschaft, B. Manufacture of Propiolic Acid. US3969200A, July 13, 1976. https://patents.google.com/patent/US3969200A/en (accessed 2023-03-14).
- (60) Bedard, R. L.; Naunheimer, C.; Towler, G. P.; Leonard, L. E.; Dudebout, R.; Woodcock, G. O.; Mittendorf, D. L. Methane Conversion Apparatus and Process Using a Supersonic Flow Reactor. US10166524B2, January 1, 2019. https://patents.google.com/patent/US10166524B2/en (accessed 2020-05-27).
- (61) Hwang, N. K.; Cha, M. S.; Lee, D. H.; Kim, S. J. Role of Plasma Chemistry in Methane Decomposition in an Arc Jet Reactor. **2008**, 5.
- (62) Fincke, J. R.; Anderson, R. P.; Hyde, T.; Wright, R.; Bewley, R.; Haggard, D. C.; Swank, W. D. *Thermal Conversion of Methane to Acetylene Final Report*; INEEL/EXT-99-01378, 774309; 2000; p INEEL/EXT-99-01378, 774309.
- (63) Dinh, D. K.; Lee, D. H.; Song, Y.-H.; Jo, S.; Kim, K.-T.; Iqbal, M.; Kang, H. Efficient Methane-to-Acetylene Conversion Using Low-Current Arcs. *RSC Adv.* **2019**, *9* (56), 32403–32413.
- (64) How acetylene is made material, making, used, processing, Raw Materials. http://www.madehow.com/Volume-4/Acetylene.html (accessed 2020-08-30).
- (65) *The new Acetylene Plant*. https://www.basf.com/global/en/who-we-are/organization/locations/europe/german-sites/ludwigshafen/production/the-production-verbund/new acetylene facility.html (accessed 2021-08-28).
- (66) Gooßen, L. J.; Rodríguez, N.; Manjolinho, F.; Lange, P. P. Synthesis of Propiolic Acids via Copper-Catalyzed Insertion of Carbon Dioxide into the CH Bond of Terminal Alkynes. *Adv. Synth. Catal.* **2010**, *352* (17), 2913–2917.
- (67) Li, F.-W.; Suo, Q.-L.; Hong, H.-L.; Zhu, N.; Wang, Y.-Q.; Han, L.-M. DBU and Copper(I) Mediated Carboxylation of Terminal Alkynes Using Supercritical CO2 as a Reactant and Solvent. *Tetrahedron Lett.* **2014**, *55* (29), 3878–3880.
- (68) Wang, X.; Lim, Y. N.; Lee, C.; Jang, H.-Y.; Lee, B. Y. 1,5,7-Triazabicyclo[4.4.0]Dec-1-Ene-Mediated Acetylene Dicarboxylation and Alkyne Carboxylation Using Carbon Dioxide. *Eur. J. Org. Chem.* **2013**, *2013* (10), 1867–1871.
- (69) Diaz, H.; Wu, Z.; Vandichel, M.; Verpoort, F. Inserting CO2 into Terminal Alkynes via Bis-(NHC)-Metal Complexes. *Catal. Lett.* **2017**, *147*.
- (70) Halpern, J.; James, B. R.; Kemp, A. L. W. Catalysis of the Hydration of Acetylenic Compounds by Ruthenium(III) Chloride. *JACS*. **1961**, *83* (19), 4097–4098.
- (71) Ogo, S.; Fukuzumi, S.-I. Method for Synthesis of Keto Acid or Amino Acid by Hydration of Acetylene Compound. EP1932824A1, June 18, 2008. https://patents.google.com/patent/EP1932824A1/en (accessed 2019-09-25).

- (72) Huddleston, J. P.; Johnson, W. H.; Schroeder, G. K.; Whitman, C. P. Reactions of Cg10062, a Cis-3-Chloroacrylic Acid Dehalogenase Homologue, with Acetylene and Allene Substrates: Evidence for a Hydration-Dependent Decarboxylation. *Biochemistry* **2015**, *54* (19), 3009–3023.
- (73) Draths, K. F.; Geiger, J. H.; Hewage, A. N. S. M.; Gavgani, H. N. Synthesis of 3-Hydroxypropionic Acid via Hydration of Acetylenecarboxylic Acid. WO2022226190A1, October 27, 2022. https://patents.google.com/patent/WO2022226190A1/en?oq=WO2022226190A1 (accessed 2023-02-27).

Chapter Two: Stereospecific Synthesis of Lactic Acid from Methane and Carbon Dioxide

Reprinted with permission from Kwiatkowski, K.; Nguyen, V.; Draths, K.; Stereospecific Synthesis

of Lactic Acid from Methane and Carbon Dioxide. Manuscript in preparation.

2.1 Introduction

Figure 2.1. Structures of D- and L- lactic acid 2a-b.

With the desire to transform methane and carbon dioxide-derived acetylenecarboxylic acid (ACA) 6 into a valuable C3 molecule, lactic acid 2 proves to be an excellent candidate. Lactic acid 2 is a C3 alpha-hydroxy acid with one chiral center (Figure 2.1). The U.S. Department of Energy (DOE) identified lactic acid 2 to be a valuable building block for commodity chemicals. Building blocks are defined as molecules with multiple functional groups and have the potential to be transformed into high-value chemicals. Lactic acid 2 has a global market value expected to reach \$9.8 billion by 2025. It has applications for food and beverages, personal care, solvents, and polymers. In the food industry, lactic acid 2 is used as a pH regulator, flavoring agent, and to prevent bacterial contamination in food processing. Due to its moisturizing and antimicrobial properties, lactic acid 2 is found in many cosmetic products.

The largest demand of lactic acid **2** is for the production of polylactic acid (PLA) which accounts for approximately 28% of market demand.⁵ PLA is a biodegradable polymer typically produced using agricultural feedstocks and is becoming prevalent as an alternative to its petroleum derived counterparts.⁶ Plastics are utilized due to their low cost, easy processability, and high durability, but they are often single-use or have a short service life. This is cause for

great environmental concern as approximately 70 million tons of plastic waste has accumulated in the environment. With this plastic eventually degrading into microplastics, there is also concern for health issues,⁷ including inflammation, oxidative stress, and cytotoxic effects.⁸ This furthers the effort to shift to using biodegradable plastics. PLA has been utilized for packaging as well as for biomedical applications including sutures, implants, tissue engineering, and drug delivery.⁹ The majority of microbes capable of degrading PLA belong to the actinomycetes family.¹⁰ Typically, these microbes will release depolymerase enzymes to break down the polymeric material into water-soluble compounds that can be transported into the cell and further digested. Lipases are capable of degrading PLA, but due to the size of the enzymes, they cannot penetrate the polymer. They are typically active after conformational changes have already begun.¹⁰ At natural weathering conditions, PLA undergoes bulk degradation as hydrolysis occurs throughout the entire sample and results in mass loss.^{10,11} Composting and anaerobic digestion results in quick degradation of PLA with 90% biodegradation in as little as 28 days.¹² PLA can also undergo thermal, oxidative, and photodegradation. ¹⁰

2.1.1 Chemical and Enzymatic Production of Lactic Acid

Figure 2.2. Synthetic production of lactic acid **2** from acetaldehyde **11** and hydrogen cyanide via lactonitrile **12**.

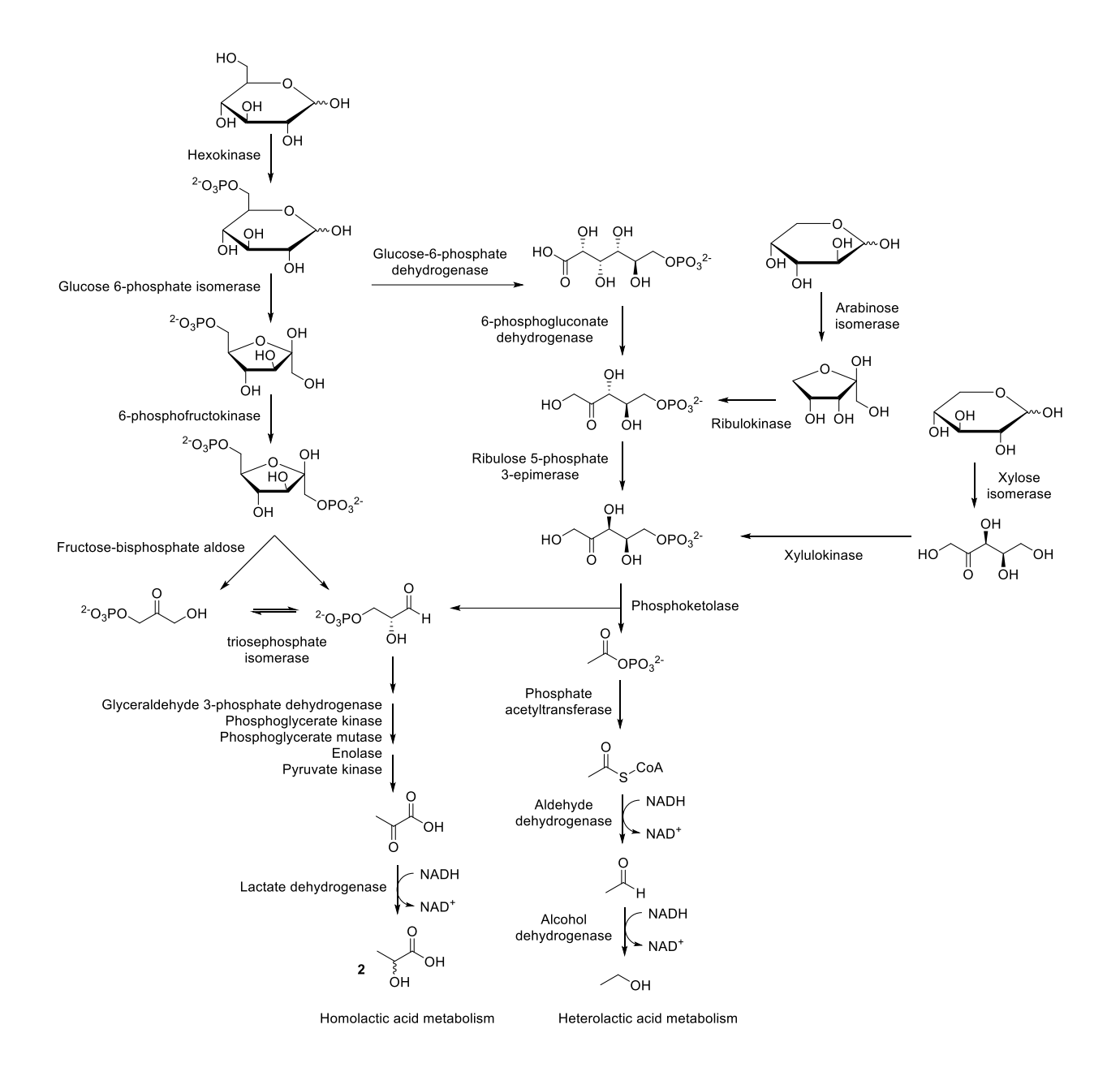


Figure 2.3. The metabolic pathways for lactic acid 2 fermentation in LAB.¹³

Lactic acid **2** can be produced via chemical synthesis or biological conversion. Monsanto (Texas, USA) was the first company to chemically produce large amounts of lactic acid **2**.⁴ Synthesis via lactonitrile **12** is the most common synthetic pathway used industrially (Figure 2.2). First, a base-catalyzed reaction of acetaldehyde **11** and hydrogen cyanide under high pressure produces lactonitrile **12** (Figure 2.2, eq. 1). Next, lactonitrile **12** is purified and hydrolyzed using sulfuric acid to produce lactic acid **2** (Figure 2.2, eq. 2). In order to produce pure lactic acid **2**, it is

then esterified to produce methyl lactate 13 (Figure 2.2, eq. 3) which is then purified via distillation and hydrolyzed to produce lactic acid 2 and methanol (Figure 2.2, eq. 4).4,14,15 The drawbacks of using chemical synthesis is that it is expensive relative to fermentation, relies on acetaldehyde 11, a petrochemical, and produces racemic lactic acid 2a-b. 15 Currently, more than 90% of lactic acid 2 is produced using microbial fermentation of biomass. 14 NatureWorks LLC is a leading producer of lactic acid 2 and PLA, and relies on microbial production of lactic acid 2.16 Microbial fermentation creates enantiomerically pure lactic acid 2.17 Most commercial PLA consists of optically pure poly-L-lactic acid (PLLA) due to the amorphous nature of racemic poly-D,L-lactic acid (PDLLA).9 Many organisms produce lactic acid 2 naturally including Lactic Acid Bacteria (LAB), Corynebacterium glutamicum, Escherichia coli, Bacillus spp., Enterobacter spp., and Pediococcus spp. 3,13,18,19 Saccharomyces cerevisiae produces lactic acid 2 when it is engineered to express lactate dehydrogenase. Many strains have been engineered using techniques such as adaptive laboratory evolution, metabolic engineering, and mutation breeding to produce highyielding mutant strains. 18 LAB is a heterogeneous group of gram-positive bacteria that is most commonly used for lactic acid 2 production at a large scale. LAB can grow aerobically or anaerobically and produce lactic acid 2 through either a homolactic (Embden-Meyerhof-Parnas pathway) or heterolactic (phosphoketolase pathway) fermentation pathway (Figure 2.3). Fermentation still presents challenges though. About 90% of lactic acid production via fermentation relies on carbohydrates such as glucose 1 from edible feedstocks like corn, 20 which puts the chemical industry in direct competition with the food industry.²¹ With the world's population expected to increase by 2 billion people in the next 30 years, 22 this is not a sustainable alternative. Lactic acid 2 has been made from a variety of carbon sources including sugars like glycerol 29, glucose 1, and xylose; sugar-containing materials such as sugarcane bagasse and whey; starchy materials like wheat and potato; lignocellulose such as rice straw, corn cob, and wheat straw; and other organic waste that contains a mixture of carbon sources, but many of these rely on fermentation.^{3,23,24} Lactic acid **2** formation also inhibits cell growth in fermentation

due to change in pH, so neutralizing agents are needed.¹⁴ For every ton of lactic acid **2** produced, a ton of CaSO₄ is produced and must be disposed of.²⁵ Nitrogen sources, vitamins, and minerals are needed to support growth of the microorganisms and add to production cost.¹⁴ More than half of the cost for lactic acid **2** production comes from downstream processing to separate it out from fermentation broth and creates a bottleneck in the process, thus requiring a need for better alternatives.¹⁵

2.1.2 Pyruvic Acid as an Intermediate

Figure 2.4. 1,3-hydration of ACA **6** to pyruvic acid **8** goes through a 3-exo-trig intermediate, while 1,4-hydration of ACA to malonic semialdehyde **9** goes through a 4-endo-dig intermediate.

Lactic acid 2 synthesis from ACA 6 can be accessed via pyruvic acid 8. Pyruvic acid 8 is formed by the 1,3-addition of water to ACA 6, which can then be converted to lactic acid 2. A 1961 Halpern and coworkers showed the RuCl₃-catalyzed hydration report phenylacetylenecarboxylic acid producing the 1,4-addition product.²⁶ All else being equal, this would predict a 1,4-addition of water to ACA 6 ²⁶ however, a 2012 patent reported RuCl₃-catalyzed hydration of ACA 6 provided pyruvic acid 8, the 1,3-addition product, in 90% yield at 0.1 mmol ACA 6 scale. 27-29 In our proposed mechanism for the formation of pyruvic acid 8, it would go through an intermediate requiring a 3-exo-trig cyclization. The formation of malonic semialdehyde 9, the 1,4-addition product, would go through an intermediate requiring a 4-endo-dig cyclization (Figure 2.4). According to Baldwin's modified rules for ring closure, a 3-exo-trig cyclization is favored, while a 4-endo-dig cyclization is disfavored. ^{28,29} Various hydration reactions on terminal alkynes have been assessed, and the catalyst used plays an important role in the formation of Markovnikov or anti-Markovnikov product. Blum and coworkers tested various terminal alkynes for hydration using RhCl₃. They observed formation of Markovnikov product with all terminal alkynes, although they observed low yields due to trimerization of alkyne starting material.³⁰ Meier and coworkers employed various catalysts for the hydration of 2-methyl-3-butyn-2-ol. The majority of catalysts produced Markovnikov product while a few resulted in polymerized starting material.³¹ Chevallier and coworkers identified catalyst [CpRu(CH₃CN)(6-DPPAP)(3-DPICon)]PF₆ (Cp: cyclopentadiene, DPPAP: 6-diphenylphosphino-N-pivaloyl-2-aminopyridine, DPICon: 3-diphenylphosphinoisoquinolone) which resulted in highly selective anti-Markovnikov hydration of terminal alkynes.³² Tokunaga and coworkers studied the anti-Markovnikov hydration of terminal alkynes using ruthenium complexes.³³

The conversion of pyruvic acid 8 to lactic acid 2 can be achieved using an NADHdependent lactate dehydrogenase (LDH) [1.1.1.27]. LDH is an important oxidoreductase in the anaerobic metabolic pathway, and is found in a variety of organisms. The structure of LDH is wellpreserved across organisms with small changes in active site amino acids. LDH is assembled as a tetramer and exists in five isomeric forms. LDH catalyzes the reversible conversion of pyruvate 8 to lactate 2 by transferring a hydride ion from NADH to pyruvate 8.34 Employing LDH at an industrial scale is hampered by the challenge of cost. Cofactor regeneration allows use of substoichiometric amounts of cofactor and can be accomplished by coupling two enzymes where reduced cofactor can be regenerated by oxidation of a cheap sacrificial substrate. Formate dehydrogenase (FDH) is widely used in cofactor regeneration however, it suffers from low dehydrogenases,37 dehydrogenases.38 activity.35,36 Phosphite alcohol alucose dehvdrogenases³⁹ are alternate enzymes capable of being coupled for cofactor regeneration, but they produce byproducts and have poor atom efficiency. Hydrogenases oxidize H₂, have 100% atom efficiency, and don't produce any carbon containing byproducts.⁴⁰

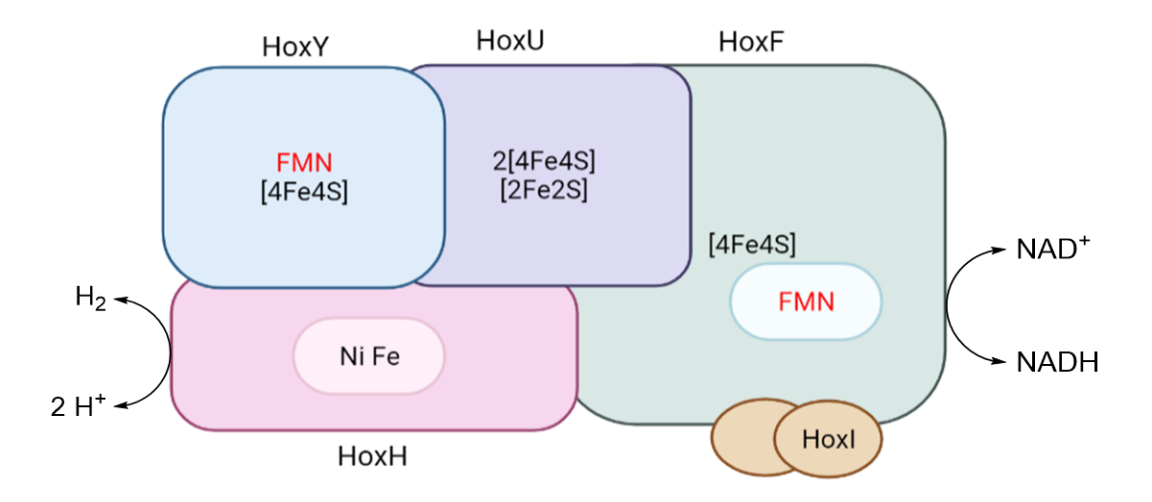


Figure 2.5. Structural representation of soluble [NAD+]-reducing hydrogenase.

Soluble hydrogenase (SH) [1.12.1.2] from *Ralstonia eutropha* strain Hf210/pGE771 was engineered by the Lenz group⁴¹ and serves as the main enzyme of interest for cofactor recycling in this chapter. SH is composed of two modules and can be further divided into four subunits, HoxHYFU as well as a Hoxl homodimer (Figure 2.5). The HoxHY dimer is a hydrogenase module and the HoxFU is an NADH-dehydrogenase module.⁴² The Hoxl dimer assists in regulatory functions and allows the binding of NADPH.^{40,42} The HoxH subunit contains the [NiFe] active site and HoxF contains the NAD+ binding site. These sites are linked by [4Fe4S] and [2Fe2S] clusters as well as one to two flavin mononucleotide molecules (depending on the species of origin).⁴⁰ The [NiFe] active site is coordinated by four cysteines, two cyanides, and one carbon monoxide.⁴⁰ The Ni²⁺ of the active site in *H. thermoluteolus* binds as a bidentate ligand to the carboxy group of a nearby glutamic acid. Purifying *R. eutropha* SH using potassium phosphate buffer between pH 6 and 7 allows Hoxl to be maintained. The purified protein can be activated by NADH or NADPH. Purifying SH at an alkaline pH results in release of the Hoxl subunit and the purified protein can only be activated by NADH.⁴²

Figure 2.6. Methane and carbon dioxide can serve as alternate starting materials for the production of lactic acid **2**. Chemical and enzymatic methods are intertwined to create a sustainable synthesis.

This chapter discusses the 1,3-hydration of acetylenecarboxylic acid **6** forming pyruvic acid **8**. A subsequent reduction to lactic acid **2** is achieved using lactate dehydrogenase with a soluble NAD+-reducing hydrogenase to recycle the cofactor. Chirality is thus created, starting with achiral molecules (Figure 2.6).

2.2 Optimization of RuCl₃-Catalyzed ACA Hydration to Pyruvic Acid

In preparation for the hydration of ACA 6 and subsequent reduction to lactic acid 2a-b, ACA 6 and pyruvic acid 8a-b were distilled prior to use. A distillation apparatus that included a short path condenser and three receiving flasks was assembled. A column containing Drierite was inserted between the distillation apparatus and the vacuum pump, and distilled material was collected at -78°C and about 12 psi pressure. ACA 6 was collected when the boiling flask reached 55-60°C, and pyruvic acid 8a-b was collected at 65°C. Distilled reagents were stored under nitrogen and exposure to air was minimized thereafter.

2.2.1 Assessing Reactions Using NMR

The hydration of ACA **6** in water results in the production of pyruvic acid **8a** and its hydrate **8b** as well as acetic acid **14**, and acetaldehyde **11a** and its hydrate **11b**. Reaction progress and product concentrations were determined by NMR. The sodium salt of 3-(trimethylsilyl)propionic-2,2,3,3-d₄ acid (TSP) served as a standard for NMR analysis. At timed intervals, an aliquot (100

μL) of the reaction was removed via syringe and combined with 600 μL of D_2O containing 10 mM TSP. Representative spectra from reaction initiation and termination are included (Figure 2.7). The resonance at δ 3.36 (s, 1H) corresponds to ACA 6. Resonances at δ 2.39 (s, 3H) and δ 1.56 (s, 3H), respectively, correspond to pyruvic acid and its hydrate 8a-b. Resonances at δ 2.24 (d, 3H) and δ 1.32 (d, 3H), respectively, correspond to acetaldehyde and its hydrate 11a-b. The resonance at δ 2.08 (s, 3H) corresponds to acetic acid 14. Product concentrations were calculated using the formula in Figure 2.7C. To determine the percent yield of each product, product concentrations were divided by the known concentration of ACA 6 (or ADCA 7 when applicable) added to initiate the reaction. At a minimum, reactions were run in duplicate, and average product concentrations are reported.

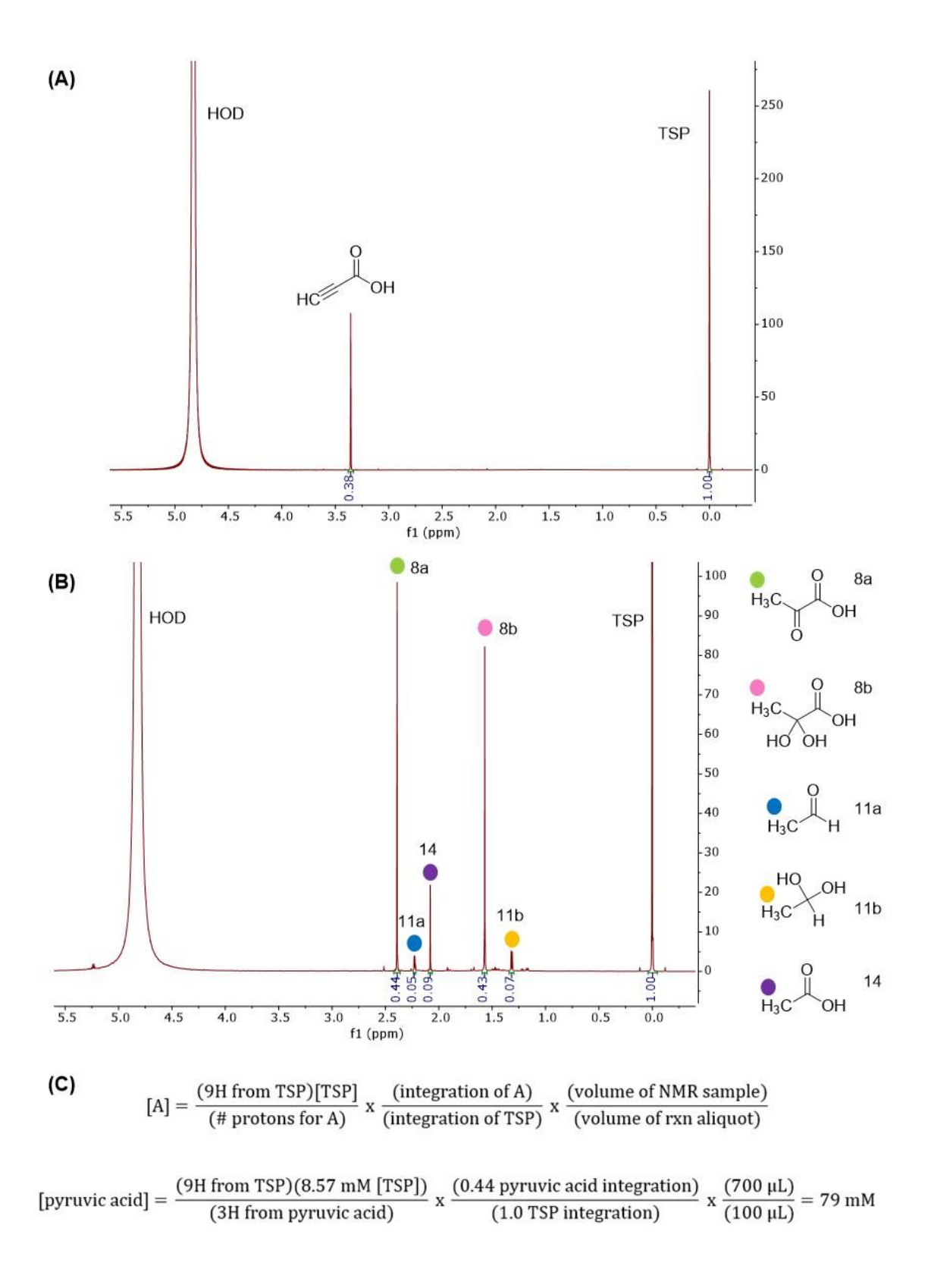


Figure 2.7. NMR spectra of RuCl₃-catalyzed hydration of ACA **6** at A) t = 0 h and B) t = 12 h. C) Sample calculation of pyruvic acid **8a-b** concentration from the spectrum provided in B).

NMR conditions were assessed to find an appropriate relaxation delay for the quantification of reactions. When a magnetic field is applied to a sample, energy absorption can result in the flipping of spin states. T₁ is the time constant at which the system relaxes back to equilibrium. Magnetic fields occur in the sample due to magnetic dipoles of nuclei in motion. Interaction between the resonating nuclear magnetic dipole and the dipole of the nucleus in motion allows energy to flow into the lattice. Because of this, nearby neighboring protons will assist in relaxation.⁴³ The lone alkyne proton on ACA 6 is expected to have a long T₁ since it doesn't have any neighboring protons to help it relax.

An NMR sample was made containing 100 μ L of a hydration reaction (250 mM ACA, 1 mol% RuCl₃, and water) and 600 μ L of 10 mM TSP in D₂O. To determine the T₁ of ACA 6, an inversion recovery experiment was run with 4 scans, a 20 s relaxation delay, 0.5 s minimum T₁ and 5 s maximum T₁ (Figure 2.9). An integral graph of peak integration versus relaxation delay was created based on the spectral data obtained for ACA 6 and TSP, and a three-parameter exponential fit was employed (Figure 2.8). The equation for the signal M(t) can be defined by M(t)=Mo[1-2(e^{-t/T1})] where M(t) is the magnetization, M₀ is the signal at thermal equilibrium state, t is the inversion recovery delay, and T₁ is the time constant.⁴⁴ This equation is represented in the form Y = B+F*exp(-X*G) in Figure 2.8 where F = -2*B. From the obtained data, the T₁ can be determined by taking 1/G which would equal 17 for ACA 6 in this case. A relaxation delay can be calculated by multiplying 5 by the T₁ value. This results in a relaxation delay (time needed between scans) of 85 s for ACA 6.

Due to instrument time limitations, quantification of ACA 6 was tested at relaxations delays of 10 s, 20 s, and 40 s. An NMR sample containing 250 mM ACA 6, 50 mM sodium formate (internal standard), 1 mol% RuCl₃, and 10% D₂O in water was prepared. Eight scans were run for each relaxation delay. Calculated ACA 6 concentrations of 249 mM, 248 mM, and 243 mM were

determined for 10 s, 20 s, and 40 s relaxation respectively. Regardless of the long T_1 value for ACA 6, a 10 s relaxation delay still resulted in accurate quantification.

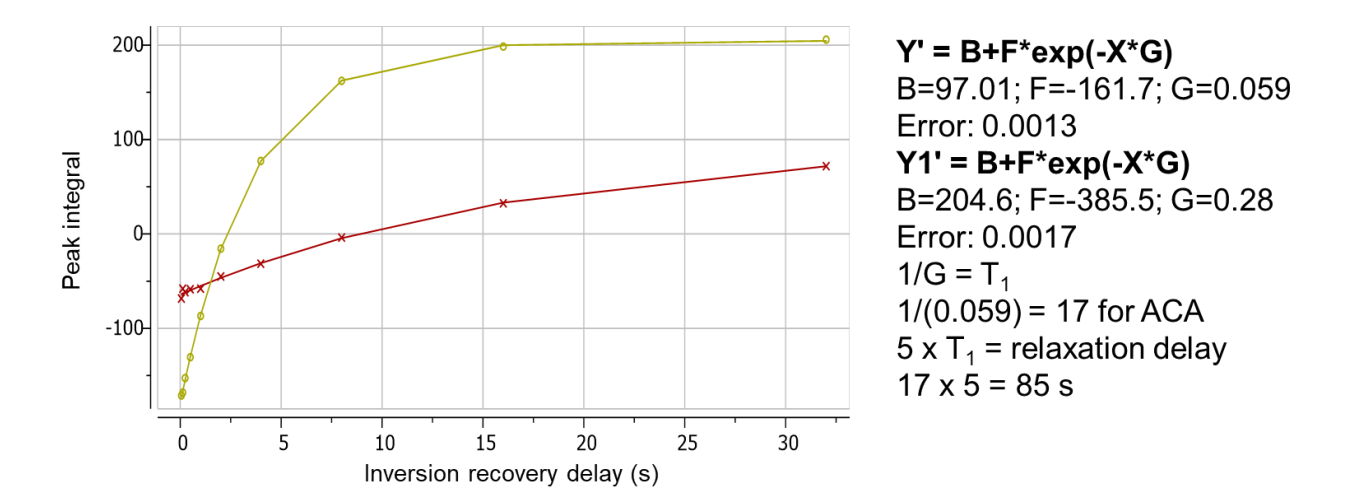


Figure 2.8. Integral graphs with a three-parameter exponential fit were created to calculate a T₁ value for ACA **6** (red line) based off TSP (yellow line) as an internal standard.

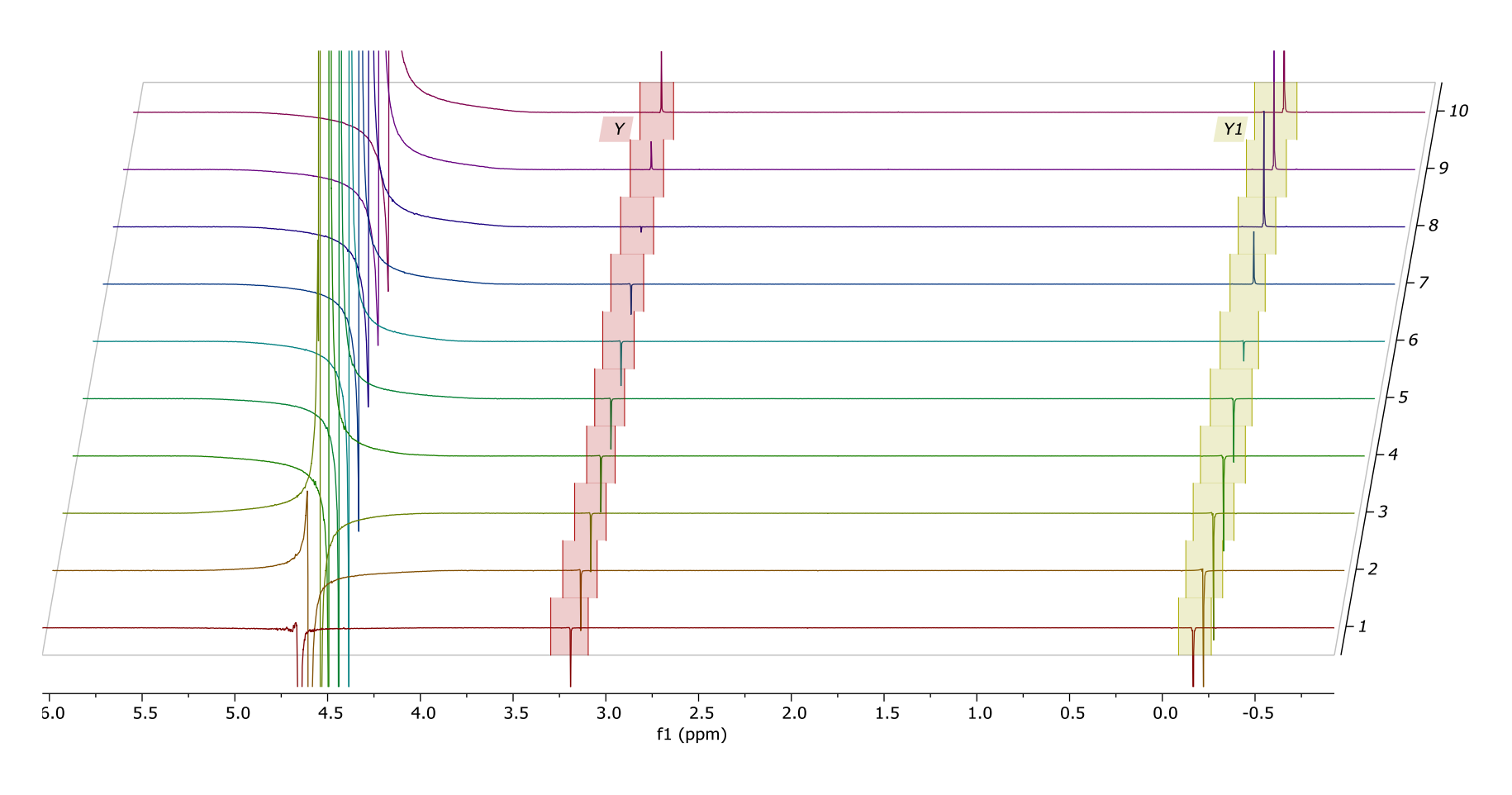


Figure 2.9. A T_1 experiment with 10 spectra at T_1 values ranging from 0.5-5 s was run to determine an appropriate relaxation delay for ACA 6.

2.2.2 Hydration of ACA in Various Solvents

The RuCl₃-catalyzed hydration of acetylenecarboxylic acid (ACA) 6 produces the 1,3-hydration product, pyruvic acid 8a-b, with malonic semialdehyde 9 as a minor product (which is manifested as acetaldehyde 11a-b). This is contrary to the 1961 report by Halpern and coworkers that would predict formation of the 1,4-hydration product, malonic semialdehyde 9 ²⁶. Reaction of 250 mM concentrations of ACA 6 with H₂O catalyzed by RuCl₃ (1 mol%) was examined in various solvents (Table 2.1). Products formed (Figure 2.10) include pyruvic acid 8a, and its hydrate 8b, acetaldehyde 11a, the hydrate of acetaldehyde 11b, and acetic acid 14. Pyruvic acid 8a and its hydrate 8b are the products of the desired 1,3-addition of H₂O to ACA 6. Competing, undesired 1,4-addition of water leads to malonic semialdehyde 9, which presumably decarboxylates to form acetaldehyde 11a and acetaldehyde hydrate 11b. Oxidation of 5a and 5b leads to acetic acid 14.

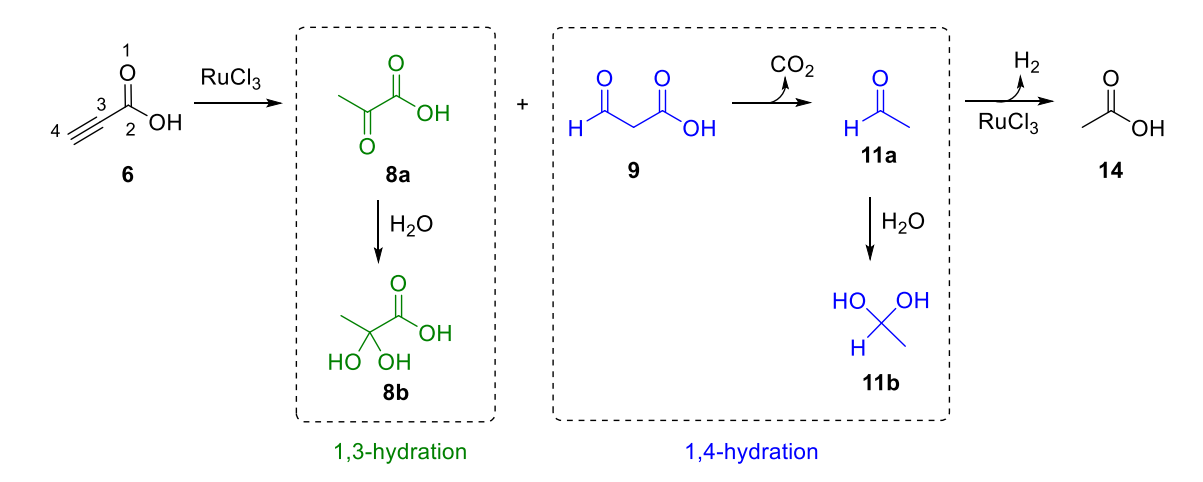


Figure 2.10. RuCl₃ catalyzed 1,3-hydration of ACA **6** to produce pyruvic acid **8a** and its hydrate **8b** and 1,4-hydration to produce malonic semialdehyde **9** as a minor product which leads to the formation of acetaldehyde **11a** and its hydrate **11b**, and subsequent oxidation to acetic acid **14**.

Table 2.1. RuCl₃-catalyzed Hydration of ACA in various solvents.

Entry ^a	Solvent	Water Equiv.	Temp (°C)	O CO ₂ H 8a	HO OH CO ₂ H 8b	О Н 11а	HO OH H	О ОН 14	CO ₂ H 6
		•	` ,	%Yield ^b (mol/mol)					
1	H ₂ O	-	100	34	30	5	5	15	0
2 ^c	THF	10	65	1	1	0	0	0	90
3^c	dioxane	10	100	31	20	0	0	17	0
4 ^d	dioxane/ PvOH	1	100	48	6	0	0	7	0
5	HOAc	0	100	102 ^c	4	0	3	-	0

^a Reactions contained 250 mM ACA, 1 mol% RuCl₃ and were run under N₂ for 12 h in solvents containing the indicated number of equivalents of H_2O . ^b Determined by ¹H NMR. ^c 50% consisted of the enol form of pyruvic acid.

Various solvents were examined for the hydration of ACA 6 to optimize pyruvic acid 8a-b production. With H₂O as solvent at 100 °C (Table 2.1, entry 1), RuCl₃ catalyzed the hydration of ACA 6 to produce a 64% combined yield of pyruvic acid 8a and its hydrate 8b. Significant yields of acetaldehyde 11a (5%), its hydrate 11b (5%), and acetic acid 14 (15%) were also formed (Table 2.1, entry 1). Only trace quantities of pyruvic acid 8a and its hydrate 8b were observed in THF at 65 °C (Table 2.1, entry 2). With dioxane as solvent at 100 °C (Table 2.1, entry 3), the reaction afforded a combined yield of 51% of pyruvic acid 8a and its hydrate 8b along with formation of acetic acid 14 (17%). In the ruthenium-catalyzed dimerization of propiolates, pivalic acid was shown to be an effective co-solvent with dioxane 45, possibly assisting with proton exchange with the ruthenium. Dioxane at 100 °C with 10 equiv. of pivalic acid (PvOH) and 1 equiv. of H₂O relative to ACA 6 (Table 2.1, entry 4) afforded a 54% combined yield of pyruvic acid 8a and its hydrate 8b along with a 7% yield of acetic acid 14. The highest combined yields at 106% of pyruvic acid 8a and its hydrate 8b were observed when RuCl₃-catalyzed hydration was run in HOAc as solvent (Table 2.1, entry 5). Error in NMR product quantitation is likely why the yield is above 100%. This NMR error also contributes to mass balance that is not 100% in other reactions. The NMR measurements are very reproducible, however. An NMR sample was run three times, and

quantification of the pyruvic acid **8a** peak resulted in an average pyruvic acid **8a** concentration of 61.8 mM with a small standard deviation of 1.0 mM.

2.2.3 Optimization of the Hydration of ACA in Water

Table 2.2. Hydration of ACA 6 and ADCA 7 in water at various conditions.

Entry ^a	Cat. mol %	[ACA] [ADCA] (mM)	Scale ^b	Temp (°C)	Time (h)	O CO₂H 8a	8b	О Н 11а	но он Н 11b	о 14	CO ₂ H 6
							%`	∕ield ^c (mol/mol))	
1	1	250	1X	100	11	34	30	5	5	15	0
2	0	250	1X	100	12	0	0	4	6	0	86
3	1	250	2X	100	11	31	28	9	11	7	1
4	1	250	8X	100	12	26	26	10	13	5	7
5	1	250	1X	90	13	30	30	9	11	6	2
6	1	250	1X	50	85	8	13	6	7	3	55
7	4	250	1X	50	145	19	20	3	5	6	2
8	1	500	1X	100	11	19	21	4	5	6	1
9	2	500	1X	100	9	13	12	3	4	4	0
10	2	500	1X	80	24	19	25	8	10	6	3
11	2	250	1X	100	6	27	26	6	7	7	0
12	0.5	250	1X	100	24	27	20	2	3	5	0
13	1	250	1X	100	11	37	44	4	5	6	0
14	2	250	1X	100	10	30	34	2	3	4	0
15	1	500	0.5X	100	12	25	36	3	3	5	1

^a All hydrations were run under N₂ with RuCl₃ as catalyst. ^b 1X scale refers to a reaction containing 20 mL H₂O, 310 μL ACA (or 574 mg ADCA), and 12 mg RuCl₃. All reactions are relative to the 1X scale. (e.g. 2X is double everything from 1X) ^c Yields determined by ¹H NMR. Reactions were run in duplicate at minimum, and average values are reported.

Although the highest pyruvic acid **8a-b** yield was seen with acetic acid **14** as the solvent, further hydration reaction conditions were tested (Table 2.2) using water as the solvent with the hope that crude reaction mixture could be used for the subsequent enzymatic reduction to lactic acid **2a-b** (Figure 2.16). Although the enzymes weren't tested in 100% acetic acid, lactate dehydrogenase is assayed in buffered aqueous solutions in routine assays. All changes to reaction conditions were made based on Table 2.1, entry 1 (Table 2.2, entry 1 included for reference) as the standard reaction. A control reaction was run at 100 °C with only ACA **6** in water

and no catalyst. A small amount of acetaldehyde 11a and its hydrate 11b were formed, with 86% ACA 6 remaining (Table 2.2, entry 2). Scaling up the reaction by a factor of 2 resulted in a 59% combined yield of pyruvic acid 8a and its hydrate 8b (Table 2.2, entry 3), and an 8X scale resulted in a slightly lower yield of 52% 8a-b (Table 2.2, entry 4). Hydration of ACA 6 at 90 °C gave a similar yield to that at 100 °C with a yield of 60% 8a-b (Table 2.2, entry 5). Reducing the temperature to 50 °C resulted in a significantly lower yield of 21% 8a-b (Table 2.2, entry 6) and increasing RuCl₃ to 4 mol% and running the hydration for 145 hours at 50 °C still only gave 39% 8a-b (Table 2.2, entry 7). Running the reactions at lower temperature required much longer reaction times which may contribute to more product loss through evaporation. Surprisingly, doubling the ACA 6 concentration (Table 2.2, entry 8) and doubling both the ACA 6 and RuCl₃ concentrations (Table 2.2, entry 9) resulted in much lower yields of 40% and 25% 8a-b respectively. By lowering the temperature to 80 °C while having doubled ACA 6 and RuCl₃ concentrations, the yield was slightly increased to 44% 2a-b (Table 2.2, entry 10). Doubling the RuCl₃ to 2 mol% and cutting it in half to 0.5 mol% resulted in lower pyruvic acid 8a-b yields of 53% (Table 2.2, entry 11) and 47% (Table 2.2, entry 12) respectively. Using ADCA 7 as the substrate at standard conditions resulted in the highest hydration in water yield of 81% pyruvic acid 8a and its hydrate 8b (Table 2.2, entry 13). Timepoints taken of the reaction show decarboxylation of ADCA 7 into ACA 6 as the reaction proceeds to hydration products (Figure 2.11). Doubling the RuCl₃ to 2 mol% in hydration of ADCA 7 resulted in a 63% yield (Table 2.2, entry 14) of pyruvic acid 8a-b which is comparable to standard conditions using ACA 6, but lower compared to standard conditions using ADCA 7. Doubling the ADCA 7 concentration also resulted in a lower yield of 61% 8a-b (Table 2.2, entry 15).

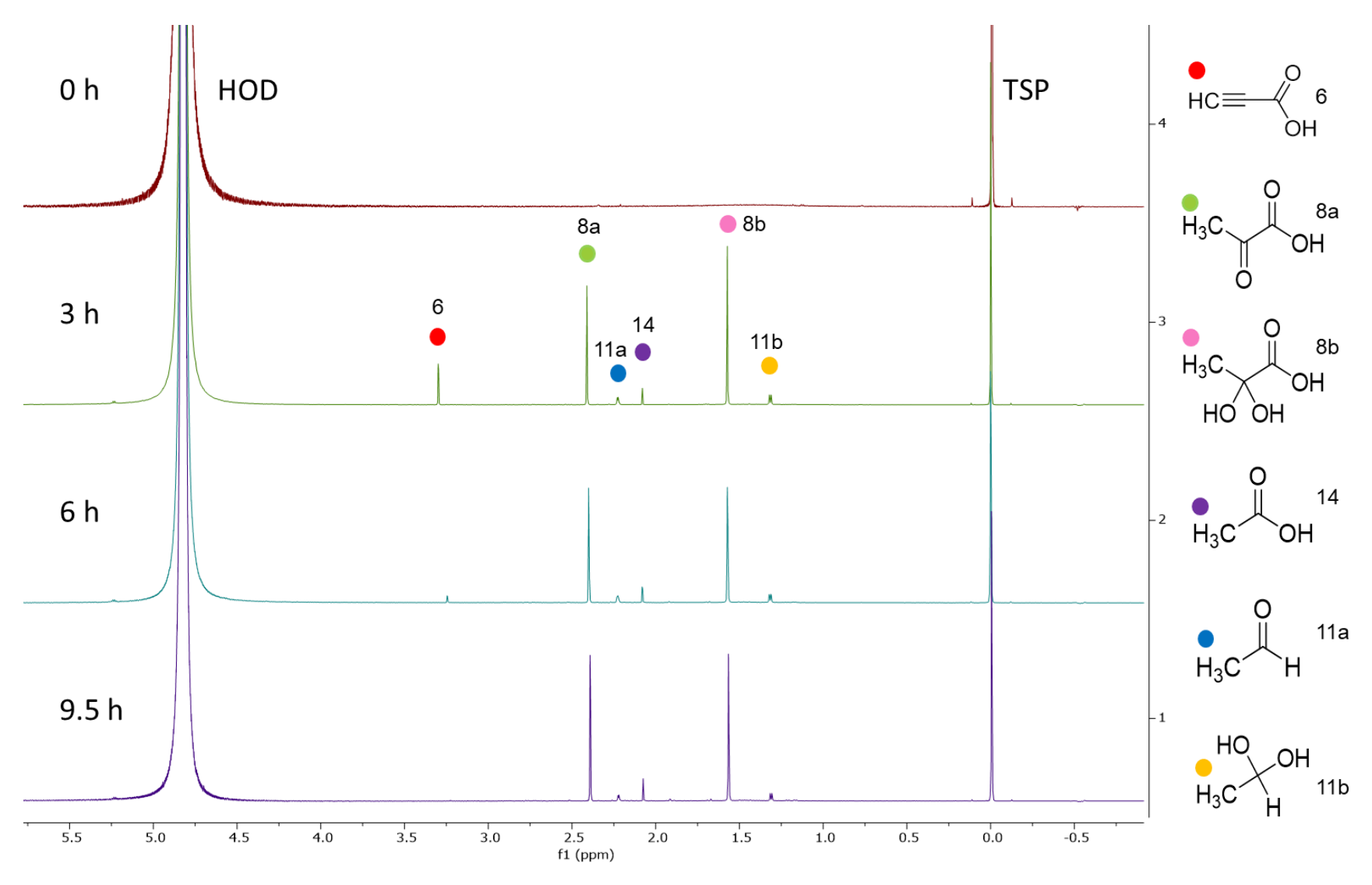


Figure 2.11. NMR spectra of timepoints taken in the Ru-catalyzed hydration of ADCA **7** show that ADCA decarboxylates to form ACA **6** as it is hydrated to then form pyruvic acid **8**.

2.2.4 Exploration of Metal Catalysts for the Hydration of ACA

Table 2.3. Catalyst Screening for the hydration of ACA **6**.

Entry	Catalyst	Cat. mol%	Time (h)	O CO₂H 8a	HO OH CO ₂ H 8b	O H 11a	HO OH H 11b	о ОН 14	CO ₂ H 6
						%Yield ^b ((mol/mol)		
1	RuCl ₃	1	11	34	30	5	5	15	0
2	IrCl ₃	1	12	27	11	14	15	13	0
3	$InCl_3$	1	11	19	4	11	13	7	0
4	$RhCl_{\mathfrak{Z}}$	1	11	14	6	9	6	12	5
5	FeCl ₃	1	16	0	1	4	7	1	73
6	BiCl ₃	1	11	0	0	3	5	0	73
7	$MoCl_3$	1	11	0	0	4	7	0	74
8	Hg(OAc) ₂	1	11	4	5	4	7	n/a	40
9	$Cu(OTf)_2$	1	11	1	1	4	7	1	58
10	$CuSO_4 \cdot 5 H_2O$	1	11	1	2	4	6	1	83
11	Cul	1	11	0	0	1	2	1	0
12	AgSbF ₆	1	11	0	0	0	1	0	0
13	$AgNO_3$	1	11	0	0	1	1	1	0
14	$Bi(NO_3)_3 \cdot 5 H_2O$	1	11	0	0	3	5	1	72

^a All hydrations were run under N₂ with 250 mM ACA as substrate. ^b Yields determined by ¹H NMR.

Additional catalysts were screened in the hydration of ACA 6 in water. RuCl₃ is included as Table 2.3, entry 1 for reference. To assess if any other metal trichloride catalysts compared to RuCl₃ in yields, IrCl₃, InCl₃, RhCl₃, FeCl₃, BiCl₃, and MoCl₃ were tested at 1 mol%. Of them, IrCl₃ performed the best, giving 38% yield of pyruvic acid 8a and its hydrate 8b (Table 2.3, entry 2), compared to 29% 8a-b shown by Ogo and coworkers at 0.1 mmol ACA 6 scale ²⁷. Although IrCl₃ performed the best in the catalyst screen, it still was well below the yields seen using RuCl₃ at these conditions. Hydration catalyzed with InCl₃ and RhCl₃ resulted in 23% (Table 2.3, entry 3) and 20% (Table 2.3, entry 4) yields 8a-b respectively. RhCl₃ yields were comparable to the 19%

8a-b seen by Ogo and coworkers at 0.1 mmol ACA **6** ²⁷. FeCl₃ showed a small yield of only 1% **8a-b** (Table 2.3, entry 5). BiBr₃ has shown Markovnikov hydration of *p*-methoxyphenylacetylene, ⁴⁶ but BiCl₃ as well as MoCl₃ didn't result in any product **8a-b** formation (Table 2.3, entries 6-7). To achieve the Markovnikov hydration product via oxymercuration-demercuration, Hg(OAc)₂ was tested, but resulted in only 9% pyruvic acid **8a-b** (Table 2.3, entry 8). The remaining catalysts screened have shown Markovnikov hydration of various alkynes, ^{46,48,49} but resulted in very low or no product formation for the hydration of ACA **6** at these conditions. Cu(OTf)₂ produced only 2% pyruvic acid **8a-b** (Table 2.3, entry 9) and CuSO₄·5 H₂O resulted in 3% pyruvic acid **8a-b** (Table 2.3, entry 10). Cul, AgSbF₆, AgNO₃, and Bi(NO₃)₃ did not result in any product **8a-b** formation (Table 2.3, entries 11-14).

2.3 Pyruvic Acid Extraction and Removal of Ruthenium

The extraction of pyruvic acid **8a-b** from crude hydration reaction mixture (run at a 2X scale, 40 mL, pH ~ 2) was compared using a standard liquid-liquid extraction method versus a continuous extraction. This was done with the initial assumption that ruthenium would need to be removed prior to the enzymatic conversion of pyruvate to lactate by lactate dehydrogenase. In the standard method, pyruvic acid **8a-b** was extracted with diethyl ether three times. The combined organic layers were washed with brine and dried using sodium sulfate. Diethyl ether was removed *in vacuo* and approximately 24% product was recovered based on NMR quantification. For continuous extraction (Figure 2.12), MTBE was used to extract pyruvic acid **8a-b** (since it doesn't readily form peroxides and the extraction will be heated) with the same solvent volume used as in the standard extraction. MTBE and crude reaction mixture were added to the continuous extractor and stirred. MTBE was added to a flask connected to the side arm and heated to maintain a constant reflux. The side flask was emptied and replaced with fresh MTBE two additional times. Each round of refluxing was left for approximately three hours. The organic layers were combined and dried with sodium sulfate. MTBE was removed *in vacuo* and

approximately 69% of product was recovered based on NMR quantification. Continuous extraction resulted in a much higher product recovery compared to the standard liquid-liquid extraction method.

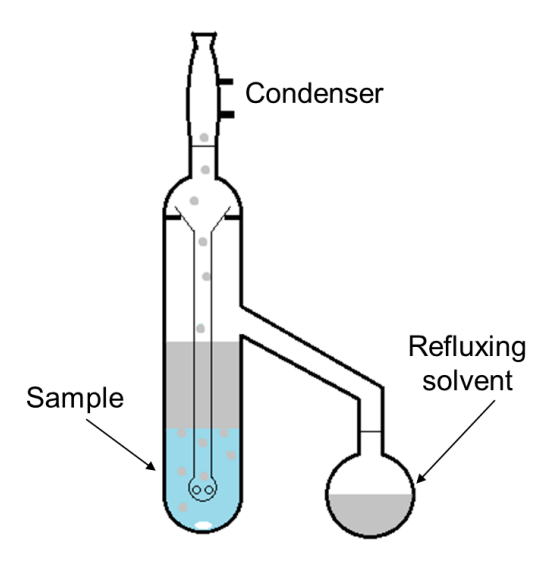


Figure 2.12. As the refluxing solvent condenses in a continuous extractor, it is mixed into the stirring sample to extract the desired material.

Removal of ruthenium from a hydration reaction was attempted using Dowex 50WX8 (H⁺ form) resin. Two Dowex columns were poured having 5 mL and 15 mL of resin respectively. The columns were acidified with 2 M HCl and rinsed with water until the flow-through had a neutral pH. Duplicate hydration reactions that were run at "standard" conditions were added to their respective columns, and the columns were eluted with water (10 CV). Pyruvic acid **8a-b** was extracted from the aqueous column flow-through using the standard extraction method described above. Approximately 23% and 6% product was recovered based on hydration reaction yields from the columns containing 5 mL and 15 mL Dowex respectively. The difference in product recovery was likely due to the increased volume of Dowex in one column. Inductively coupled plasma- optical emission spectrometry (ICP-OES) was used to compare the removal of ruthenium between a hydration reaction treated only with a standard diethyl ether extraction versus the two reactions run through Dowex columns followed by diethyl ether extraction. ICP-OES is an

analytical method that allows determination of the atomic composition of a sample. The sample is aerosolized and passed through a high energy argon plasma which ionizes the sample through collisional excitation. Once the ions transition back to a lower energy state, they release characteristic wavelengths. These wavelengths can be used to identify and quantify elements in a sample. First, a calibration curve for each characteristic ruthenium wavelength was made using 0 ppm, 0.08 ppm, 0.4 ppm, 2 ppm, and 10 ppm ruthenium standards all prepared in 2% nitric acid to matrix match samples (Figure 2.13). The samples for analysis were prepared in 2% nitric acid in order to digest any organics in the sample. Assuming no ruthenium was removed from the samples, a concentration of 12 ppm would be observed. The sample that was extracted only and the samples that were run through Dowex columns followed by extraction all showed significantly less ruthenium at the four wavelengths measured, ranging from 0.05 to 0.07 ppm ruthenium. Comparing the three samples, the reaction that was run through 15 mL of Dowex resin followed by extraction showed the lowest ruthenium concentrations, however, there was no significant difference amongst the three ruthenium removal methods (Table 2.4).

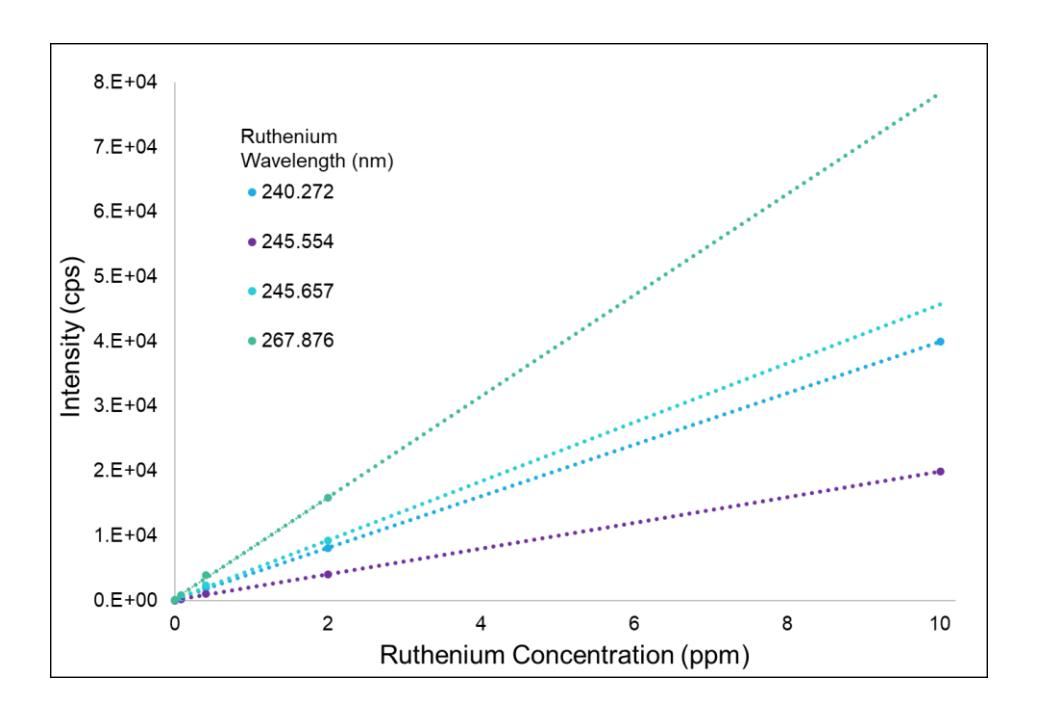


Figure 2.13. Calibration curves for ruthenium standards at four standard wavelengths associated with ruthenium. (cps: counts per second)

Table 2.4. The removal of ruthenium was compared using diethyl ether extraction to running samples through a Dowex column followed by extraction. Similar ruthenium concentrations were seen in each method.

	Ru Concentration (ppm)						
Sample	Ru Wavelength (nm)						
	240.272	245.554	245.657	267.876			
Extraction Only	0.072	0.076	0.059	0.075			
5 mL Dowex & Extraction	0.060	0.066	0.051	0.051			
15 mL Dowex & Extraction	0.057	0.061	0.047	0.049			

2.4 Proposed Mechanism for the Hydration of ACA

Figure 2.14. The proposed mechanism for the RuCl₃-catalyzed hydration of ACA **6** in water goes through a metal vinylidene intermediate followed by a 3-exo-trig cyclization.

The proposed mechanism for the RuCl₃-catalyzed hydration of ACA 6 (Figure 2.14) starts with interaction between the ruthenium and the alkyne functional group of ACA 6. Ruthenium has been shown to undergo 1,2-hydrogen shifts when interacting with terminal alkynes to form a metal vinylidene.⁵⁰ We then propose that anchimeric assistance of the C-1 carboxylic acid could result in a 3-exo-trig cyclization to form a methylene oxiranone. This key intermediate could explain why pyruvic acid 8a-b is the product formed instead of malonic semialdehyde 9 which would require an unfavored 4-endo-dig cyclization. Water could then break open the strained ring and a proton

could be transferred, resulting in neutral oxygen atoms. Electrons from the carbon-hydrogen bond could then be pushed between the carbon atoms, with electrons being pushed onto the ruthenium and an enol resulting. Addition of a proton to the alkene could result in a carbocation intermediate where the electrons from the carbon-ruthenium bond could be used to reform the enol. The enol could then tautomerize to the keto form, resulting in pyruvic acid **8a-b**.

2.5 Production of Lactic Acid

Pyruvic acid **8a-b** produced from the RuCl₃-catalyzed hydration of ACA **6** can be enzymatically reduced to form lactate **2a-b**. Reaction of pyruvate **8a-b** with D-lactate dehydrogenase yields D-lactate **2a** and reaction with L-lactate dehydrogenase yields L-lactate **2b**. Oxygen tolerant, NAD+-reducing soluble hydrogenase was used to recycle cofactor.

2.5.1 Purification and Characterization of Enzymes

L-Lactate dehydrogenase (L-LDH) from rabbit muscle, and D-lactate dehydrogenase from Lactobacillus leichmannii (D-LDH) were purchased from Roche. Lactate dehydrogenase activity was measured by monitoring the decrease in absorbance at 340 nm, corresponding to the consumption of NADH (ϵ = 6220 M⁻¹ cm⁻¹). Measurements were made at 30 °C. Assays contained NADH, LDH and pyruvate **8a-b** in 50 mM Tris-HCl (pH 8 at 30°C). The reaction was initiated by addition of pyruvate **8a-b** and A₃₄₀ was recorded.

Table 2.5. Representative specific activity of L-LDH, D-LDH, and SH.

Enzyme	Specific Activity (U mg ⁻¹)				
L-LDH	10.7				
D-LDH	6.2				
SH	26.0				

The protocol for overexpression and purification of soluble hydrogenase (SH) was adapted from the Lenz group.⁵¹ Soluble hydrogenase is naturally produced by *Ralstonia eutropha* with a

physiological function of reducing H₂, CO₂, and O₂ during cell growth.⁴⁰ *R. eutropha* Hf210 pGE771 was engineered for overexpression of SH and operates under control of the native SH promoter. The hoxF gene of SH is equipped with a *strep*-tag II-encoding sequence at the 5' end.⁴⁰ One liter of *R. eutropha* Hf210 pGE771 culture was grown to an OD₄₃₆ of 10-12 and pelleted. For protein purification, the resuspended cell pellet was flushed with argon and passed twice through a chilled French press cell into an argon-flushed centrifuge tube. Cellular debris was separated from cell lysate by centrifugation and filtered through a syringe filter. SH was purified via column chromatography using *strep*-Tactin Sepharose resin 50% suspension. The *strep*-tag (WSHPQFEK) binds to the engineered streptavidin resin. SH was eluted from the column using desthiobiotin which competitively binds to the resin. Purified SH was stored at -80 °C in 50 mM KH₂PO₄, pH 7.0, containing 5% glycerol. Protein concentration was determined by Bradford analysis, and purity was assessed using SDS-PAGE (Figure 2.15).

Soluble hydrogenase activity was measured by monitoring the increase in absorbance at 365 nm, corresponding to production of NADH (ϵ = 3480 M⁻¹ cm⁻¹). Although the maximum absorbance of NADH lies at 340 nm, the absorbance increase remains linear for longer when measured at 365 nm. Measurements were made at 30 °C. ^{41,51} Assays (final volume 2 mL) contained NAD+ and soluble hydrogenase (SH) in 50 mM Tris-HCI (pH 8 at 30°C). The reaction was sealed, saturated with hydrogen, and initiated by addition of SH via syringe and A₃₆₅ was recorded.

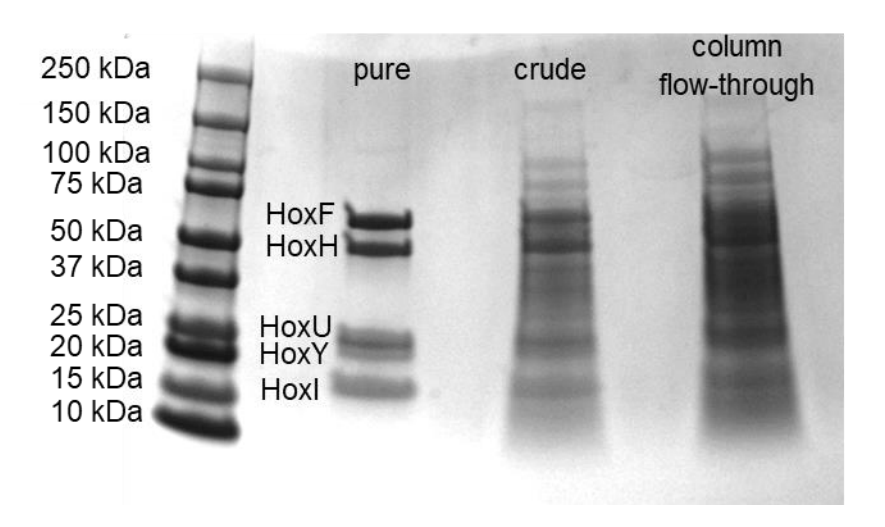


Figure 2.15. SDS-PAGE gel of SH showing purified protein, crude protein, and column flow-through before elution of SH. Subunits HoxF: 68 kDa, HoxH: 55 kDa, HoxU: 26 kDa, HoxY: 23 kDa, and HoxI: 19 kDa are seen.

Figure 2.16. Pyruvic acid **8a-b** produced via RuCl₃-catalyzed hydration used in the lactate dehydrogenase conversion to lactic acid **2a-b** with soluble hydrogenase added for cofactor recycling.

2.5.2 Preparation for Using Crude Hydration Mixture to Produce Lactic Acid

Reactions for the production of lactic acid **2a-b** contained pyruvic acid **8a-b**, NAD⁺, LDH, and SH (final volume 4 mL) and were run in 50 mM Tris-HCl (pH 8 at 30 °C). Reaction flasks were sealed with septa and placed in a 30 °C water bath. Hydrogen was bubbled in using a needle, with a second needle used to relieve pressure. Reaction progress and product concentrations were determined by 1 H NMR. At timed intervals, an aliquot (490 µL) of the reaction was removed via pipette and combined with 100 µL of D₂O containing 10 mM TSP and 10 µL concentrated H₂SO₄. The turnover number (TON) for conversion of NAD⁺ to NADH was calculated by dividing the final concentration of lactate **2a-b** by the concentration of NAD⁺ in the reaction. An authentic

pyruvate **8a-b** reaction (12 mM pyruvate) with 0.1 mM NAD⁺ gave a 95% conversion **2b** and a TON of 116, and 1 mM NAD⁺ resulted in 97% conversion **2b** with a TON of 12 (Figure 2.18). Since pyruvate **8a-b** produced via hydration will be used directly for the production of lactate **2a-b**, the components of the crude reaction mixture had to be tested with LDH and SH to determine if they would interfere with enzyme activity. The activity of L-LDH and SH (Figure 2.17) was assayed in the presence of 5 μ M, 50 μ M, and 500 μ M acetaldehyde **11a-b**, acetate **14**, and RuCl₃, and compared to the relative control reaction which did not contain any of the components. Even with excess amounts of hydration components added, activity did not significantly decrease for either enzyme. Rather, an increase in SH activity was seen with 5 μ M and 50 μ M RuCl₃.

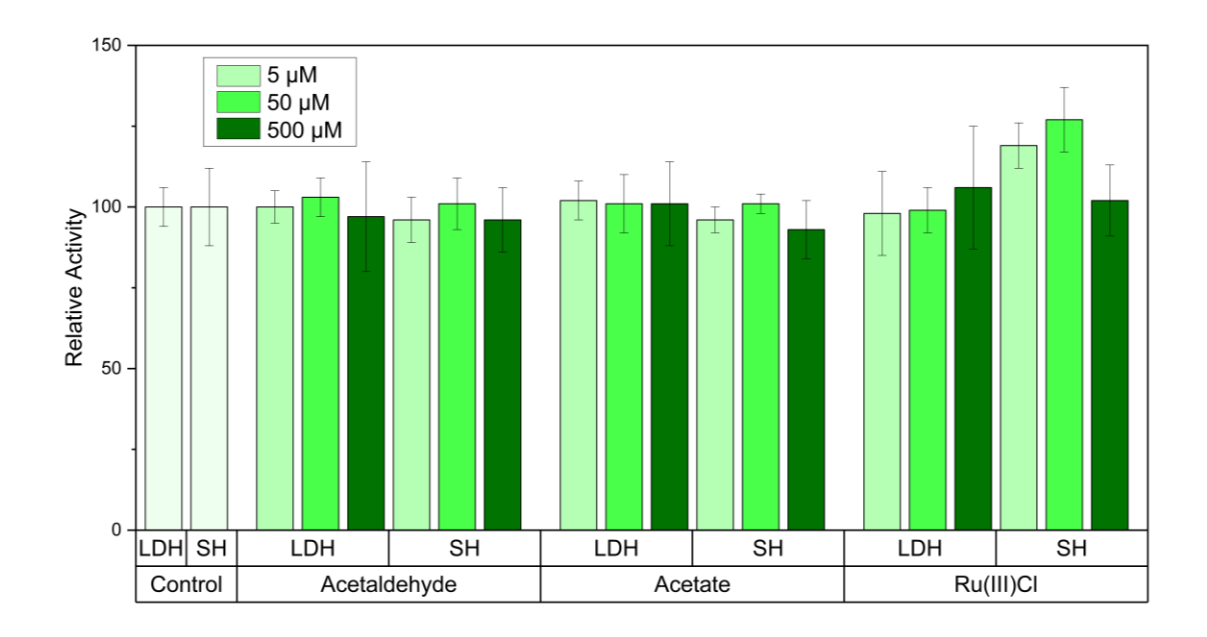


Figure 2.17. LDH and SH activity in the presence of 5 μ M, 50 μ M, and 500 μ M acetaldehyde **11**, acetate **14**, and RuCl₃. The controls are normalized to 100% activity, and the assays containing a hydration reaction component are relative to the respective control.

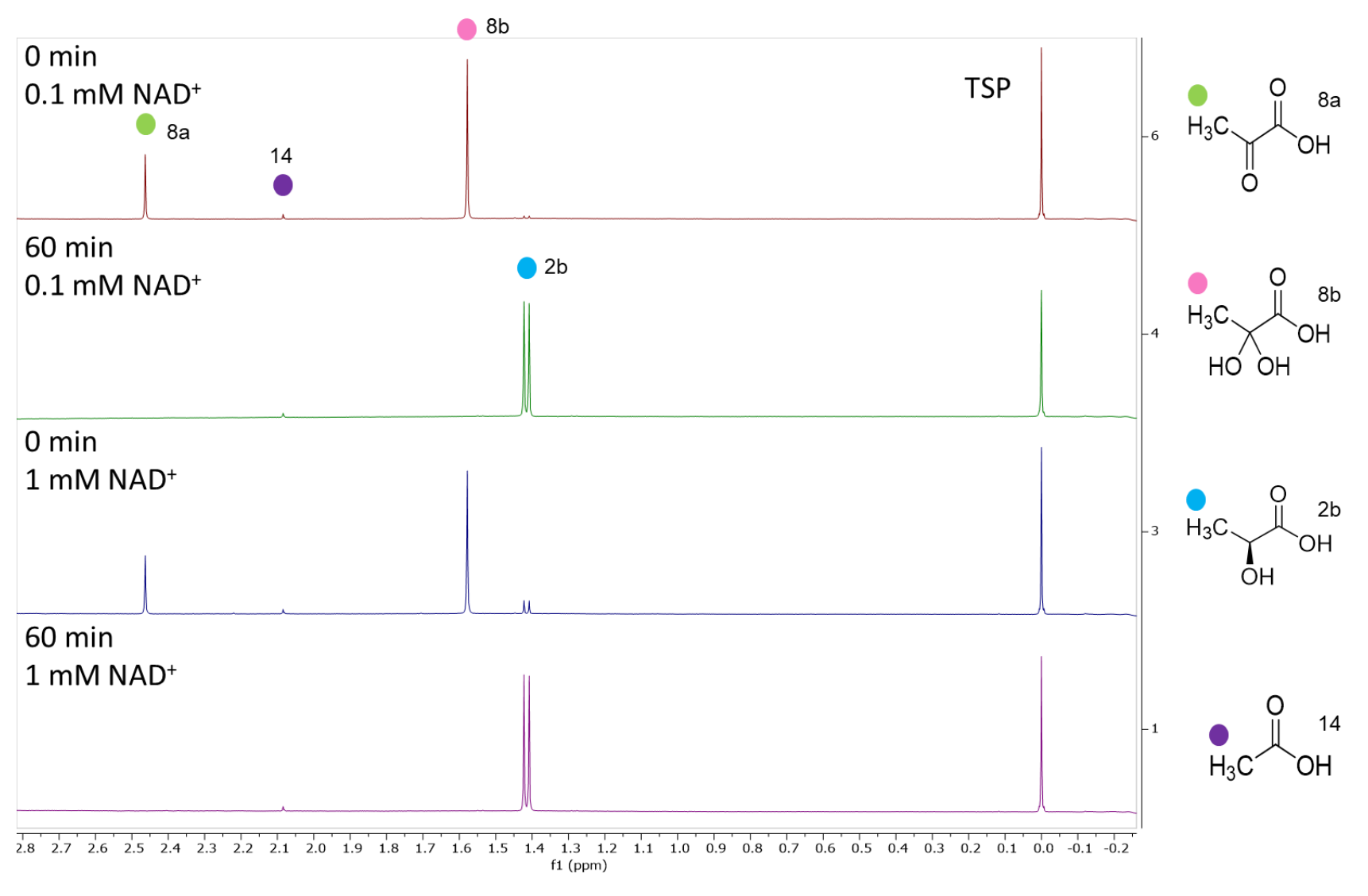


Figure 2.18. NMR spectra of initial and final timepoints taken in the enzymatic conversion of authentic pyruvic acid **8** to L-lactic acid **2b** using L-LDH and SH at 0.1 mM NAD⁺ and 1 mM NAD⁺.

2.5.3 Production of Lactic Acid with Cofactor Recycling

Table 2.6. Lactate dehydrogenase-catalyzed conversion of pyruvate 8 to lactate 2.

Entry	[pyruvate] (mM)	-		[NAD+] (mM)	NAD+ TON ^b	О ОН ОН 2 а	OH OH 2b	
	,				()		%Yield ^c (r	mol/mol)
1	12	-	0.4	2.6	1	12	n.d.	95
2	12	-	0.4	2.6	0.1	117	n.d.	97
3	12	0.2	-	5.3	1	12	100	n.d.
4	12	0.2	-	5.3	0.1	116	94	n.d.
5	12	-	2.4	23.5	0.01	1224	n.d.	98
6	12	-	2.4	23.5	0.001	2560	n.d.	22

^a All reactions were run in 50 mM Tris-HCl, pH 8, final volume 4 mL, at 30 °C with constant H₂ bubbling. ^bNAD+ TON (turnover number) = final [lactate] in mM/ [NAD+] in mM ^c Yields determined by ¹H NMR. n.d. is not determined.

D- and L-Lactate **2a-b** can be produced from pyruvate **8a-b** generated from the hydration of ACA **6**. A hydration reaction with 103 mM combined pyruvic acid **8a-b** concentration, run at the conditions of Table 2.1, entry 1 was used for lactate production **2a-b** (Figure 2.16). The crude mixture was added to reactions without any purification. Using L-LDH, SH, and pyruvate **8a-b** produced via hydration, the 1 mM NAD+ reaction resulted in a 95% conversion **2b** and an NAD+ TON of 12 (Table 2.6, entry 1, Figure 2.20) The 0.1 mM NAD+ reaction gave a 97% conversion **2b** and an NAD+ TON of 117 (Table 2.6, entry 2, Figure 2.21). Figure 2.19a depicts the decrease in pyruvate **8a-b** and increase in L-lactate **2b** at 0.1 and 1 mM NAD+. Using crude pyruvate **8a-b**, SH, and D-LDH, reaction with 1 mM NAD+ resulted in 100% conversion **2a** and an NAD+ TON of 12 (Table 2.6, entry 3, Figure 2.22). Using 0.1 mM NAD+ gave a 94% conversion **2a** and an NAD+ TON of 116 (Table 2.6, entry 4, Figure 2.23) Figure 2.19b depicts the decrease in pyruvate **8a-b** and increase in D-lactate **2a** at 0.1 and 1 mM NAD+. Lowering NAD+ concentration even further in the conversion to L-lactate **2b** still resulted in cofactor recycling. A % conversion of 98% was achieved with 0.01 mM NAD+ and an NAD+ TON of 1224 (Table 2.6, entry 5, Figure 2.24). Figure 2.19c shows the reaction traces for the production of L-lactate **2b** at 0.01 mM NAD+. Using 0.001

mM NAD⁺ resulted in a lower % conversion of 22% **7b**, but it resulted in the highest NAD⁺ TON of 2560 (Table 2.6, entry 6).

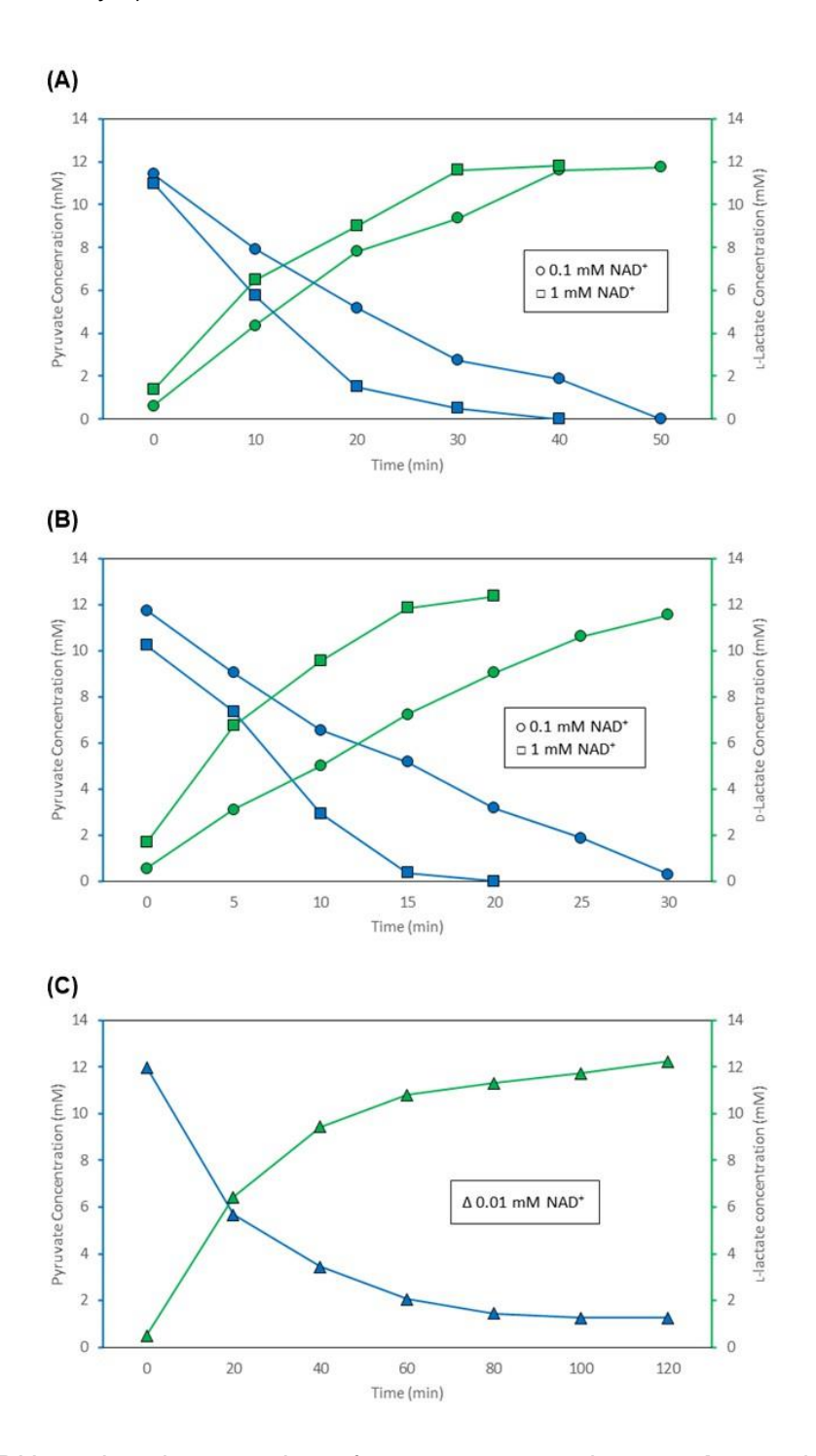


Figure 2.19. LDH-catalyzed conversion of pyruvate **8** to L-lactate **2b** or D-lactate **2a**. Substoichiometric amounts of added NAD⁺ are recycled with SH. a) L-LDH in the presence of 0.1 and 1 mM NAD⁺ b) D-LDH in the presence of 0.1 and 1 mM NAD⁺ c) L-LDH in the presence of 0.01 mM NAD⁺.

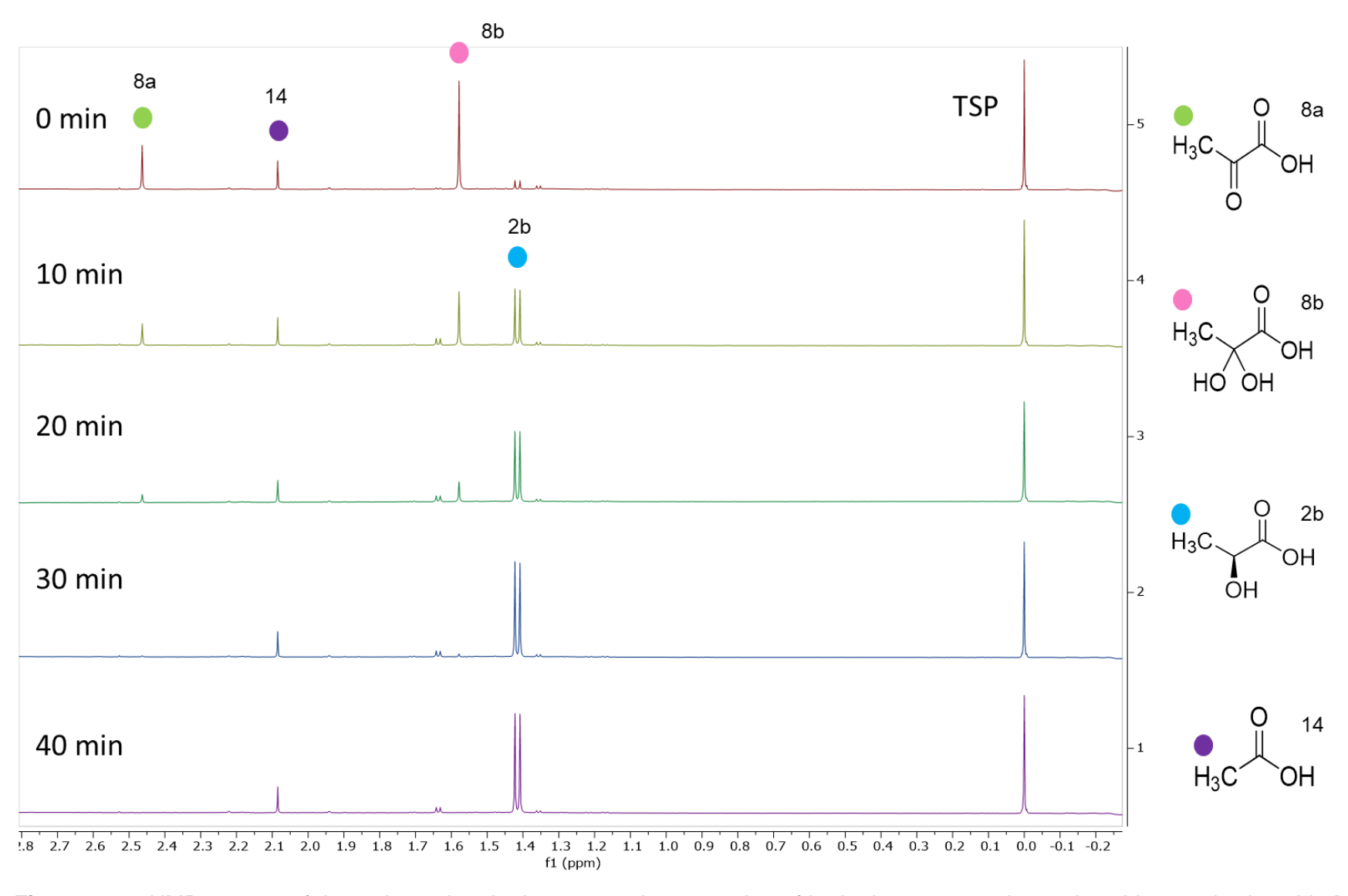


Figure 2.20. NMR spectra of timepoints taken in the enzymatic conversion of hydration-generated pyruvic acid **8** to L-lactic acid **2b** using L-LDH and SH in the presence of 1 mM NAD⁺.

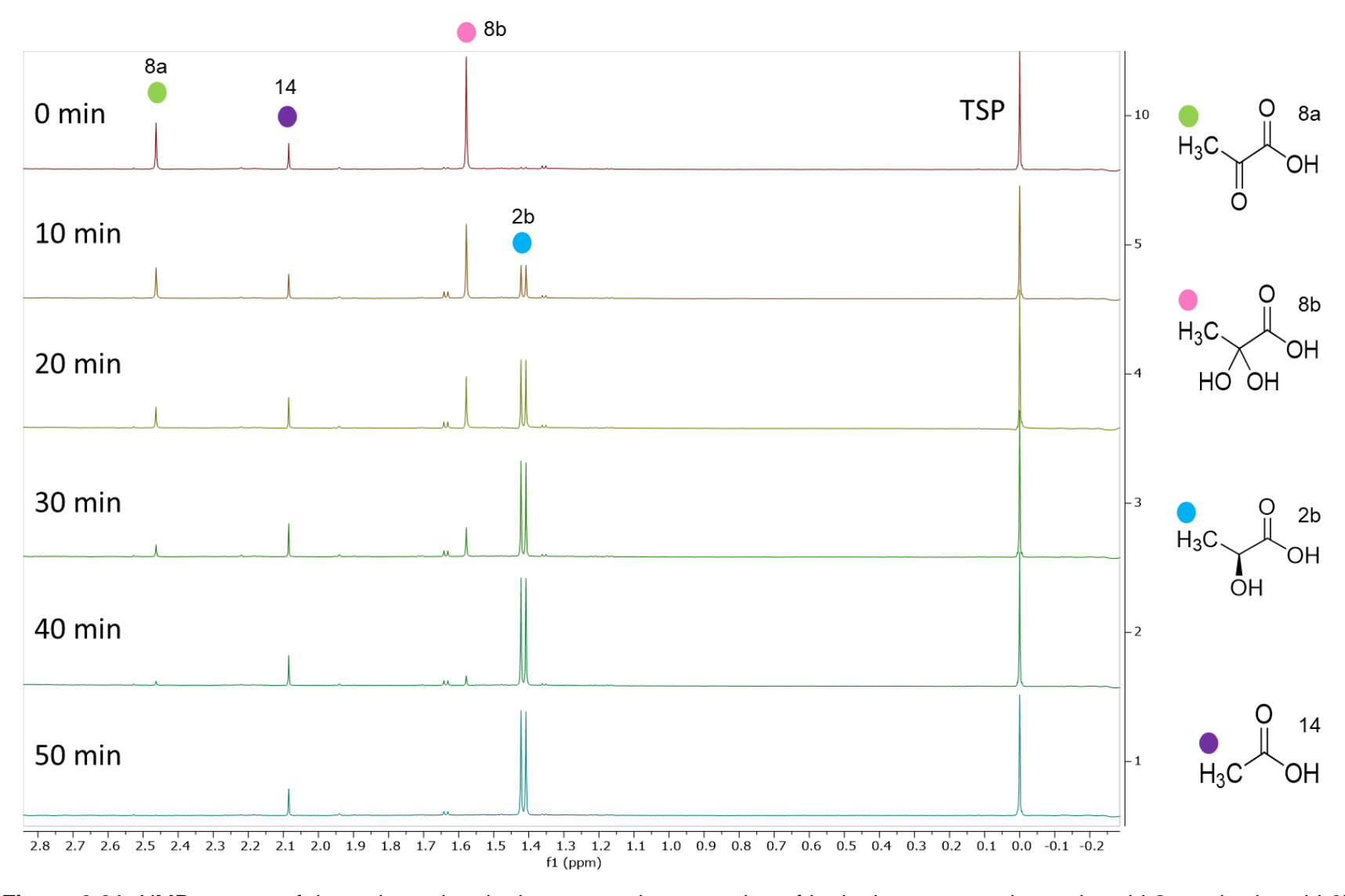


Figure 2.21. NMR spectra of timepoints taken in the enzymatic conversion of hydration-generated pyruvic acid **8** to L-lactic acid **2b** using L-LDH and SH in the presence of 0.1 mM NAD⁺.

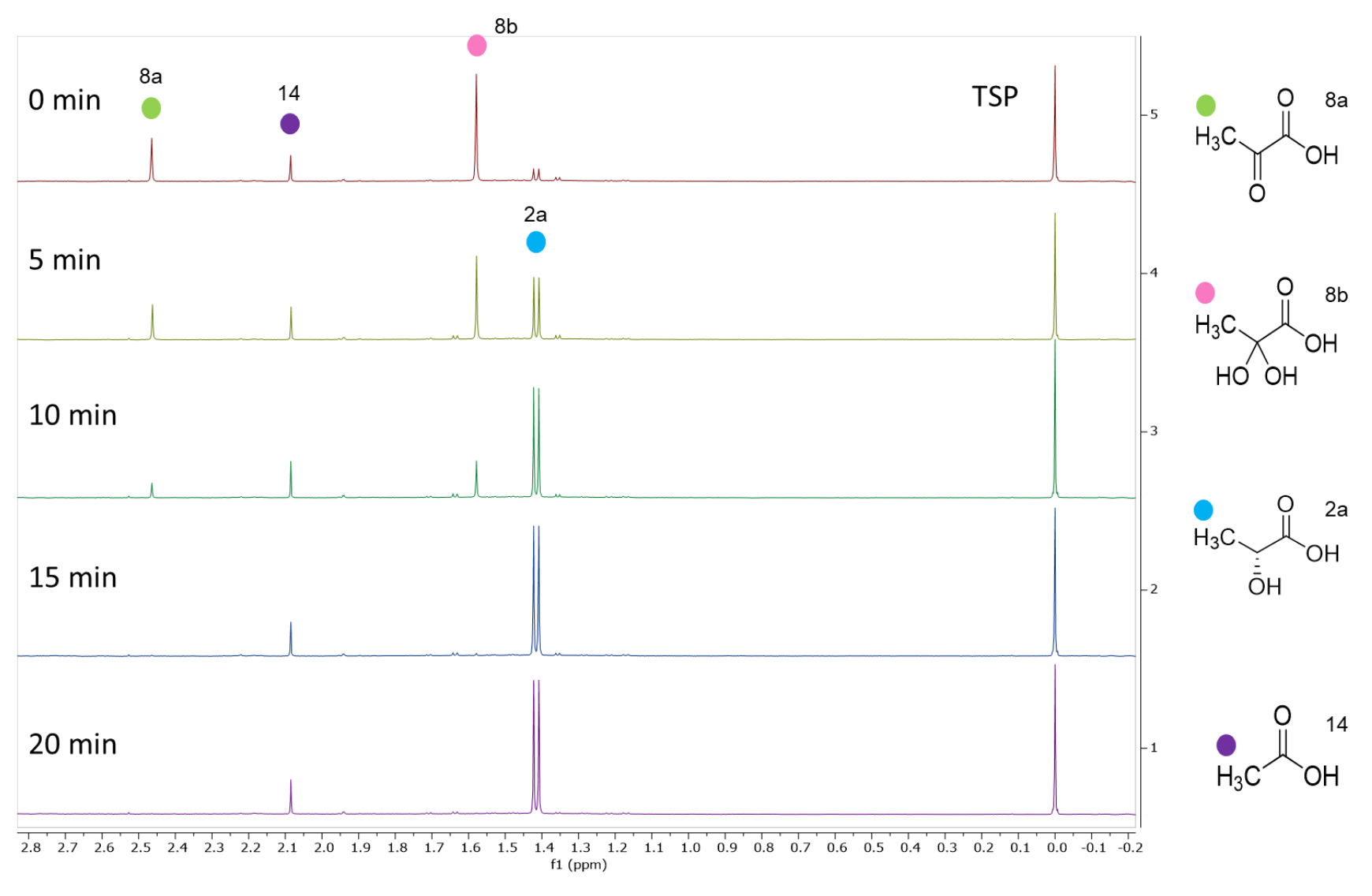


Figure 2.22. NMR spectra of timepoints taken in the enzymatic conversion of hydration-generated pyruvic acid **8** to D-lactic acid **2a** using D-LDH and SH in the presence of 1 mM NAD⁺.

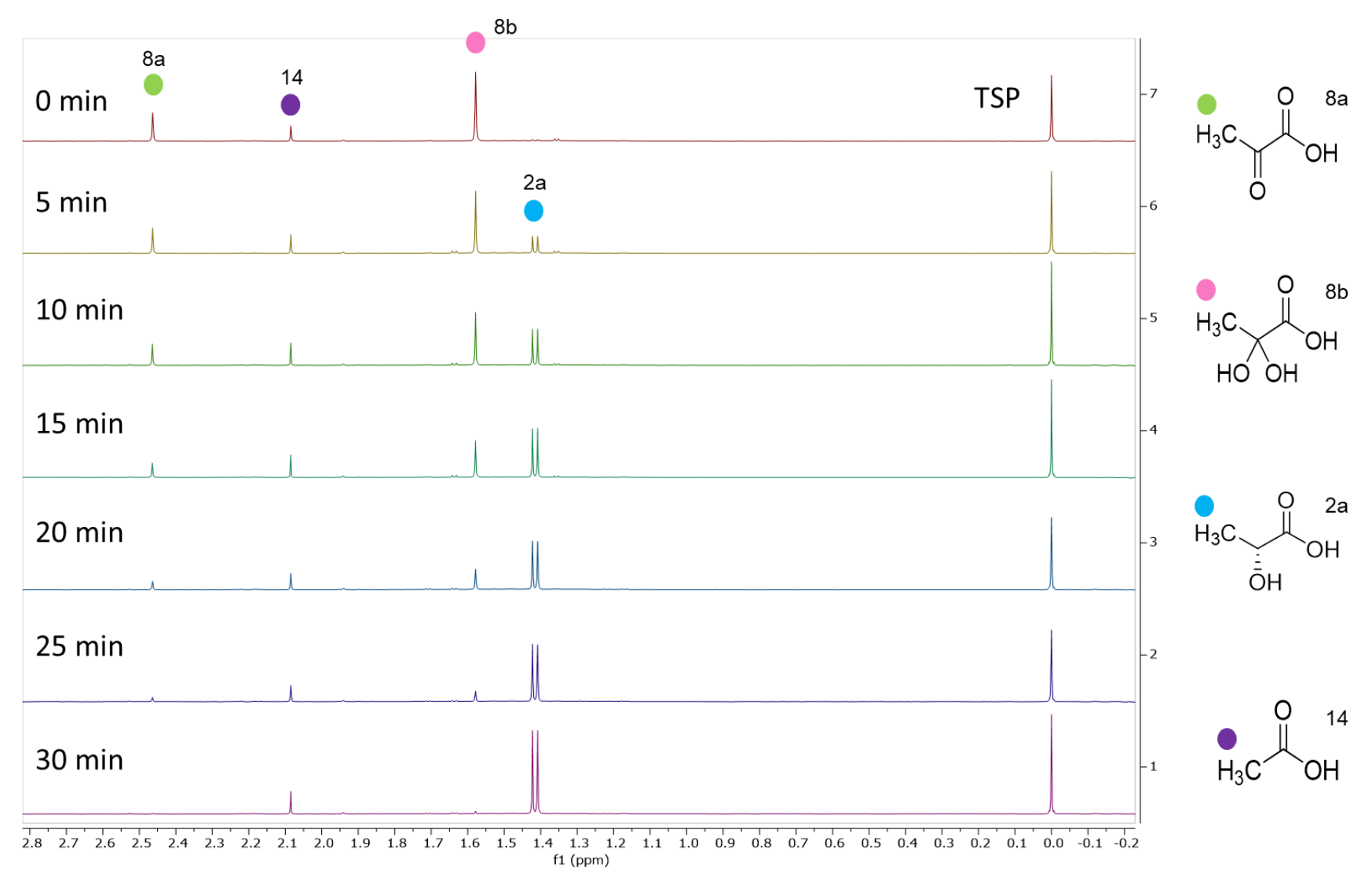


Figure 2.23. NMR spectra of timepoints taken in the enzymatic conversion of hydration-generated pyruvic acid **8** to D-lactic acid **2a** using D-LDH and SH in the presence of 0.1 mM NAD⁺.

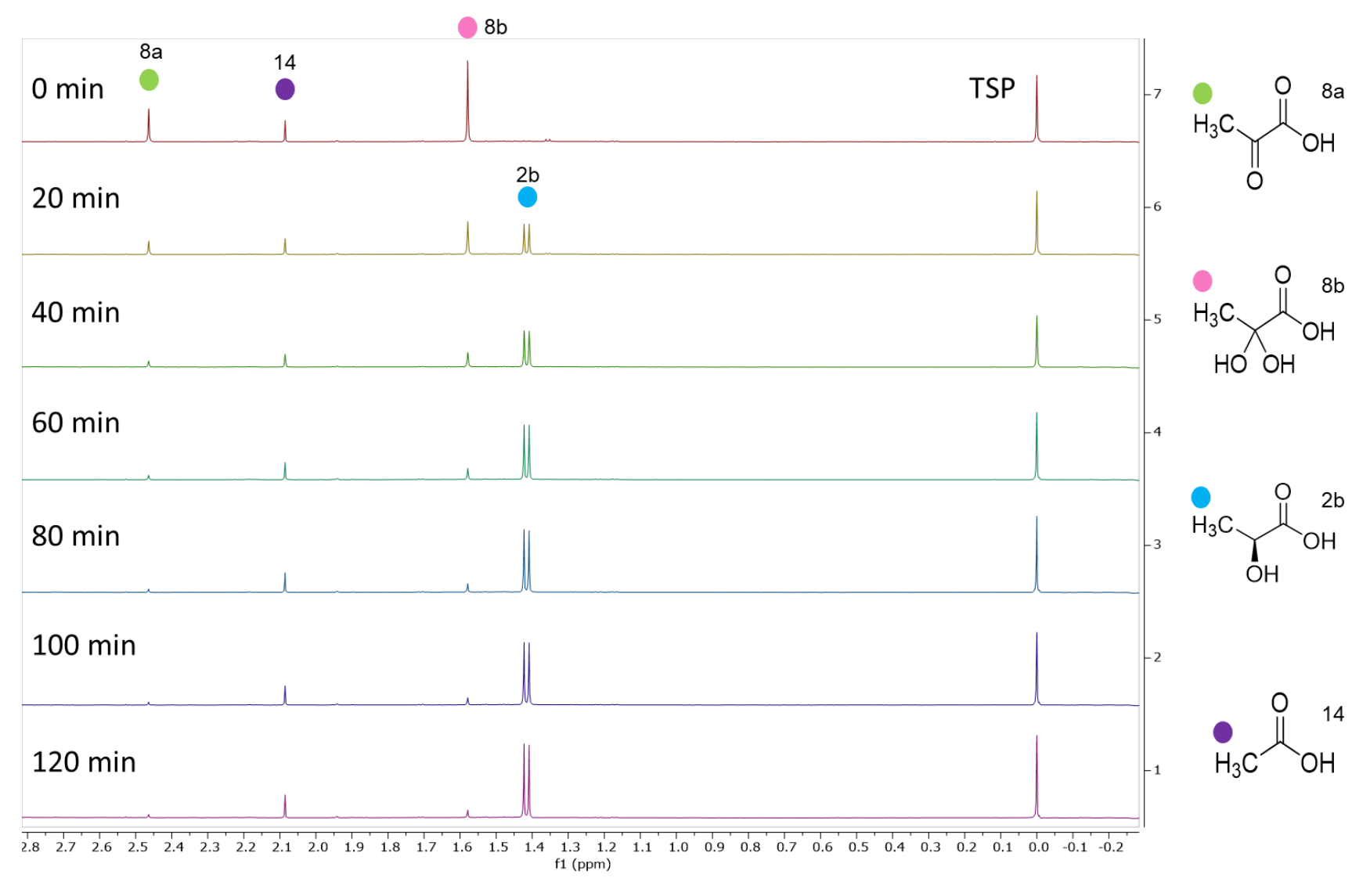


Figure 2.24. NMR spectra of timepoints taken in the enzymatic conversion of hydration-generated pyruvic acid **8** to L-lactic acid **2b** using L-LDH and SH in the presence of 0.01 mM NAD⁺.

2.6 Conclusion

Lactic acid 2 is an important building block for commodity chemicals with applications in food and beverages, personal care, solvents, and polymers. Methane and carbon dioxide have been proposed as alternate starting materials for the synthesis of D- and L-lactic acid 2a-b as current production mostly relies on edible feedstocks. RuCl₃-catalyzed hydration of ACA 6 results in pyruvic acid 8 as the main product. The hydration of ACA 6 in acetic acid 14 resulted in the highest yield of pyruvic acid 8a-b at 106%, but hydration of ACA 6 was further studied in water because of the subsequent reduction to lactic acid 2. Hydration of ACA 6 in water gave a 64% yield of pyruvic acid 8, and hydration of ADCA 7 resulted in an 81% pyruvic acid 8 yield. Crude hydration reaction mixture was used in the enzymatic reduction to lactic acid 2 as studies showed the components of the reaction would not negatively affect enzyme activity. Coupled LDH and SH resulted in NAD+ TON up to 2,560 with quantitative conversion of pyruvate 8 to lactate 2. For future work, this system could be transitioned to a continuous flow system. Lactate dehydrogenase, soluble hydrogenase, and cofactor could be immobilized to allow reuse of the system, making it more economical. Wang and coworkers successfully immobilized LDH, glucose dehydrogenase (GDH), and NADH onto porous glass beads with a polyethylene glycol (PEG) linker to achieve shuttling of cofactor between enzymes on an immobilized system.⁵² Lenz and coworkers immobilized SH onto Amberlite anionic resin with crosslinked phenol-formaldehyde matrix using a methoxy PEG linker.⁵³ Immobilization of SH resulted in increased stability and halflife. For additional future work, both enzymes could also be tested in a pressurized system to assess activity. This would increase hydrogen solubility, reducing the amount needed as it wouldn't require it to be constantly bubbled into the reaction. Additionally, pyruvic acid 8 produced from the hydration of ADCA 7 could be tested for the production of lactic acid 2. Overall, this synthesis provides a method for producing lactic acid 2 from methane and carbon dioxide without the expensive downstream processing of fermentation, while still providing high stereospecificity unlike in chemical synthesis methods.

REFERENCES

- (1) Werpy, T.; Petersen, G. *Top Value Added Chemicals from Biomass: Volume I -- Results of Screening for Potential Candidates from Sugars and Synthesis Gas*; DOE/GO-102004-1992, 15008859; 2004.
- (2) Li, F.; Wei, X.; Sun, Q.; Guo, Y.; Liu, J. Production of L-Lactic Acid in Saccharomyces Cerevisiae Through Metabolic Engineering and Rational Cofactor Engineering. *Sugar Tech* **2022**, *24* (4), 1272–1283.
- (3) Nwamba, M. C.; Sun, F.; Mukasekuru, M. R.; Song, G.; Harindintwali, J. D.; Boyi, S. A.; Sun, H. Trends and Hassles in the Microbial Production of Lactic Acid from Lignocellulosic Biomass. *Environ. Technol. Innov.* **2021**, *21*, 101337.
- (4) Komesu, A.; Oliveira, J. A. R. de; Martins, L. H. da S.; Maciel, M. R. W.; Maciel Filho, R. Lactic Acid Production to Purification: A Review. *BioResources* **2017**, *12* (2), 4364–4383.
- (5) Lactic Acid Market Share | Industry Report, 2021-2028. https://www.grandviewresearch.com/industry-analysis/lactic-acid-and-poly-lactic-acid-market (accessed 2021-07-13).
- (6) Elsawy, M. A.; Kim, K.-H.; Park, J.-W.; Deep, A. Hydrolytic Degradation of Polylactic Acid (PLA) and Its Composites. *Renew. Sustain. Energy Rev.* **2017**, *79*, 1346–1352.
- (7) Taib, N.-A. A. B.; Rahman, M. R.; Huda, D.; Kuok, K. K.; Hamdan, S.; Bin Bakri, M. K.; Bin Julaihi, M. R. M.; Khan, A. A Review on Poly Lactic Acid (PLA) as a Biodegradable Polymer. *Polym. Bull.*
- (8) Bhuyan, Md. S. Effects of Microplastics on Fish and in Human Health. *Front. Environ. Sci.* **2022**, *10*.
- (9) Saini, P.; Arora, M.; Kumar, M. N. V. R. Poly(Lactic Acid) Blends in Biomedical Applications. *Adv. Drug Deliv. Rev.* **2016**, *107*, 47–59.
- (10) Teixeira, S.; Eblagon, K. M.; Miranda, F.; Pereira, M. F. R.; Figueiredo, J. L. Towards Controlled Degradation of Poly(Lactic) Acid in Technical Applications. *C-J. Carbon Res.* **2021**, 7 (2), 42.
- (11) Budin, S.; Jaafar, M. Comparative Study on Mechanical Properties of Virgin and Recycled Polylactic Acid Aging in Natural Weathering and Seawater Environment. *Polym. Bull.* **2021**.
- (12) Choe, S.; Kim, Y.; Won, Y.; Myung, J. Bridging Three Gaps in Biodegradable Plastics: Misconceptions and Truths About Biodegradation. *Front. Chem.* **2021**, *9*.
- (13) Grewal, J.; Sadaf, A.; Yadav, N.; Khare, S. K. Chapter 5 Agroindustrial Waste Based Biorefineries for Sustainable Production of Lactic Acid. In *Waste Biorefinery*; Bhaskar, T., Pandey, A., Rene, E. R., Tsang, D. C. W., Eds.; Elsevier, 2020; pp 125–153.
- (14) Jantasee, S.; Kienberger, M.; Mungma, N.; Siebenhofer, M. Potential and Assessment of Lactic Acid Production and Isolation a Review. *J. Chem. Technol. Biotechnol.* **2017**, *92* (12), 2885–2893.

- (15) Kumar, A.; Thakur, A.; Panesar, P. S. Lactic Acid and Its Separation and Purification Techniques: A Review. *Rev. Environ. Sci. Biotechnol.* **2019**, *18* (4), 823–853.
- (16) Abdel-Rahman, M. A.; Tashiro, Y.; Sonomoto, K. Recent Advances in Lactic Acid Production by Microbial Fermentation Processes. *Biotechnol. Adv.* **2013**, *31* (6), 877–902.
- (17) Fei, Q.; Liang, B.; Tao, L.; Tan, E. C. D.; Gonzalez, R.; Henard, C. A.; Guarnieri, M. T. Biological Valorization of Natural Gas for the Production of Lactic Acid: Techno-Economic Analysis and Life Cycle Assessment. *Biochem. Eng. J.* **2020**, *158*, 107500.
- (18) Tian, X.; Chen, H.; Liu, H.; Chen, J. Recent Advances in Lactic Acid Production by Lactic Acid Bacteria. *Appl. Biochem. Biotechnol.* **2021**, *193* (12), 4151–4171.
- (19) Gao, T.; Wong, Y.; Ng, C.; Ho, K. L-Lactic Acid Production by Bacillus Subtilis MUR1. *Bioresour. Technol.* **2012**, *121*, 105–110.
- (20) Wang, Y.; Meng, H.; Cai, D.; Wang, B.; Qin, P.; Wang, Z.; Tan, T. Improvement of L-Lactic Acid Productivity from Sweet Sorghum Juice by Repeated Batch Fermentation Coupled with Membrane Separation. *Bioresour. Technol.* **2016**, *211*, 291–297.
- (21) Lane, S.; Dong, J.; Jin, Y.-S. Value-Added Biotransformation of Cellulosic Sugars by Engineered Saccharomyces Cerevisiae. *Bioresour. Technol.* **2018**, *260*, 380–394.
- (22) *Population*. United Nations. https://www.un.org/en/global-issues/population (accessed 2021-08-28).
- (23) Kim, J.; Kim, Y.-M.; Lebaka, V. R.; Wee, Y.-J. Lactic Acid for Green Chemical Industry: Recent Advances in and Future Prospects for Production Technology, Recovery, and Applications. *Fermentation.* **2022**, *8* (11), 609.
- (24) Thygesen, A.; Tsapekos, P.; Alvarado-Morales, M.; Angelidaki, I. Valorization of Municipal Organic Waste into Purified Lactic Acid. *Bioresour. Technol.* **2021**, *342*, 125933.
- (25) Bozell, J. J.; Petersen, G. R. Technology Development for the Production of Biobased Products from Biorefinery Carbohydrates—the US Department of Energy's "Top 10" Revisited. *Green Chem.* **2010**, *12* (4), 539–554.
- (26) Halpern, J.; James, B. R.; Kemp, A. L. W. Catalysis of the Hydration of Acetylenic Compounds by Ruthenium(III) Chloride. *JACS.* **1961**, *83* (19), 4097–4098.
- (27) Ogo, S.; Fukuzumi, S.-I. Method for Synthesis of Keto Acid or Amino Acid by Hydration of Acetylene Compound. EP1932824A1, June 18, 2008. https://patents.google.com/patent/EP1932824A1/en (accessed 2019-09-25).
- (28) Baldwin, J. E. Rules for Ring Closure. *J. Chem. Soc. Chem. Commun.* **1976**, No. 18, 734–736.
- (29) Alabugin, I. V.; Gilmore, K.; Manoharan, M. Rules for Anionic and Radical Ring Closure of Alkynes. *JACS.* **2011**, *133* (32), 12608–12623. https://doi.org/10.1021/ja203191f.

- (30) Blum, J.; Huminer, H.; Alper, H. Alkyne Hydration Promoted by RhCl3 and Quaternary Ammonium Salts. *J. Mol. Catal.* **1992**, *75* (2), 153–160.
- (31) Meier, I. K.; Marsella, J. A. Hydration of Acetylenic Compounds without Using Mercury. *J. Mol. Catal.* **1993**, *78* (1), 31–42. https://doi.org/10.1016/0304-5102(93)87031-3.
- (32) Chevallier, F.; Breit, B. Self-Assembled Bidentate Ligands for Ru-Catalyzed Anti-Markovnikov Hydration of Terminal Alkynes. *Angew. Chem. Int. Ed.* **2006**, *45* (10), 1599–1602.
- (33) Tokunaga, M.; Suzuki, T.; Koga, N.; Fukushima, T.; Horiuchi, A.; Wakatsuki, Y. Ruthenium-Catalyzed Hydration of 1-Alkynes to Give Aldehydes: Insight into Anti-Markovnikov Regiochemistry. *JACS.* **2001**, *123* (48), 11917–11924.
- (34) Farhana, A.; Lappin, S. L. Biochemistry, Lactate Dehydrogenase. In *StatPearls*; StatPearls Publishing: Treasure Island (FL), 2022.
- (35) Hoelsch, K.; Suehrer, I.; Heusel, M.; Weuster-Botz, D. Engineering of Formate Dehydrogenase: Synergistic Effect of Mutations Affecting Cofactor Specificity and Chemical Stability. *Appl. Microbiol. Biotechnol.* **2013**, *97* (6), 2473–2481.
- (36) Tishkov, V. I.; Popov, V. O. Protein Engineering of Formate Dehydrogenase. *Biomol. Eng.* **2006**, *23* (2–3), 89–110.
- (37) Johannes, T. W.; Woodyer, R. D.; Zhao, H. Efficient Regeneration of NADPH Using an Engineered Phosphite Dehydrogenase. *Biotechnol. Bioeng.* **2007**, *96* (1), 18–26.
- (38) Lutz, J.; Mozhaev, V. V.; Khmelnitsky, Y. L.; Witholt, B.; Schmid, A. Preparative Application of 2-Hydroxybiphenyl 3-Monooxygenase with Enzymatic Cofactor Regeneration in Organic-Aqueous Reaction Media. *J. Mol. Catal. B-Enzym.* **2002**, *19*, 177–187.
- (39) Vazquez-Figueroa, E.; Chaparro-Riggers, J.; Bommarius, A. S. Development of a Thermostable Glucose Dehydrogenase by a Structure-Guided Consensus Concept. *Chembiochem.* **2007**, *8* (18), 2295–2301.
- (40) Lauterbach, L.; Lenz, O.; Vincent, K. A. H2-Driven Cofactor Regeneration with NAD(P)+-Reducing Hydrogenases. *FEBS J.* **2013**, *280* (13), 3058–3068.
- (41) Lauterbach, L.; Lenz, O. Catalytic Production of Hydrogen Peroxide and Water by Oxygen-Tolerant [NiFe]-Hydrogenase during H2 Cycling in the Presence of O2. *JACS.* **2013**, *135* (47), 17897–17905.
- (42) Burgdorf, T.; Linden, E. van der; Bernhard, M.; Yin, Q. Y.; Back, J. W.; Hartog, A. F.; Muijsers, A. O.; Koster, C. G. de; Albracht, S. P. J.; Friedrich, B. The Soluble NAD+-Reducing [NiFe]-Hydrogenase from Ralstonia Eutropha H16 Consists of Six Subunits and Can Be Specifically Activated by NADPH. *J. Bacteriol.* **2005**, *187* (9), 3122–3132.
- (43) Joseph B. Lambert, Scott Gronert, Herbert F. Shurvell, David A. Lightner. *Organic Structural Spectroscopy*, second.; Pearson: New Jersey, 2011.
- (44) Data Analysis For T1 Measurements Using Mnova. www2.chemistry.msu.edu. (accessed 2023-02-09)

- (45) Manikandan, R.; Jeganmohan, M. Ruthenium-Catalyzed Dimerization of Propiolates: A Simple Route to α-Pyrones. *Org. Lett.* **2014**, *16* (3), 652–655.
- (46) Ötvös, S. B.; Szécsényi, Z.; Fülöp, F. Bismuth(III)-Catalyzed Hydration of Terminal Alkynes: Sustainable Synthesis of Methyl Ketones in Batch and Flow. *ACS Sustain. Chem. Eng.* **2019**, 7 (15), 13286–13293.
- (47) Li, M.; Long, Y.; Deng, Z.; Zhang, H.; Yang, X.; Wang, G. Ruthenium Trichloride as a New Catalyst for Selective Production of Dimethoxymethane from Liquid Methanol with Molecular Oxygen as Sole Oxidant. *Catal. Commun.* **2015**, *68*, 46–48.
- (48) Hassam, M.; Li, W.-S. Copper-Catalyzed Markovnikov Hydration of Alkynes. *Tetrahedron* **2015**, *71* (18), 2719–2723.
- (49) Li, L.; Herzon, S. B. Regioselective Reductive Hydration of Alkynes To Form Branched or Linear Alcohols. *JACS.* **2012**, *134* (42), 17376–17379.
- (50) Roh, S. W.; Choi, K.; Lee, C. Transition Metal Vinylidene- and Allenylidene-Mediated Catalysis in Organic Synthesis. *Chem. Rev.* **2019**, *119* (6), 4293–4356.
- (51) Lenz, O.; Lauterbach, L.; Frielingsdorf, S. Chapter Five O₂-Tolerant [NiFe]-Hydrogenases of Ralstonia Eutropha H16: Physiology, Molecular Biology, Purification, and Biochemical Analysis. In *Methods in Enzymology*; Armstrong, F., Ed.; Enzymes of Energy Technology; Academic Press, 2018; Vol. 613, pp 117–151.
- (52) El-Zahab, B.; Jia, H.; Wang, P. Enabling Multienzyme Biocatalysis Using Nanoporous Materials. *Biotechnol. Bioeng.* **2004**, *87* (2), 178–183.
- (53) Herr, N.; Ratzka, J.; Lauterbach, L.; Lenz, O.; Ansorge-Schumacher, M. B. Stability Enhancement of an O2-Tolerant NAD+-Reducing [NiFe]-Hydrogenase by a Combination of Immobilisation and Chemical Modification. *J. Mol. Catal. B: Enzym.* **2013**, *97*, 169–174.

Chapter Three: The Enzymatic Production of 3-Hydroxypropionic Acid from Acetylenecarboxylic Acid

Portions reprinted with permission from Hewage, A. M.; Kwiatkowski, K.; Silva, K. L. S.; Sreedhar, D.; Lee, E.; Nayebi, H.; Geiger, J. H.; Draths, K.; An Original Biosynthetic Route to 3-Hydroxypropionic Acid. Manuscript in preparation.

3.1 Introduction

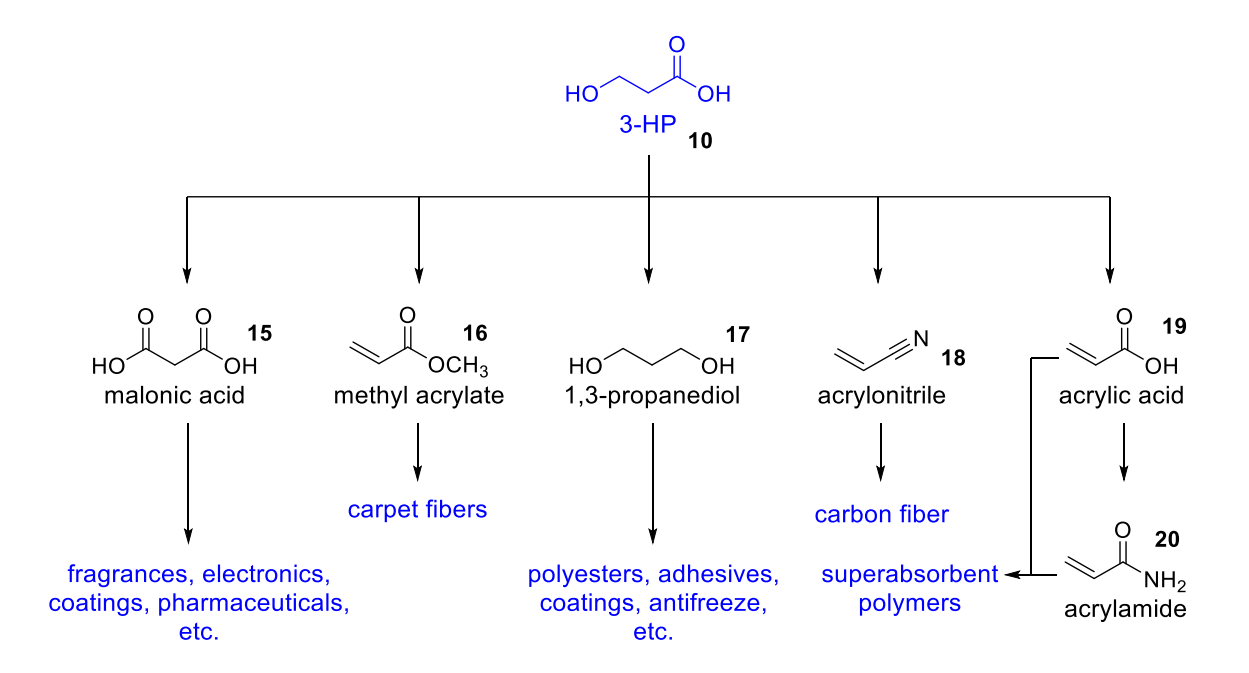


Figure 3.1. 3-HP **10** can be converted into many commodity chemicals with important applications.

3-Hydroxypropionic acid (3-HP) **10** is an achiral, three-carbon carboxylic acid with a β-hydroxyl moiety. It has been identified by the U.S. Department of Energy (DOE) to be a top 12 building block for commodity and specialty chemicals. ¹ 3-HP **10** is critical to biorefinery as it can be converted to important commodity chemicals including malonic acid **15**, methyl acrylate **16**, 1,3-propanediol **17**, acrylonitrile **18**, acrylic acid **19**, acrylamide **20** (Figure 3.1). ¹ These chemicals have applications as adhesives, coatings, carpet fibers, carbon fiber, super absorbent polymers, among others. ² Of these secondary chemicals, acrylic acid **19** has the largest market with **7**.3

million tons produced in 2020.3 When polymerized, acrylic acid 19 forms a hydrogel which is subsequently used to manufacture super absorbent polymers. 4 Cargill, Novozymes, and BASF developed a biobased synthesis of acrylic acid 19 from 3-HP 10, but later changed their synthetic route to use lactic acid 2 instead.⁵ The current industrial synthesis of acrylic acid 19 relies on the gas-phase oxidation of propylene at temperatures up to 300 °C.6 This synthesis is reliant on the petrochemical industry as propylene is a by-product of ethylene production by steam cracking, and petroleum refining.⁷ Acrylonitrile 18, another possible product from 3-HP 10, is used in the production of carbon fiber, which is employed in aircrafts, the automotive industry, and the sporting industry. Carbon fiber as a material has sought after properties including being lightweight, having high thermal and chemical resistance, and other desirable mechanical properties.8 Current production of acrylonitrile 18 relies on the Sohio process where propylene is converted to acrylonitrile 18 using a bismuth molybdate-based catalyst. Karp and coworkers, at the National Renewable Energy Laboratory (NREL), developed a renewable synthesis for acrylonitrile 18 relying on microbially produced 3-HP 10.9 In this study, they used an engineered E. coli strain to produce 3-HP 10 from glucose 1 at a titer of 25.8 g/L. Ethyl 3-HP 21 was isolated from the fermentation broth and converted to acrylonitrile 18 using TiO2 and temperatures up to 310 °C (Figure 3.2). First, ethyl 3-HP 21 is dehydrated to form ethyl acrylate 22 and water. Through aminolysis, ethyl acrylate 22 is converted to acrylamide 20 and ethanol 23. Acrylamide 20 is then dehydrated to form acrylonitrile 18. A techno-economic analysis of this process starting from lignocellulose predicted a selling price of \$0.89/lb for acrylonitrile 18, which falls in the range of selling price for fossil fuel-based acrylonitrile 18 of \$0.40 - \$1.00/lb.9 Using this technology, companies including Cargill and MATRIC will produce the biobased acrylonitrile 18, which will then be polymerized to form carbon fiber by a Portuguese company who will then hand it off to the Ford Motor Company. 10 3-HP 10 itself can also be polymerized to form a biodegradable polymer with a high glass transition temperature and high heat stability. This polymer has potential to be used for surgical biocomposite material, or for controlled drug release.² 3-HP **10** is used as an adhesive, coating, and antistatic agent. It can also be used as a food preservative due to its antibacterial properties. 3-HP **10** has an expected market value of more than USD 10 billion per year.³

Dehydration

Nitrilation

O 21
$$TiO_2$$
 O 22 $+ H_2O$

Nitrilation

O 22 $+ NH_3$ TiO_2 O 20 $+ H_2O$

NH₂ $+ H_2O$

O 20 $+ NH_2$ $+ H_2O$

O 20 $+ NH_2$ $+ H_2O$

Figure 3.2. Renewable acrylonitrile production via dehydration of ethyl 3-HP **21**, aminolysis of ethyl acrylate **22**, and dehydration of acrylamide **20**.⁹

3.1.1 Production of 3-HP from Glucose and Glycerol

A diverse group of microorganisms are able to produce 3-HP **10** naturally, but because these pathways deviate from core metabolism, a limited amount of 3-HP **10** is produced.¹¹ To produce 3-HP **10** on a commercial scale, genetically engineered organisms are necessary to allow for high efficiency. Inexpensive substrates are also necessary, so glucose **1** and glycerol **29** are the two most commonly explored starting materials for the production of 3-HP **10**.¹² Glucose **1** is a renewable sugar that is most often obtained from the hydrolysis of corn starch. Using glucose **1** as a starting material however puts the food industry in competition with the chemical industry, so alternative starting materials are necessary.^{13,14} 3-HP **10** production from glucose **1** can follow several pathways. The malonyl-CoA pathway is the most well-studied of the glucose **1**

pathways (Figure 3.3). First, glucose **1** is converted to acetyl-CoA **24** through glycolysis. Acetyl-CoA **24** is then converted to malonyl-CoA **25** using acetyl-CoA carboxylase (ACC).¹³ ACC is common in many microorganisms as it participates in fatty acid metabolism.¹¹ Heterologous expression of ACC in *E. coli* resulted in a 40% increase in 3-HP **10** production.¹⁵ Malonyl-CoA **25** is then converted to malonic semialdehyde **9**, which is converted to 3-HP **10** using malonyl-CoA reductase (MCR),¹³ a bifunctional enzyme. However, the reduction of malonyl-CoA **25** to malonic semialdehyde **9** by the C-terminal of MCR was rate limiting. To increase 3-HP **10** production, MCR can be dissected into MCR-C and MCR-N which resulted in increased K_{cat}/K_m (4x higher for MCR-C) values for the fragments with their respective substrates.¹⁶

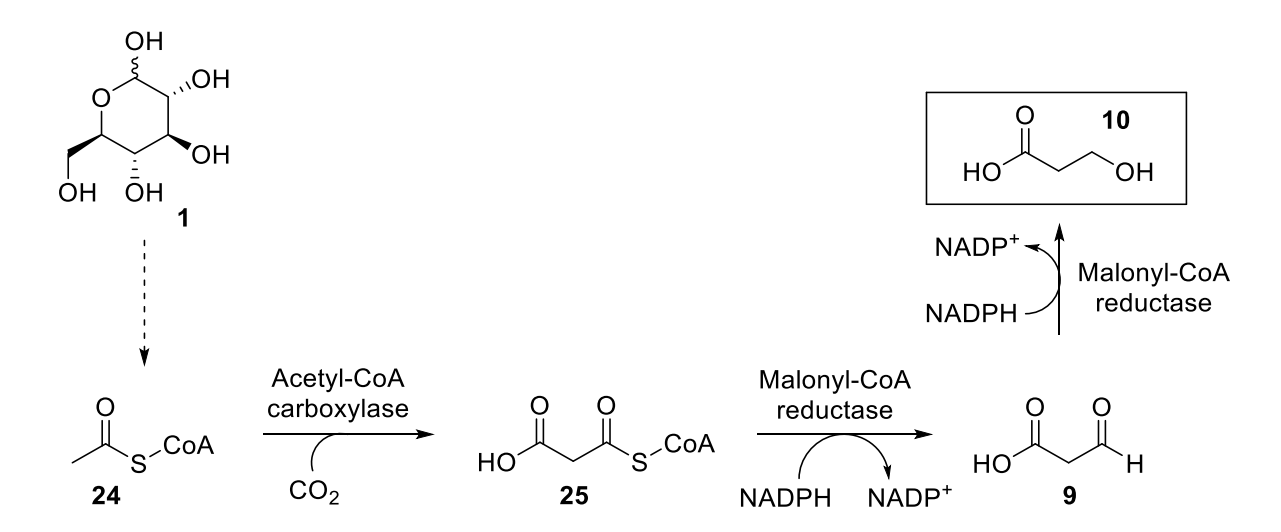


Figure 3.3. Conversion of glucose 1 to 3-HP 10 via the malonyl-CoA pathway. 13

The β -alanine pathway is a second pathway that can afford 3-HP 10 biosynthesis (Figure 3.4). First, glucose 1 is converted through multiple steps to acetyl-CoA 24, which enters the TCA cycle. Fumarate 26 is a resulting intermediate which can be transformed into aspartate 27 by a highly active aspartase. Aspartate 27 can then be transformed into β -alanine 28 using aspartate- α -decarboxylase. β -Alanine-pyruvate aminotransferase then cleaves an amino group and converts β -alanine 28 into malonic semialdehyde 9.13 Pyruvate 8 is simultaneously converted into L-alanine, which can be converted back into β -alanine 28.11 Malonic semialdehyde 9 is then

converted to 3-HP **10** using malonic semialdehyde reductase, 3-hydroxypropionate dehydrogenase, or 3-hydroxyisobutyrate dehydrogenase.¹³ Since this pathway relies on the TCA cycle, intermediate metabolites are byproducts and make downstream separation more challenging.¹¹ Additional glucose **1** pathway options include the propionyl-CoA pathway, the glycerate pathway, and the lactate pathway.¹³

Figure 3.4. Conversion of glucose **1** to 3-HP **10** via the β -alanine pathway.¹³

Glycerol **29** is a waste product of biodiesel production,³ and is produced in the transesterification of animal fats and vegetable oils.¹⁷ Biodiesel has been promoted with the hopes of reducing greenhouse gas emissions and moving towards energy independence. This process however, uses methanol which is a product of the petrochemical industry.¹⁸ Using glycerol **29** as a substrate for 3-HP **10** production is still in its infancy for industry.³ In the conversion of glycerol **29** to 3-HP **10**, it can either follow the CoA-independent pathway or CoA-dependent pathway (Figure 3.5). Regardless of the pathway, both begin with the conversion of glycerol **29** to 3-hydroxypropanal **30** via coenzyme B₁₂-dependent glycerol dehydratase. In the CoA-independent pathway, 3-hydroxypropanal **30** is then converted to 3-HP **10** using NAD⁺-dependent aldehyde dehydrogenase.¹⁹ The CoA-independent pathway is the most used among engineered organisms, but it has little natural relevance due to the low activity of aldehyde dehydrogenase in

wild type bacteria. 19,20 It is a simpler pathway in comparison to the CoA-dependent pathway because it does not produce ATP or require CoA.²¹ In the CoA-dependent pathway, 3hydroxypropanal 30 is converted to 3-hydroxypropanoyl-CoA 31 using NAD+-dependent propionaldehyde dehydrogenase in the presence of CoA. 3-Hydroxypropanoyl-CoA 31 is then converted to 3-HP 10 via a 3-hydroxypropanoyl-phosphate 32 intermediate using phosphotransacylase and ADP-dependent propionate kinase. 11,19 Both of these pathways go through a 3-hydroxypropanal 30 intermediate which is highly toxic and can stop 3-HP 10 production with 15-30 mM. These pathways also rely on coenzyme B₁₂ which is a biologically active form of vitamin B₁₂. ¹² To keep production costs low, strains that naturally produce vitamin B₁₂ are necessary. Because of this, Klebsiella pneumoniae is an important candidate for the production of 3-HP 10 from glycerol 29, but it poses a variety of public health concerns due to the broad variety of infections it can cause including pneumonia, urinary tract infections, and soft tissue infections.¹³ In organisms that produce vitamin B₁₂, the synthesis of coenzyme B₁₂ is still unsatisfactory under aerobic conditions. Coenzyme B₁₂ can also be inactivated during the conversion of 3-HP 10 to 3-hydroxypropanal 30 which requires external addition, leading to cost increase.21

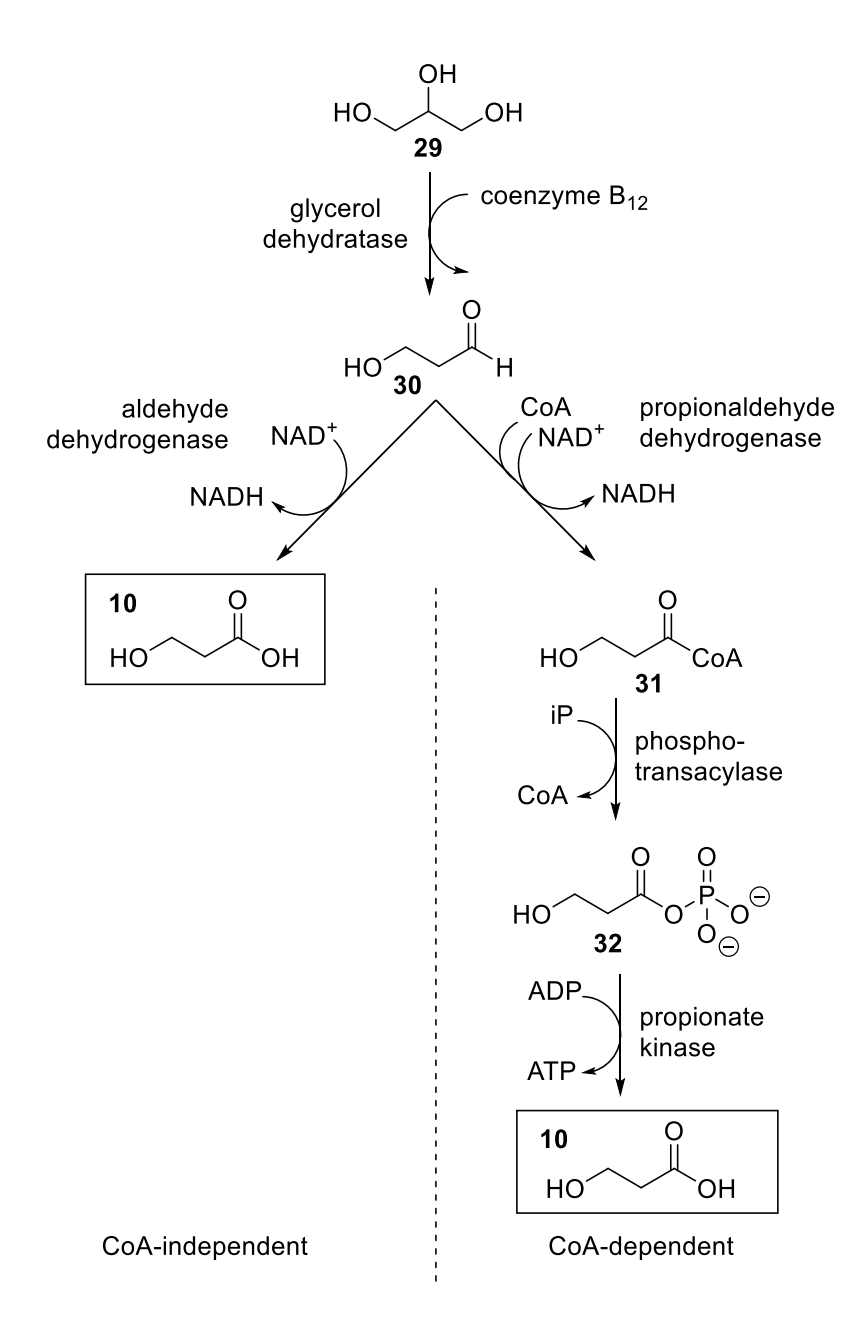


Figure 3.5. Conversion of glycerol **29** to 3-HP **10** via the CoA-independent and CoA-dependent pathways.¹⁹

In addition to the challenges mentioned above, producing 3-HP **10** via fermentation suffers from toxicity issues as well as challenging downstream processing. *E. coli* and *K. pneumoniae* are two common hosts for the biosynthesis of 3-HP **10**, but 3-HP **10** concentrations greater than 300 mM result in growth inhibition¹¹ due to disturbance of cytoplasmic pH.²² This is compared to the industrially desirable concentration of 1 M 3-HP **10**. The pH of the fermentation broth can be

maintained by adding an ammonia solution or NaOH, but a high anion content in later stages of the fermentation results in a lower production of 3-HP **10**¹¹ due to increased osmotic stress to the cells. Park and coworkers generated an *E. coli* strain through adaptive evolution that could tolerate up to 800 mM 3-HP **10**. There were 13 mutations observed with a mutation in *yieP* likely contributing mainly to the increased 3-HP tolerance.²² It was discovered that a deletion in *yieP* allows for the overexpression of YohJK1 which functions as a 3-HP **10** transporter and increases tolerance.²³

In the fermentation production of 3-HP 10, there are three main challenges that plague downstream processing. First, 3-HP 10 is a soluble extracellular compound, making it challenging to isolate from fermentation broth. Lactic acid 2 is a byproduct of 3-HP 10 production, and due to the structural similarity, they are extremely challenging to separate. The addition of base for pH maintenance also causes the need for removal of ions in the purification process. The second challenge is that 3-HP 10 decomposes when exposed to high temperatures, so traditional distillation methods are not practical, and high concentrations of 3-HP 10 results in polymerization. Above the processing is energy intensive, requires a complex process, and therefore increases production cost. A 3-HP 10 recovery method patented by Cargill begins with centrifugation to remove cells. The supernatant is then concentrated and acidified to lower the pH between 1-3. An ion exchanger is then used to remove ions, and 3-HP 10 is extracted. Distillation is accomplished by applying heat and vacuum. By increasing 3-HP 10 concentration and applying heat in distillation, caution must be taken to avoid degradation and polymerization.

3.1.2 Enzymatic Conversion of ACA to 3-HP

Figure 3.6. Enzymatic conversion of ACA **6** to 3-HP **10** using Cg10062(E114N), MmsB, and either SH or PTDH to recycle cofactor.

ACA 6 can act as a bridge to allow for production of commodity chemicals using methane and carbon dioxide (Figure 3.6). 3-HP 10 synthesis from ACA 6 can be accessed via malonic semialdehyde (MSA) 9. To convert ACA 6 to MSA 9, tautomerase Cg10062 was selected due to its hydratase/decarboxylase activity with ACA 6. The tautomerase superfamily contains over 11,000 proteins and are characterized as having an N-terminal proline situated in the active site and a β-α-β fold.²⁶ Cg10062 is a 149-amino acid protein originating from *Corynebacterium glutamicum*, and the biological function is not known. Cg10062 was found to share the same six active site residues (Pro-1, His-28, Arg-70, Arg-73, Tyr103, and Glu-114) as previously discovered tautomerase *cis*-CaaD although they are only 34% identical in sequence.²⁷ Both enzymes exist as homo-trimers. Cg10062 catalyzes the hydration of ACA 6, but also the hydration-dependent decarboxylation, resulting in 19% MSA 9 and 81% acetaldehyde 11. *cis*-CaaD facilitates the hydration of ACA 6 to MSA 9 without decarboxylation, albeit at a slower rate than Cg10062.²⁶ To achieve a high yield of MSA 9, it is unfavorable to produce acetaldehyde 11 due to the immediate loss of carbon from the substrate. Whitman and coworkers have mutated active site residues of Cg10062 in order to find a mutant capable of producing MSA 9 as the only

detected product. They report two active site mutants, Cq10062(E114Q) and Cq10062(E114D), that show only hydratase activity, but at a slower rate compared to wild type.²⁸ Additional studies were done by Amaya Mathes Hewage in attempt to identify a hydratase-only mutant with greater activity. Various mutants were created using rational mutagenesis including E114A, Y103A, H28A, E114D-Y103F, and E114N. Mutants including Y103F, E114D, and E114Q were created to compare to results from Whitman and coworkers. Mutant Cg10062(E114N) resulted in hydratase only activity with a catalytic efficiency (k_{cat}/K_m of 4.08 x 10⁴ M⁻¹ s⁻¹) 4-fold and 20-fold higher than E114Q and E114D, respectively. Cq10062(E114N) still has a lower catalytic efficiency relative to wild-type Cg10062 (k_{cat}/K_m of 12.4 x 10⁴ M⁻¹ s⁻¹).^{29,30} To understand the mechanism, crystals were grown of wild-type Cg10062 and variants (E114N, E114D, H28A, R73A, and Y103F), and they were soaked in ACA 6 to trap intermediates. In the proposed mechanism (Figure 3.7), the first step would be nucleophilic attack on ACA 6 by Pro-1, resulting in a 3-(N-prolyl)-acrylate 33 intermediate as seen in E114D. The 3-(N-prolyl)-acrylate 33 can tautomerize from its enamine to its iminium 34 form as captured in Y103F, which can then decarboxylate leading to acetaldehyde 11 formation, or undergo attack by water to form 3-(N-prolyl)-3-hydroxypropionate 35 as seen in R73A or H28A. Tyr-103 forms a hydrogen bond with Glu-114, likely helping to position it for deprotonation of the water molecule that will attack the substrate. By shortening the 114 sidechain, the attacking water molecule is able to form four hydrogen bonds where Pro-1 is protonated and acting as a hydrogen bond donor. Therefore, E114D and E114N likely bypass iminium formation which results in no decarboxylation. The 3-(N-prolyl)-3-hydroxypropionate 35 intermediate leads to formation of MSA 9 when the covalent bond breaks to Pro-1, and the hydroxyl group is converted to an aldehyde.^{26,29}

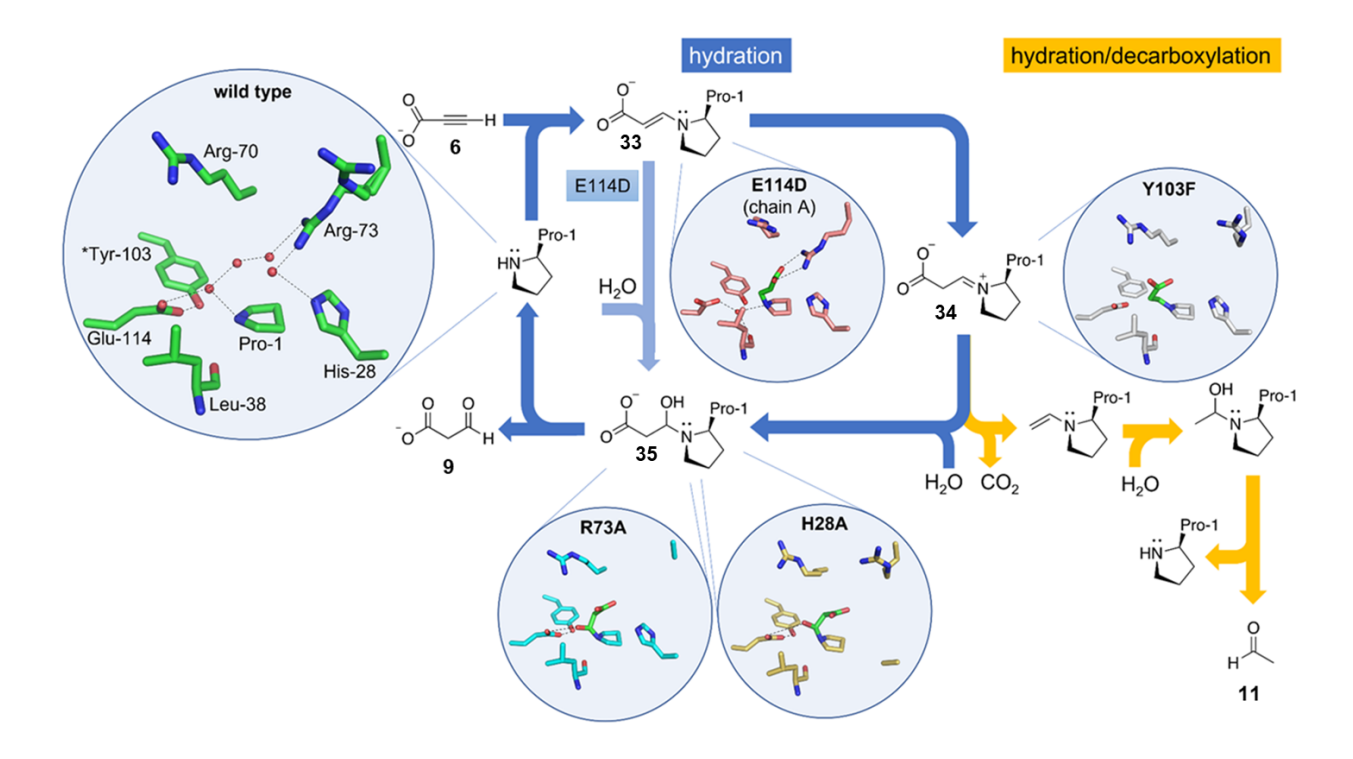


Figure 3.7. Mechanism for the hydration of ACA **6** leading to MSA **9** or decarboxylation leading to acetaldehyde **11**.

To convert MSA **9** to 3-HP **10**, NADH-dependent 3-hydroxyisobutyrate dehydrogenase (MmsB) [1.1.1.31] can be employed. MmsB is classified as an NAD+ oxidoreductase and catalyzes the reversible conversion of L-3-hydroxyisobutyrate to methylmalonate semialdehyde. It is found in a variety of organisms and is essential for valine metabolism. MmsB exists as a homo-tetramer.^{31,32} It has substrate promiscuity as it is capable of catalyzing the oxidation of L-3-hydroxyisobutyrate, L-serine, and other 3-hydroxyacids.³¹ Since MmsB utilizes NADH as cofactor, soluble hydrogenase (SH) [1.12.1.2] and phosphite dehydrogenase (PTDH) [1.20.1.1] will be utilized in two separate systems to recycle cofactor, allowing for the use of sub-stoichiometric amounts of cofactor.

Table 3.1. Substrate specificity of MmsB.31

Substrate	V _{max} K _m		V _{max} /K _m
	(U/mg)	(mg)	V max/ INm
L-3-hydroxyisobutyrate	345	0.12	2,875
L-serine	190	18	10.6
2-methyl-DL-serine	213	44	4.8
3-hydroxypropionate	188	83	2.3

As described further in chapter 2, SH is purified from *Ralstonia eutropha* strain Hf210/pGE771 and was engineered by the Lenz group.³³ SH utilizes hydrogen as an inexpensive sacrificial substrate and produces only protons as a product, making it a favorable recycling enzyme. PTDH was discovered in *Pseudomonas stutzeri* and catalyzes the NAD(P)*-dependent oxidation of phosphite to phosphate. The active enzyme exists as a homo-dimer and contains a "Rossman"-type fold with a GxxGxGxxG motif.³⁴ Three important catalytic residues in PTDH are His-292 which acts as a base to activate the nucleophilic attack of water on phosphite, Glu-266 which helps to orient and regulate the pKa of the histidine, and Arg-237 which is involved in positioning phosphite prior to nucleophilic attack.³⁵ Wild-type PTDH has cofactor specificity for NAD* over NADP* and has low thermostability. Through directed evolution, Zhao and coworkers relaxed the cofactor specificity of PTDH and improved thermostability, resulting in a PTDH variant with more than 7,000-fold longer half-life at 45 °C compared to wild-type. The resulting mutant that will be used for studies in this chapter is defined as PTDH 12X-A176R.^{34,36,37}

Figure 3.8. Enzymatic conversion of ACA 6 to 3-HP 10 using Cg10062(E114N), YdfG, and PTDH.

A prior synthesis of 3-HP **10** starting from ACA **6** was developed by Amaya Mathes Hewage. ACA **6** was converted to MSA **9** using Cg10062(E114N) followed by subsequent reduction to 3-HP **10** using NADPH-dependent 3-hydroxy acid dehydrogenase (YdfG) from *E. coli.* PTDH was coupled to recycle cofactor (Figure 3.8). Starting with 100 mM ACA **6**, this synthesis was demonstrated with as low as 0.001 eq NADP+ relative to ACA **6**.^{29,30} This chapter discusses the 1,4-hydration of ACA **6** via Cg10062(E114N) to form MSA **9**. Subsequent reduction to 3-hydroxypropionic acid **10** is achieved using 3-hydroxyisobutyrate dehydrogenase (MmsB). Two cofactor recycling systems are compared having either soluble NAD+-reducing hydrogenase or phosphite dehydrogenase as a coupled enzyme (Figure 3.6). These new synthetic routes were designed in comparison with the prior route using YdfG. MmsB and YdfG have similar catalytic efficiencies (k_{cat}/K_m) of 4.55 x 10⁴ M⁻¹ s⁻¹ and 4.41 x 10⁴ M⁻¹ s⁻¹, respectively, but MmsB has a 14-fold higher turnover number (k_{cat}) relative to YdfG.^{29,30} Using MmsB to reduce MSA **9** to 3-HP **10** also allows for the use of NADH, a less expensive cofactor relative to NADPH.

3.2 Creation of a Plasmid for MmsB Production

The MmsB gene was amplified from *P. putida* KT2440 genomic DNA (Figure 3.9) using KK035 MmsB fwd and KK036 MmsB rev primers with Ndel and Xhol restrictions sites at the 5' and 3' ends, respectively. It was cloned into the pET-21a(+) vector at the Ndel and Xhol sites. This vector encodes for ampicillin resistance, a T7 promoter, and an N-terminal His₆-tag. Plasmid construction was verified using Sanger sequencing. The resulting plasmid was named pKK1.1025 (Figure 3.10).

TAATACGACTCACTATAGGGGAATTGTGAGCGGATAACAATTCCCCCTCTAGAAATAATTTTG TTTAACTTTAAGA<mark>AGGAG</mark>ATATACAT<mark>ATG</mark>CGTATCGCATTCATCGGCCTGGGCAACATGGG CGCGCCCATGGCCCGCAACCTGATCAAGGCCGGGCATCAGCTGAACCTGTTCGACCTGAA CAAGGCCGTGCTGGCCGAGCTGGCAGAACTGGGCGGCAGATCAGCCCCTCGCCCAAG TAGCGTGTACTTGAACGAGGACGGCGTACTGGCCGGTATTCGTCCTGGCACGCCGACCGT TGACTGCAGCACCATCGACCCGCAGACCGCACGTGACGTGTCCAAGGCCGCAGCGGCAA AGGCCTGGACATGGGGGATGCGCCGGTTTCCGGTGGTACTGGCGCGGCGGCGGCCGG CACCCTGACGTTCATGGTCGGCGCCAGTACCGAGTTGTTCGCCAGCCTCAAGCCGGTACT GGAGCAGATGGGCCGCAACATCGTGCACTGCGGGGAAGTCGGTACCGGCCAGATCGCCA AGATCTGCAACAACCTGCTGGCATTTCGATGATCGGCGTGTCCGAGGCCATGGCCC TGGGTAACGCGCTGGGTATCGATACCAAGGTGCTGGCCGGCATCATCAACAGTTCGACCG GGCGTTGCTGGAGCTCGGACACCTACAACCCGTGGCCGGGCATCATCGAAACCGCACCT GCATCGCGTGGCTACACCGGTGGCTTTGGCGCCGAACTCATGCTCAAGGACCTGGGGTT GGCCACCGAAGCGCACGCCAGGCACACCAACCGTGATTCTCGGTGCCGTGGCCCAGC AGCTGTACCAGGCCATGAGCCTGCGAGGCGAGGGTGGCAAGGACTTCTCGGCCATCGTC

Figure 3.9. Nucleotide sequence of MmsB. Various elements have been highlighted: P_{T7} (green); lac operator (magenta); RBS (red); Met-1 of native protein (blue); His₆-tag (yellow).

Table 3.2. Primers used for the construction and sequencing of MmsB plasmid pKK1.1025.

Primer	Sequence
KK035 MmsB fwd	GGAGTACCATATGCGTATCGCATTCATCG
KK036 MmsB rev	CACCTCTTCTCGAGATCCTTCTTGCGATAACCCTC
KK037 Seq fwd	ACCATCGACCCGCAGAC
KK038 Seq rev	TGTTGATGATGCCGGCCAG

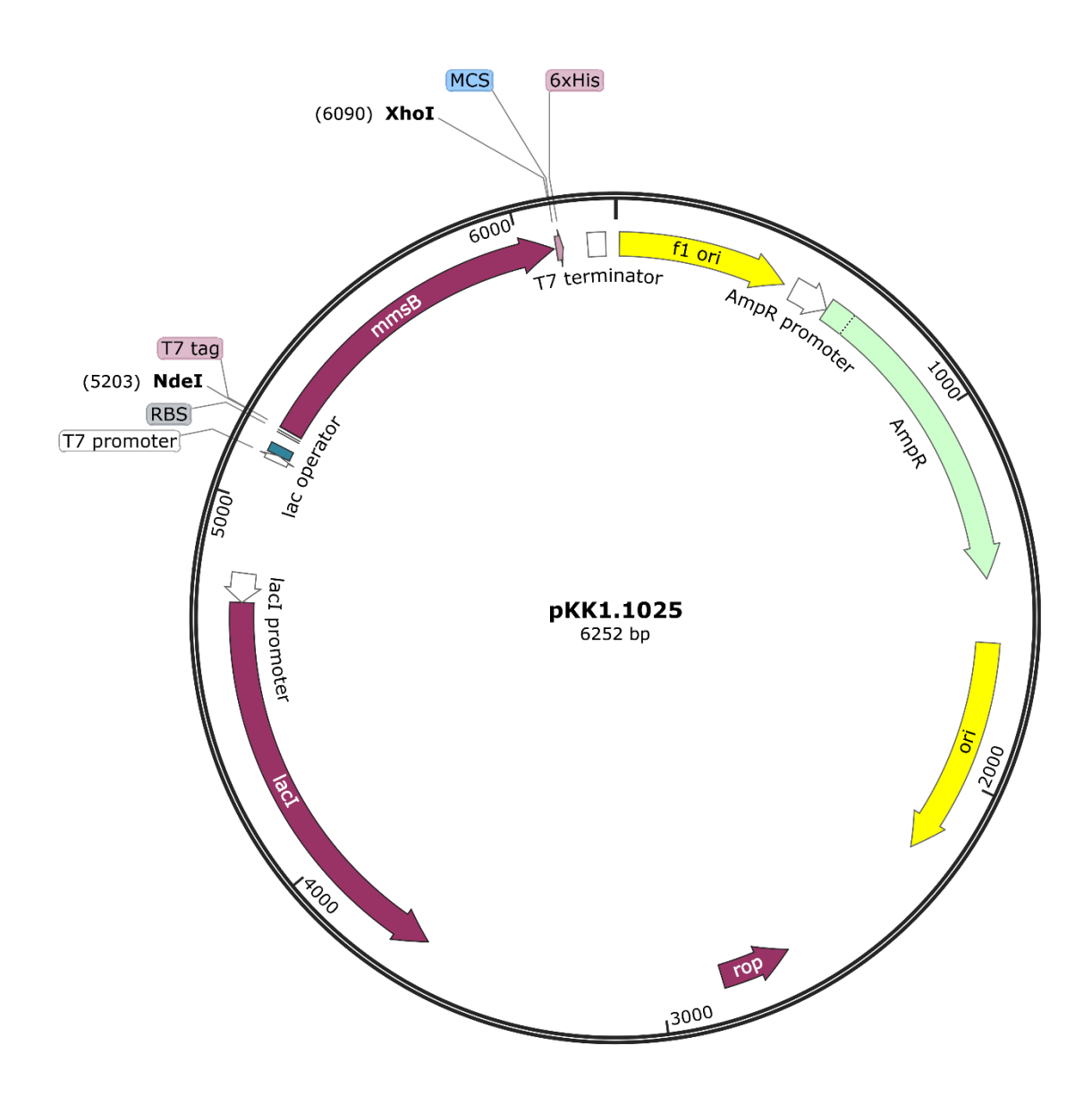


Figure 3.10. Plasmid used for the expression of MmsB.

Table 3.3. Strains and plasmids used throughout this chapter.

Strain/Plasmid	Genotype/Description	Reference/ Source
E. coli DH5α	F^- φ80/acZΔM15 Δ(/acZYA-argF)U169 recA1 endA1 hsdR17(r_K^- , m_K^+) phoA supE44 λ^- thi-1 gyrA96 relA1	Invitrogen
E. coli BL21	fhuA2 [lon] ompT gal [dcm] ΔhsdS	Invitrogen
E. coli BL21(DE3)	F^- omp T hsd S_B (r_B^- , m_B^-) gal dcm (DE3)	Invitrogen
pET-21a(+)	Ap ^R , <i>lacl, P</i> ₇₇ pMB1 replicon	Invitrogen
pAS2.100	P _{T7} cg10062(E114N) in pET-21a(+)	this study
pET15b-12x	<i>P</i> _{T7} <i>ptdh</i> in pET-15b	Addgene ³⁷
pKK1.1025	P _{T7} mmsB in pET-21a(+)	this study

3.3 Purification and Characterization of Enzymes

Cg10062(E114N), MmsB, and PTDH were purified using the same protocol. *E. coli* BL21(DE3) containing the appropriate plasmid was cultured in LB/Ap media, and protein was overexpressed through induction with IPTG. Cell pellets were stored at -20 °C. For purifications, thawed cell pellets were resuspended and passed through a chilled French press cell. Cellular debris was separated from cell lysate by centrifugation and filtered through a syringe filter. The proteins were purified on an ÄKTA Start FPLC equipped with a HisTrap FF 5 mL nickel affinity column. His6-tagged protein was eluted from the column using an imidazole gradient. Purified protein was stored at -20 °C in 100 mM potassium phosphate, pH 8.0, containing 20% ethylene glycol. Protein concentration was determined by Bradford analysis or dilution with Guanidine HCl, and purity was assessed using SDS-PAGE (Figure 3.11). The purification for soluble hydrogenase is described in chapter 2, section 2.5.1.

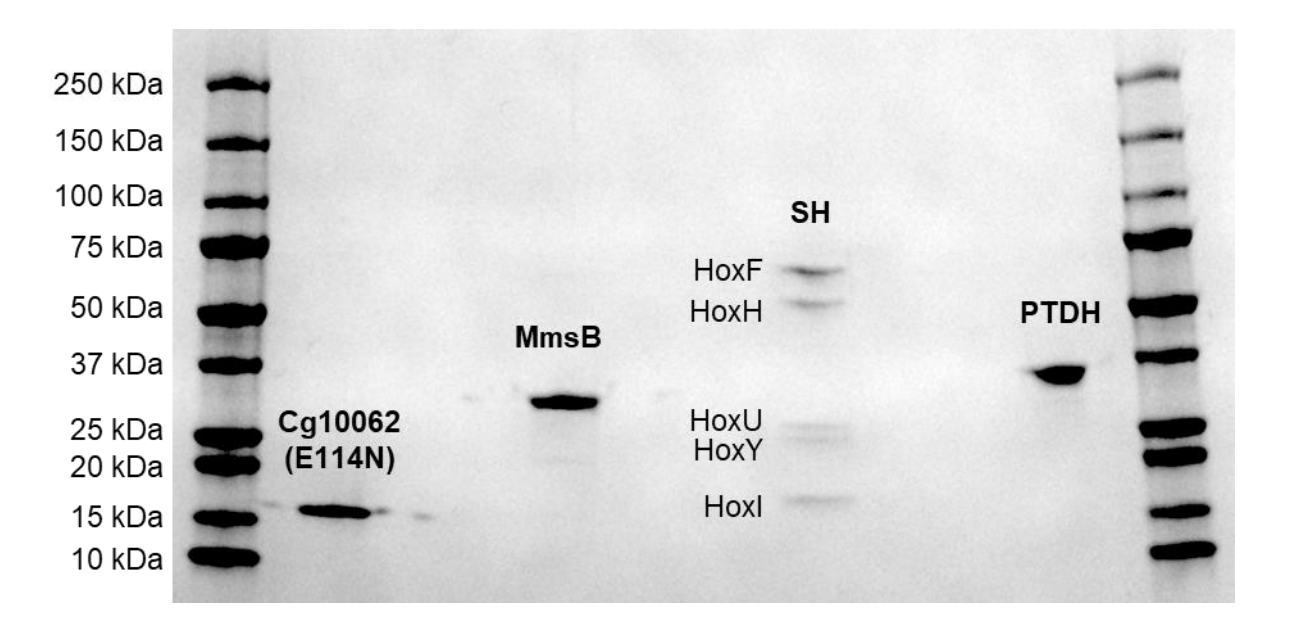


Figure 3.11. SDS-PAGE of purified Cg10062(E114N) (19 kDa), MmsB (31 kDa), SH (HoxF: 68 kDa, HoxH: 55 kDa, HoxU: 26 kDa, HoxY: 23 kDa, HoxI: 19 kDa), and PTDH (37 kDa).

Figure 3.12. The activity of Cg10062(E114N) is measured by coupling MSAD and ADH which allows the oxidation of NADH to be monitored at 340 nm.

Cg10062(E114N) activity was measured using a coupled enzyme assay (Figure 3.12) where ACA 6 was hydrated using Cg10062(E114N) to form malonic semialdehyde 9. This was then decarboxylated using malonic semialdehyde decarboxylase (MSAD) to form acetaldehyde 11. The reduction of acetaldehyde 11 by NADH-dependent alcohol dehydrogenase (ADH) was monitored by following the oxidation of NADH at 340 nm (ϵ = 6220 M⁻¹ cm⁻¹). All coupling enzymes were added in excess to allow measurement of Cg10062(E114N) activity. Assays (final volume 1 mL) contained Cg10062(E114N), MSAD, ADH, NADH, and ACA 6 in 100 mM potassium phosphate pH 8. The reaction was initiated by addition of ACA 6 and A₃₄₀ was recorded.

Figure 3.13. The hydration of ACA **6** by Cg10062(E114N) was coupled to the reduction of MSA **9** to 3-HP **10** by MmsB. Enzyme activity was followed by the loss of absorbance at 340 nm due to NADH oxidation.

The specific activity of MmsB was measured (Figure 3.13) by generating MSA **9** *in situ* from the Cg10062(E114N)-catalyzed hydration of ACA **6**. The reduction of MSA **9** by NADH-dependent MmsB was monitored by following the oxidation of NADH at 340 nm (ϵ = 6220 M⁻¹ cm⁻¹). Assays (final volume 1 mL) contained Cg10062(E114N), MmsB, NADH and ACA **6** in 100 mM potassium phosphate pH 8. ACA **6** and Cg10062(E114N) were mixed in buffer and left to sit 15 min before MmsB and NADH were added.

Figure 3.14. PTDH activity was monitored following the reduction of NADP+ at 340 nm.

The specific activity of PTDH was measured (Figure 3.14) by monitoring the reduction of NADP⁺ at 340 nm (ϵ = 6220 M⁻¹ cm⁻¹). Assays (final volume 1 mL) contained PTDH, NADP⁺ and sodium phosphite in 100 mM potassium phosphate pH 8. The assays were initiated with the addition of sodium phosphite and A₃₄₀ was recorded.

$$H_2 \xrightarrow{\text{SH}} H$$

NAD⁺

NADH

Figure 3.15. SH activity was monitored following the reduction of NAD⁺ at 365 nm.

Soluble hydrogenase activity was measured (Figure 3.15) by monitoring the increase in absorbance at 365 nm, corresponding to production of NADH (ϵ = 3480 M⁻¹ cm⁻¹). Measurements were made at 30 °C. ^{33,38} Assays (final volume 2 mL) contained NAD+ and soluble hydrogenase (SH) in 50 mM Tris-HCl (pH 8 at 30°C). The reaction was sealed, saturated with hydrogen, and initiated by addition of SH via syringe and A₃₆₅ was recorded.

Table 3.4. Representative specific activity of Cg10062(E114N), MmsB, PTDH, and SH.

Enzyme	Specific Activity (U mg ⁻¹)
Cg10062(E114N)	4.4
MmsB	172
PTDH	1.1
SH	26

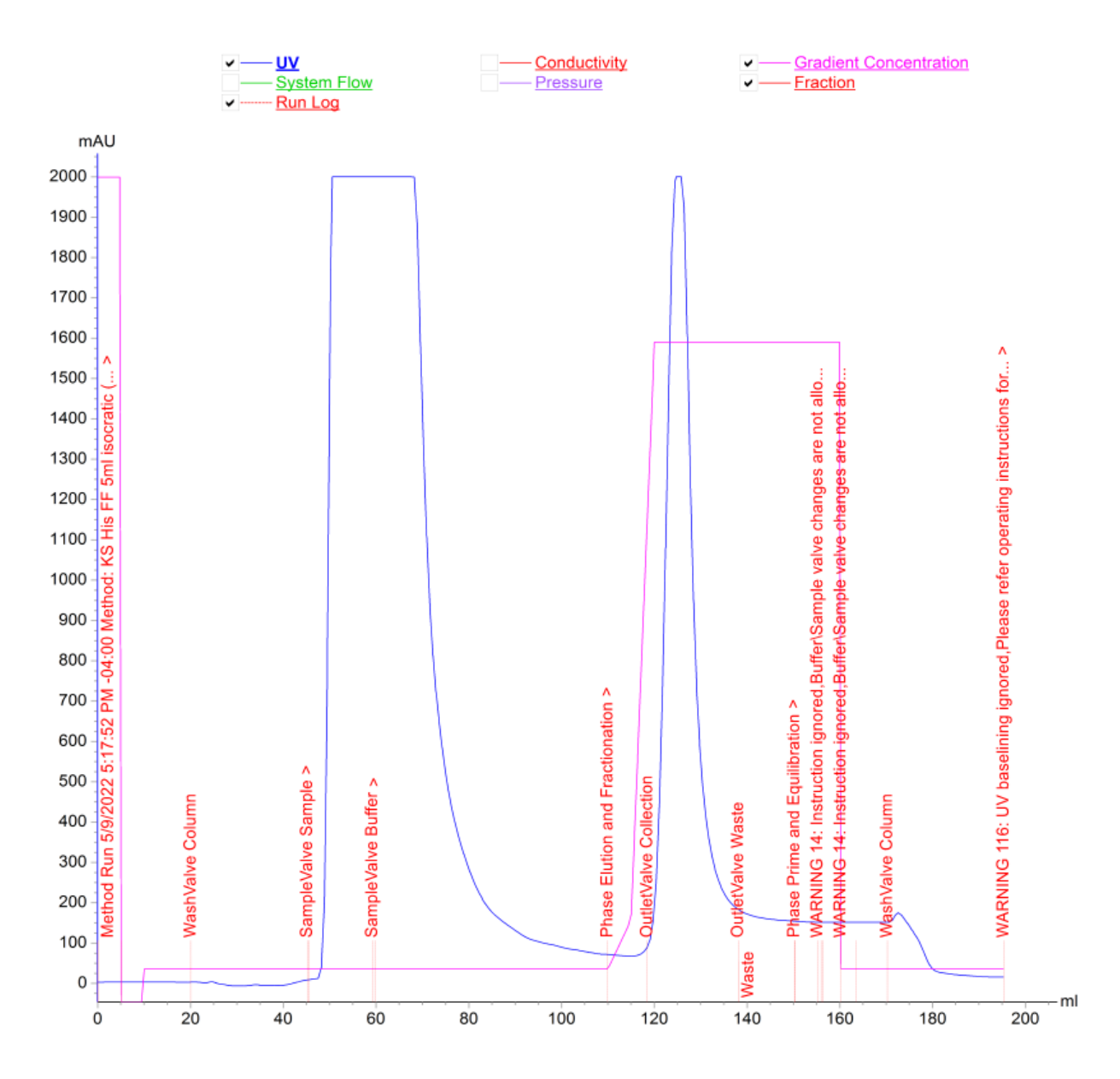


Figure 3.16. FPLC trace for the purification of Cg10062(E114N).

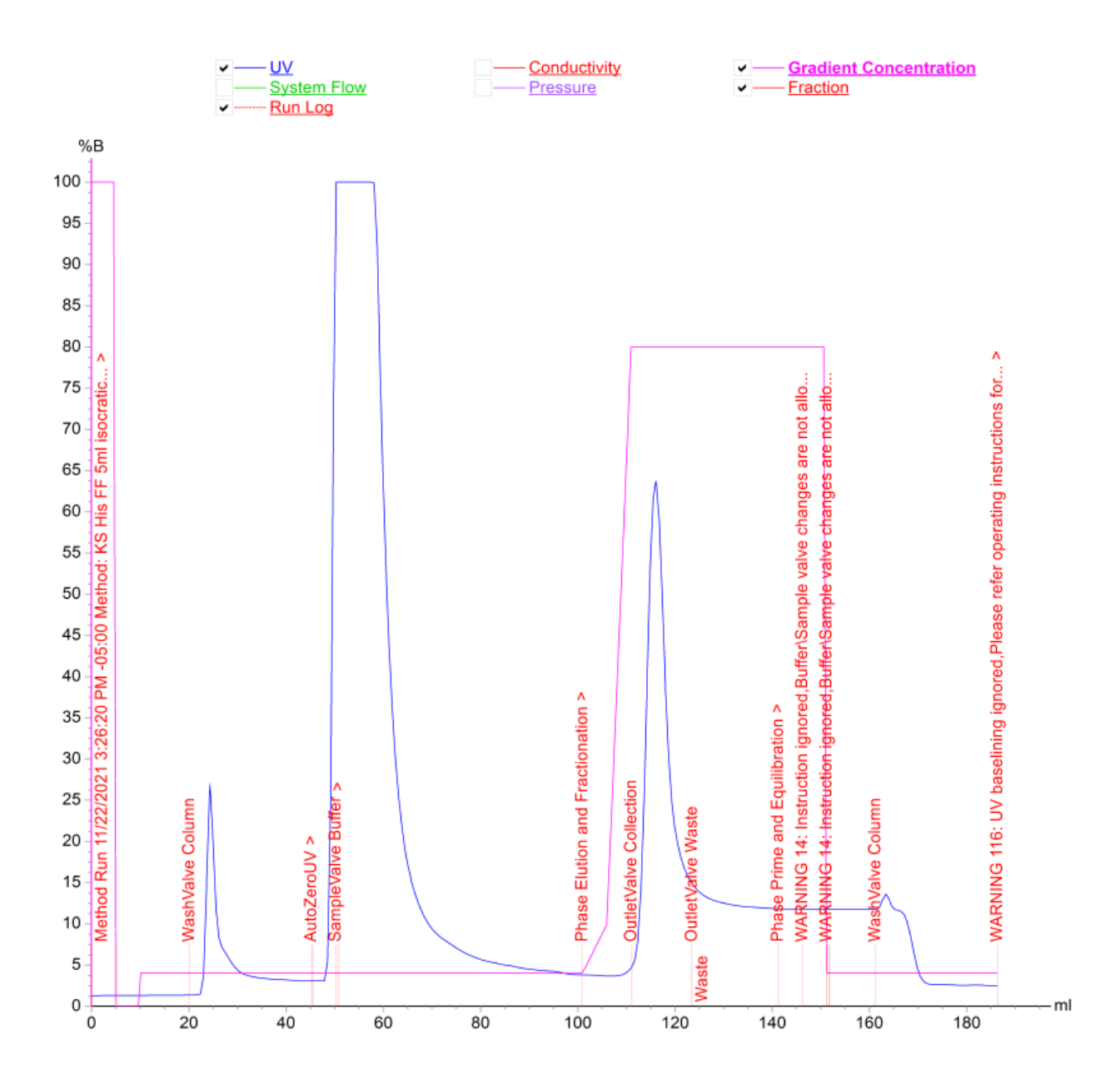


Figure 3.17. FPLC trace for the purification of MmsB.

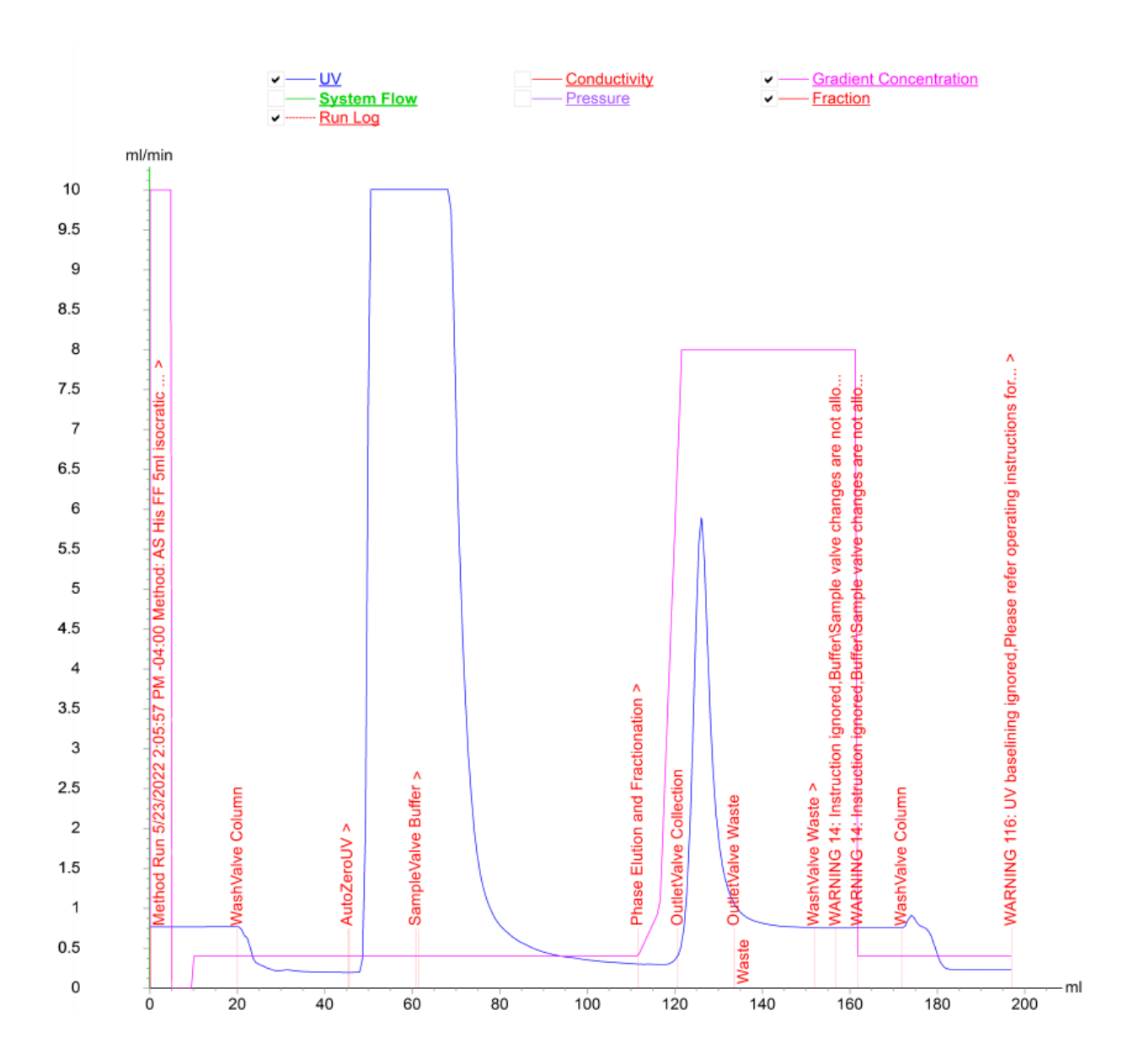


Figure 3.18. FPLC trace for the purification of PTDH.

3.3.1 MmsB Kinetics

The kinetic parameters of MmsB were determined using the coupled enzyme assay shown in Figure 3.13. All assays were carried out in triplicate at 25 °C in 100 mM potassium phosphate pH 8 with a final volume of 1 mL. All stock solutions for the assays were prepared in 100 mM potassium phosphate pH 8. The kinetic parameters (Figure 3.19) of MmsB were measured by generating MSA **9** *in situ* from the Cg10062(E114N)-catalyzed hydration of ACA **6**. The assays contained Cg10062(E114N), MmsB and NADH. ACA **6** (50 – 10,000 μ M) and Cg10062(E114N) were mixed in buffer and left to sit 15 min before MmsB and NADH were added. OriginPro was used to fit the data to a Michaelis Menten model. A K_m of 2220 \pm 192 μ M and a k_{cat} of 101 \pm 5 s⁻¹ were observed (Figure 3.19).

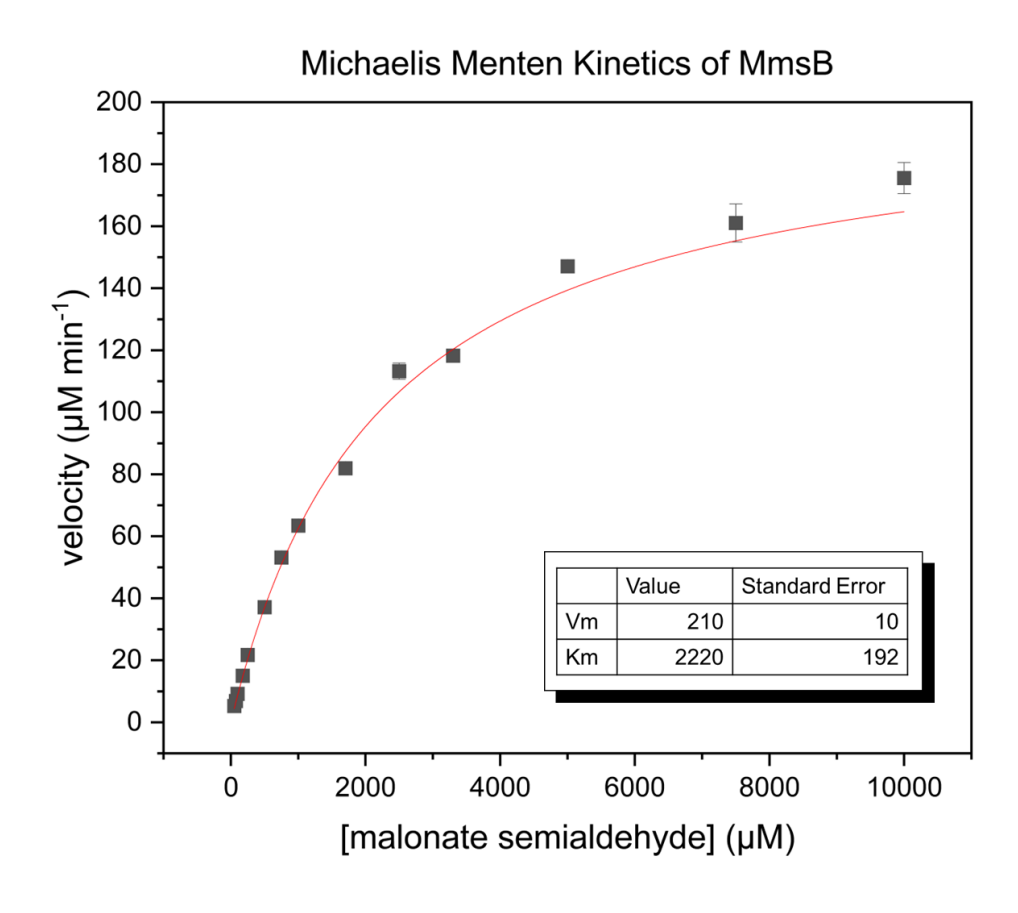


Figure 3.19. Michaelis Menten kinetic parameters of MmsB. Cg10062(E114N) and ACA **6** were used to generate MSA **9** in situ to monitor MmsB activity.

3.4 Enzymatic Synthesis of 3-HP

Figure 3.20. Enzymatic conversion of ACA 6 to 3-HP 10 using Cg10062(E114N), MmsB, and SH.

An *in vitro* synthesis was developed to produce 3-HP **10** from ACA **6**. This system utilizes Cg10062(E114N) for ACA **6** hydration to MSA **9** and relies on NADH-dependent MmsB from *P. putida* to reduce MSA **9** to 3-HP **10**. To further improve the economic viability, O₂-tolerant and soluble NAD+-reducing hydrogenase SH is coupled for cofactor regeneration (Figure 3.20). SH utilizes hydrogen as a cheap and environmentally friendly sacrificial substrate.

3.4.1 Buffer dependence of Cg10062(E114N), MmsB, and SH

pH dependence studies were carried out for Cg10062(E114N), MmsB, and SH in order to determine the optimum buffer and pH conditions for this system. The pH dependence of Cg10062(E114N) (Figure 3.21) and MmsB (Figure 3.22) was measured using four buffer systems: 100 mM potassium phosphate, 50 mM Tris-HCl, 50 mM bis-tris propane and 50 mM HEPES buffers for pH 6.5–8.0, 7.0–9.0, 7.0–9.0 and 7.0–8.0, respectively. The pH dependance of SH (Figure 3.23) was measured in a subset of these buffers including 100 mM potassium phosphate, 50 mM bis-tris propane and 50 mM HEPES buffers for pH 7.0-8.0. Each respective assay was carried out as described above. Cg10062(E114N) had the highest activity at pH 8.0 for all buffers with slightly higher activity in potassium phosphate and HEPES. The highest MmsB activity was also observed at pH 8.0 in all buffers except the phosphate buffer which had the highest activity at pH 7.0. The highest activity for SH was recorded at pH 8.0 in bis-tris propane. Although the phosphate buffer was not optimal for all three enzymes collectively, 3-HP 10 synthesis was carried

out in 100 mM potassium phosphate pH 8.0 as it is more economical than bis-tris propane. Potassium phosphate was used instead of sodium phosphate, due to the fact that sodium ions inhibit SH activity.³⁹

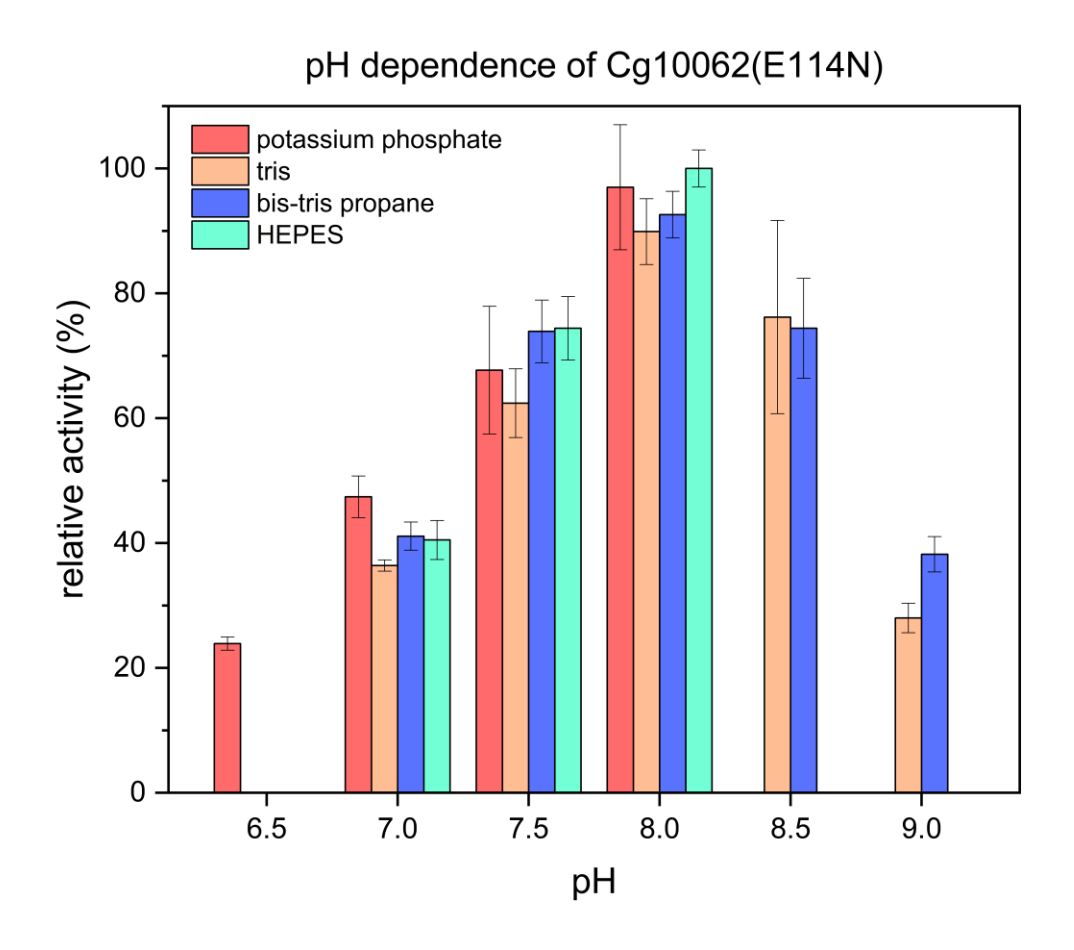


Figure 3.21. pH dependence of Cg10062(E114N) in four buffer systems at various pH values assayed in triplicate.

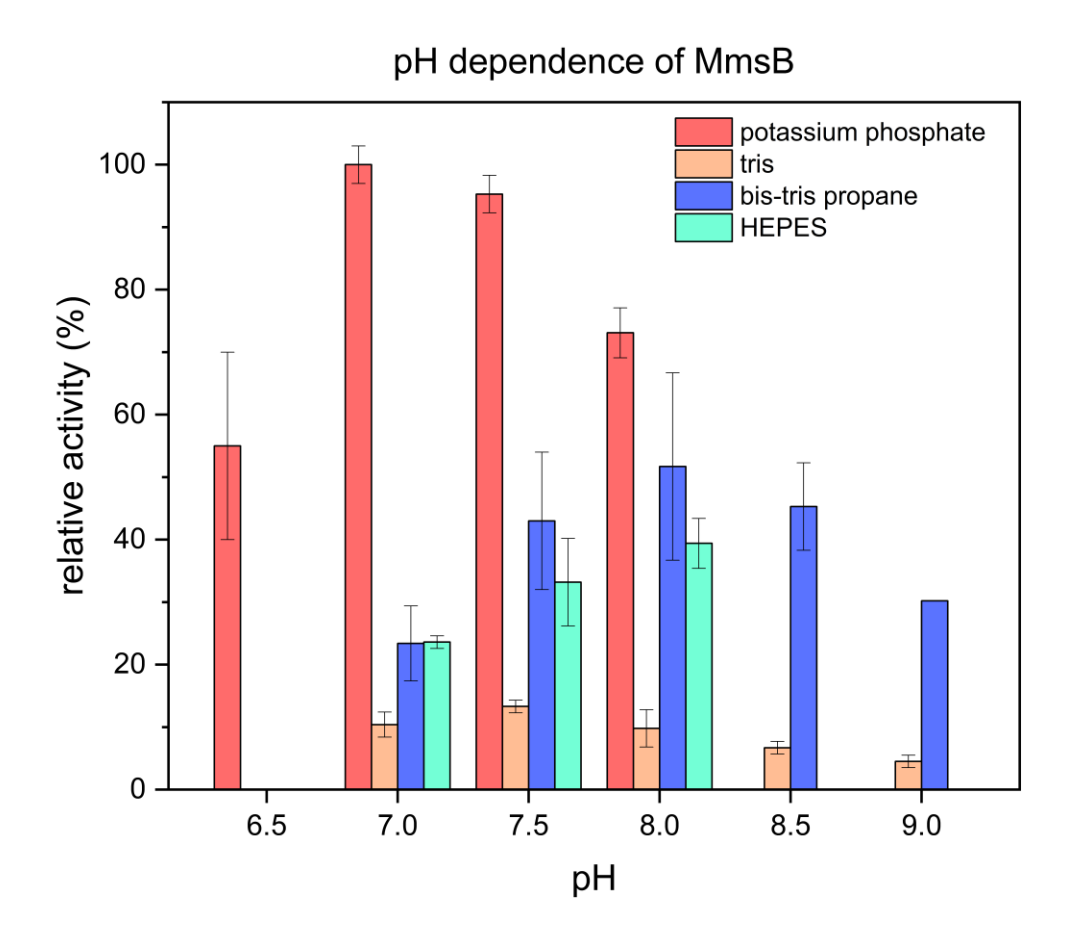


Figure 3.22. pH dependence of MmsB in four buffer systems at various pH values assayed in triplicate.

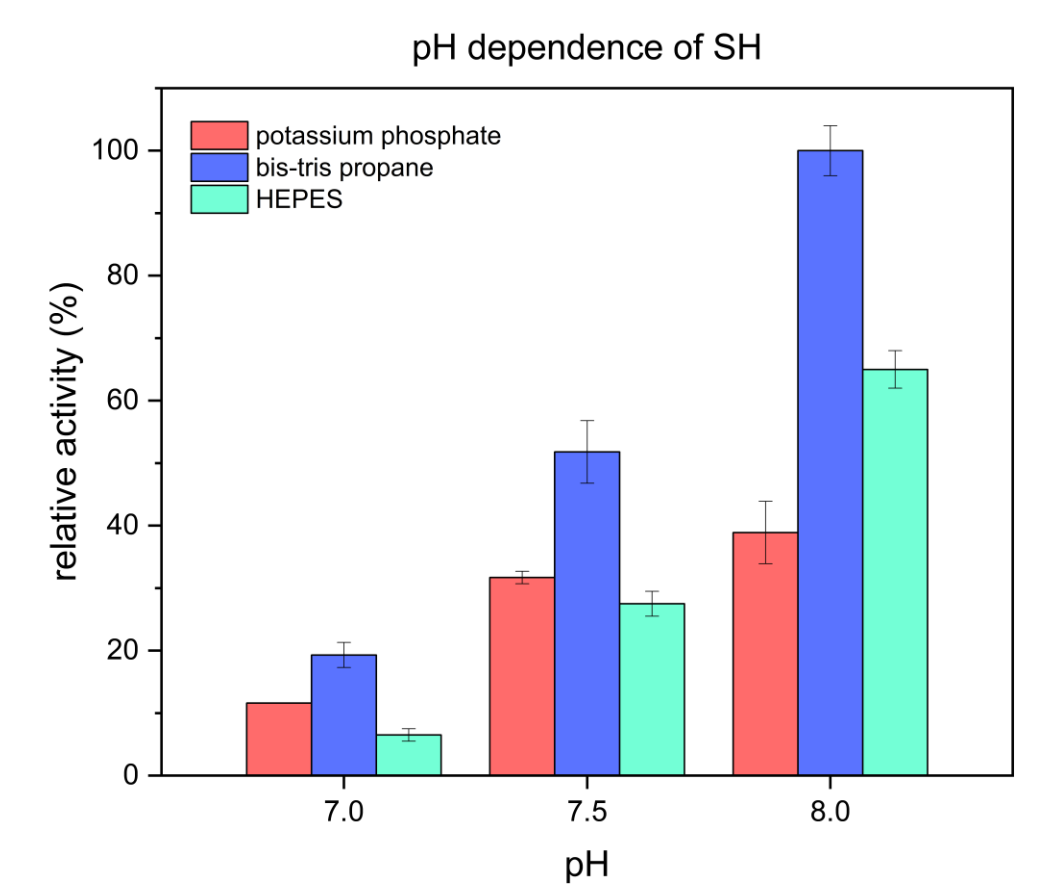


Figure 3.23. pH dependence of SH in three buffer systems at various pH values assayed in triplicate.

3.4.2 Hydrogen Delivery to Reaction

Table 3.5. Reaction components in the conversion of ACA 6 to 3-HP 10.

					0.01 eq	0.1 eq
Figure	[ACA] (mM)	Cg10062 (E114N) U	MmsB U	SH U	[NAD ⁺] (mM)	[NAD ⁺] (mM)
3.24	25	3.1	0.7	9.8	0.25	2.5
3.27	100	3	12	22	0.25	-
3.29	100	3	12	33	0.25	-

The conversion of ACA 6 to 3-HP 10 was carried out on a 4 mL scale. All stock solutions were prepared in 100 mM potassium phosphate, pH 8. Each reaction was carried out in a stoppered pear-shaped flask attached to a manifold. For all reactions, samples were analyzed by ¹H NMR. At timed intervals, an aliquot (490 μL) of the reaction was removed via pipette and combined with 100 μL of D₂O containing 10 mM TSP and 10 μL concentrated H₂SO₄. For SH to act as an efficient coupling enzyme, hydrogen was bubbled into each reaction. However, this resulted in no conversion as the starting ACA 6 remained in the reaction. To determine why this result was observed, a reaction monitoring only the hydration of ACA 6 to MSA 9 by Cq10062(E114N) was run. No conversion was seen indicating that the bubbling hydrogen was affecting Cg10062(E114N). Control experiments indicated that this effect was not the result of the hydrogen itself but, the act of bubbling in a gas to the reaction. Nitrogen gas was bubbled into a reaction with ACA 6 and Cg10062(E114N) and no conversion was observed. Additional efforts made using gas dispersion tubes to reduce the size of the bubble did not remedy the loss of activity. Using gas dispersion tubes made it more difficult to control the flow of hydrogen into the reactions and foaming still occurred. To work around this situation, ACA 6 can be hydrated to MSA 9 before hydrogen is bubbled into the reaction for subsequent reduction to 3-HP 10. Starting with 12.5 mM ACA 6, quantitative conversion to 3-HP 10 was achieved using two substoichiometric concentrations of NAD+ (0.2 and 0.02 equiv.) when the syntheses were carried out in two consecutive steps (Figure 3.24) (Table 3.5). All reaction components except MmsB were added at the beginning of each reaction. Once the ACA 6 was fully converted to MSA 9, MmsB was added to each reaction along with hydrogen bubbling, to complete the reduction of MSA 9 to 3-HP 10. The reactions were characterized and quantified using ¹H NMR to allow for detection of MSA 9 (Figures 3.25 and 3.26). Although MSA 9 can undergo spontaneous decarboxylation, 40 the short time span of these reactions did not result in loss of product.

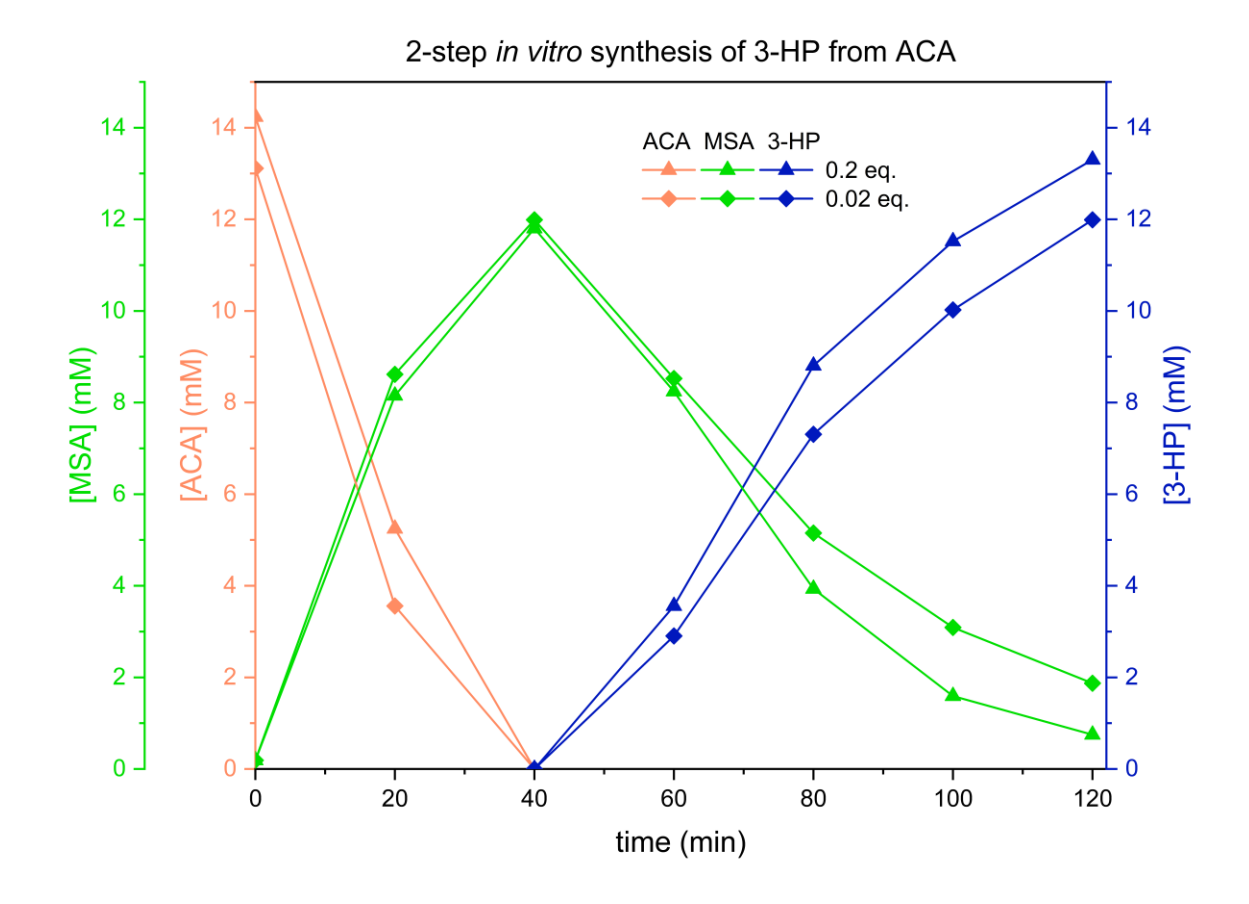


Figure 3.24. Two-step quantitative conversion of ACA **6** to 3-HP **10** with hydrogen bubbled into the reaction starting at 40 minutes.

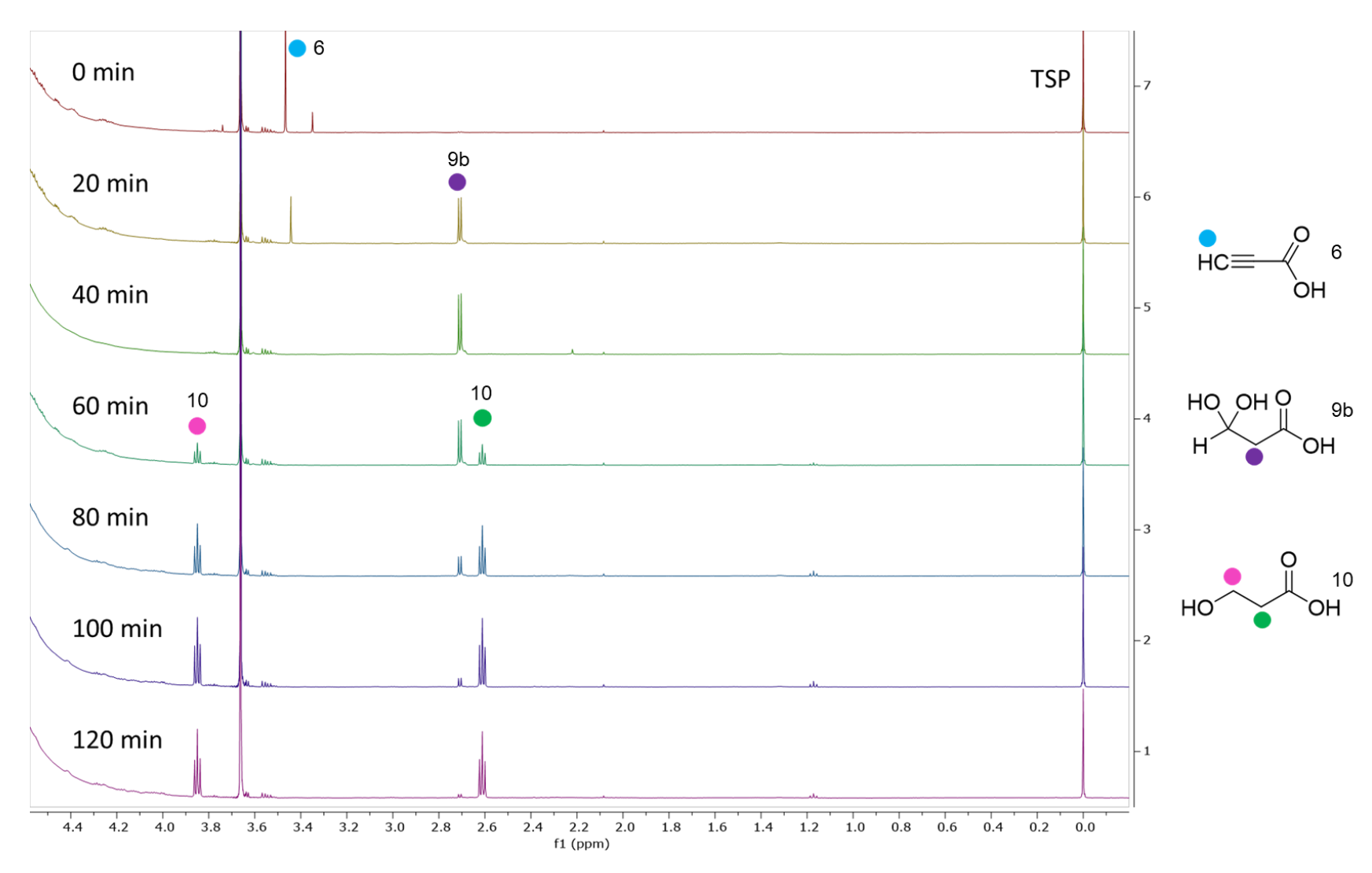


Figure 3.25. ¹H NMR spectra for the two-step quantitative conversion of ACA 6 to 3-HP 10 containing 0.2 eq NAD⁺.

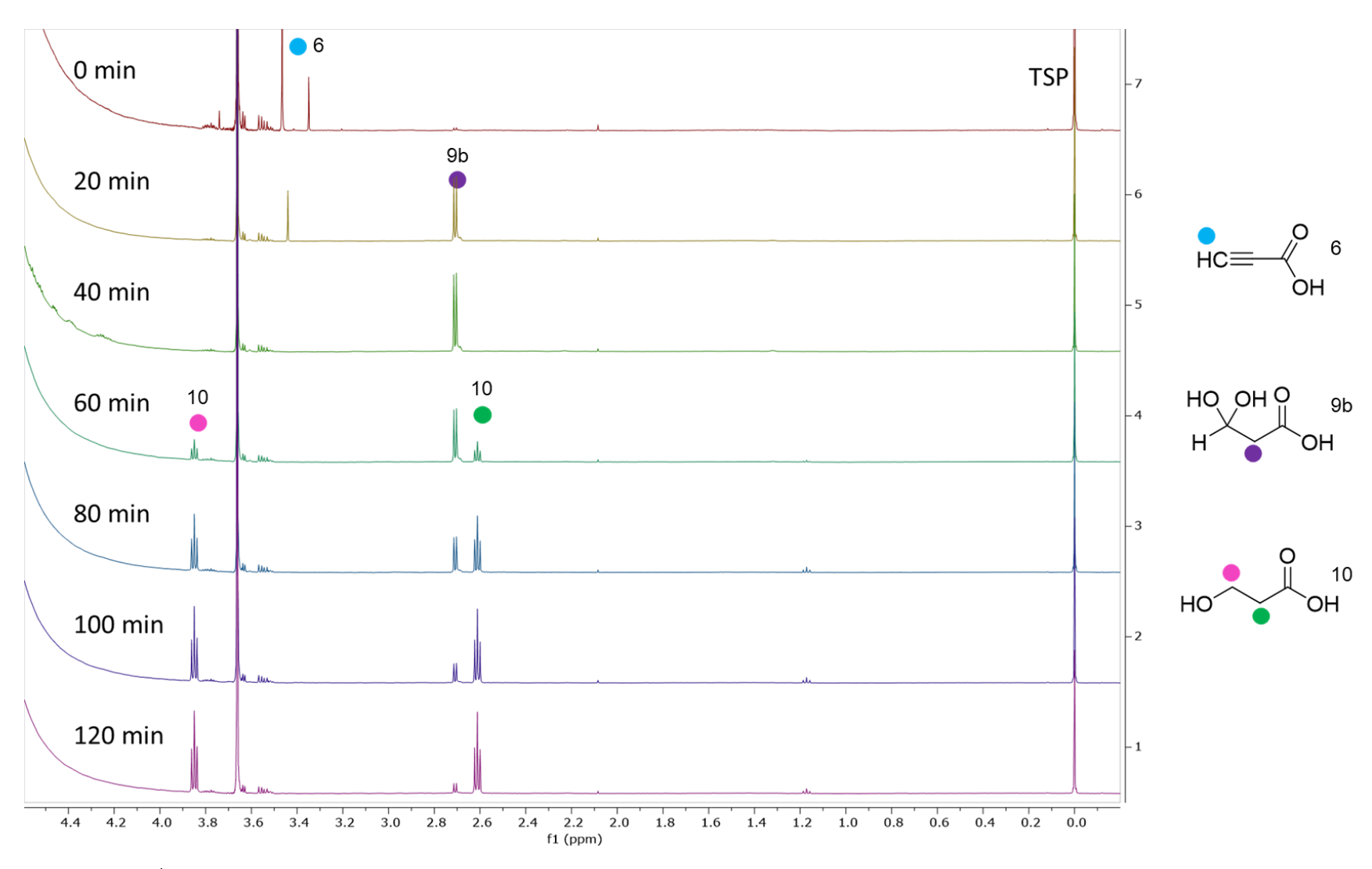


Figure 3.26. ¹H NMR spectra for the two-step quantitative conversion of ACA 6 to 3-HP 10 containing 0.02 eq NAD⁺.

This method however did not work for reactions starting with a higher concentration of ACA 6 due to the longer time required for conversion of ACA 6 to MSA 9. This resulted in accumulation of MSA 9 which decarboxylated and resulted in low mass balance at the end of the reactions. Reactions observing the hydration of ACA 6 to MSA 9 showed that Cg10062(E114N) retained activity when hydrogen was supplied to the headspace. The subsequent reduction to 3-HP 10, however, showed slow conversion as hydrogen only has a solubility of 0.8 mM in water at 1 atm pressure.⁴¹ Gentle stirring of the reactions resulted in faster conversion as it was able to improve hydrogen solubility.

3.4.3 Production of 3-HP Using Cg10062(E114N), MmsB, and SH

When using higher ACA **6** concentration, the reactions must be done in one step to avoid buildup and subsequent decarboxylation of MSA **9**. Reactions were assessed using 100 mM ACA **6** for direct comparison to the work done by Amaya. Starting with a higher concentration of ACA **6** also allows for simpler downstream processing. At the 100 mM ACA **6** scale, all reaction components were added at the start of the reaction and hydrogen was supplied to the headspace while the reactions were gently stirred to improve hydrogen solubility (Table 3.5). Excess coupling enzymes were necessary for complete conversion of MSA **9** to product, otherwise a low mass balance was observed at the conclusion of the reactions. When using 22 U SH, two replicates approached complete conversion, but great variation amongst replicates was observed (Figures 3.27 & 3.28). With increased SH, duplicate reactions with Cg10062(E114N) (2 U), MmsB (12 U) and SH (33 U) resulted in greater than 90% conversion (Figures 3.29 & 3.30). Minimal hydrogen solubility remains a limiting factor, contributing to the high unit amount of SH required. SH has a K_m of 11.9 \pm 0.9 μ M for H_s.⁴²

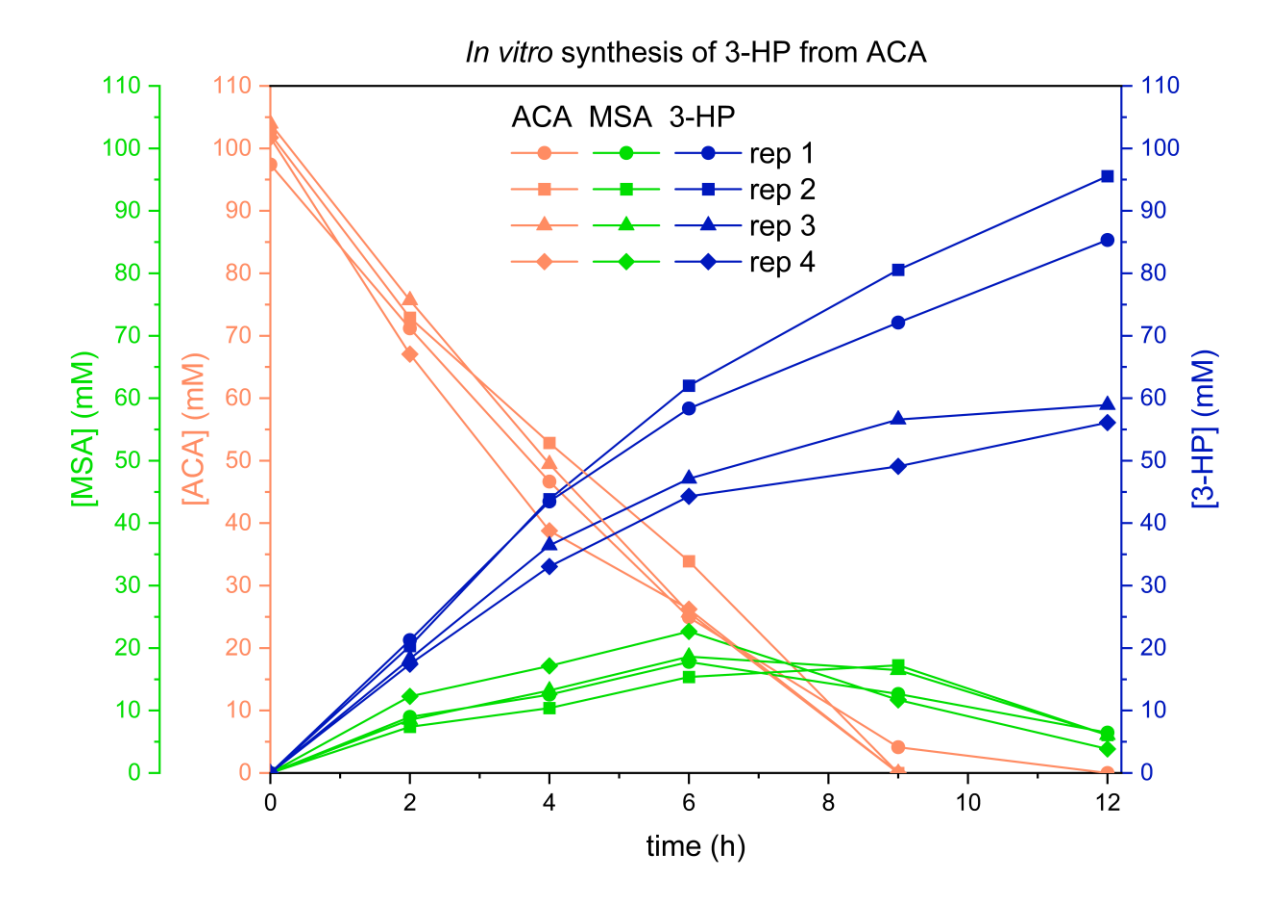


Figure 3.27. Four replicates of the conversion of 100 mM ACA **6** to 3-HP **10** shows deviation in the final [3-HP] that is formed when using 22 U SH.

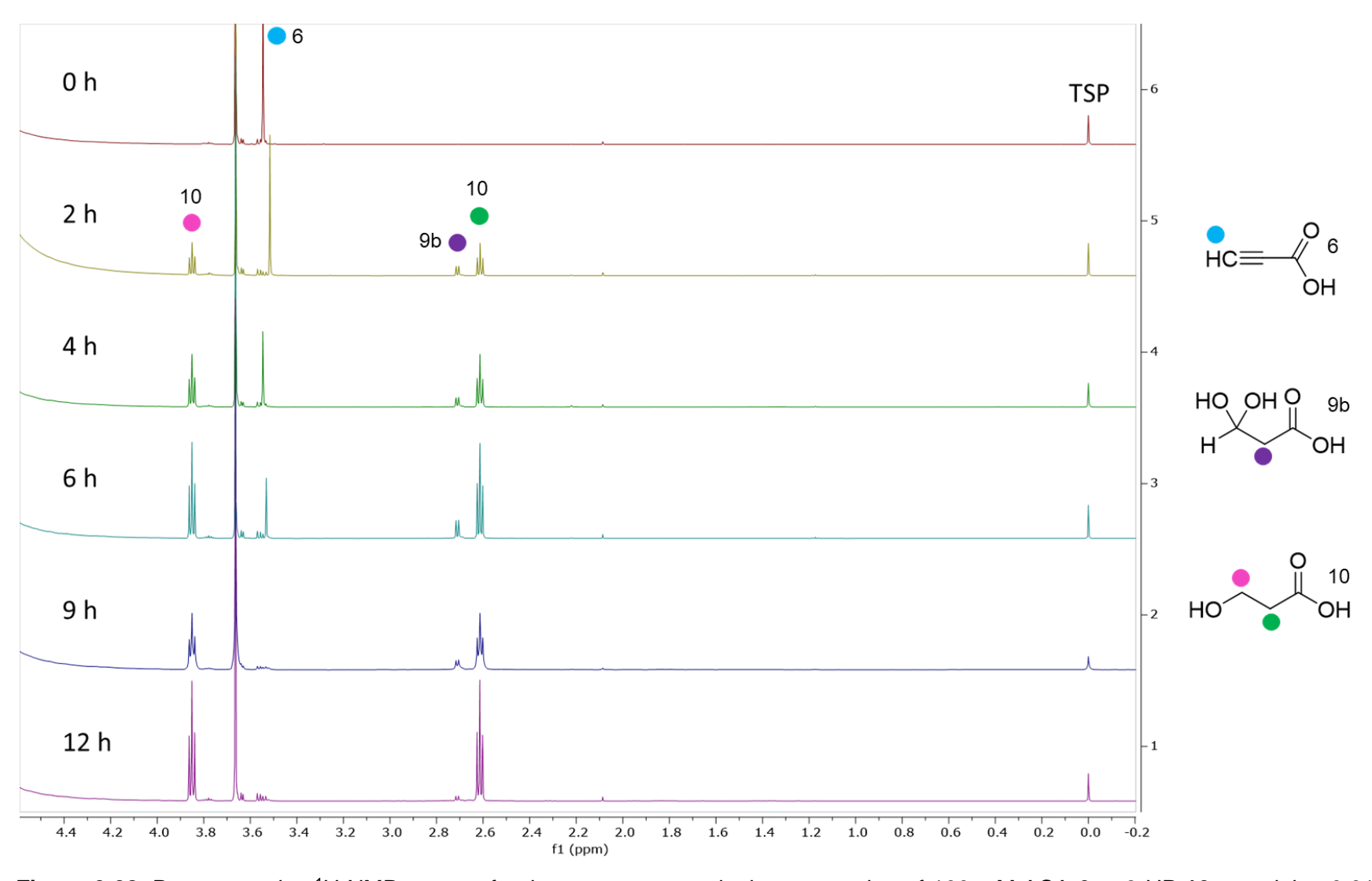


Figure 3.28. Representative ¹H NMR spectra for the one-step quantitative conversion of 100 mM ACA **6** to 3-HP **10** containing 0.01 eq NAD⁺ and 22 U SH.

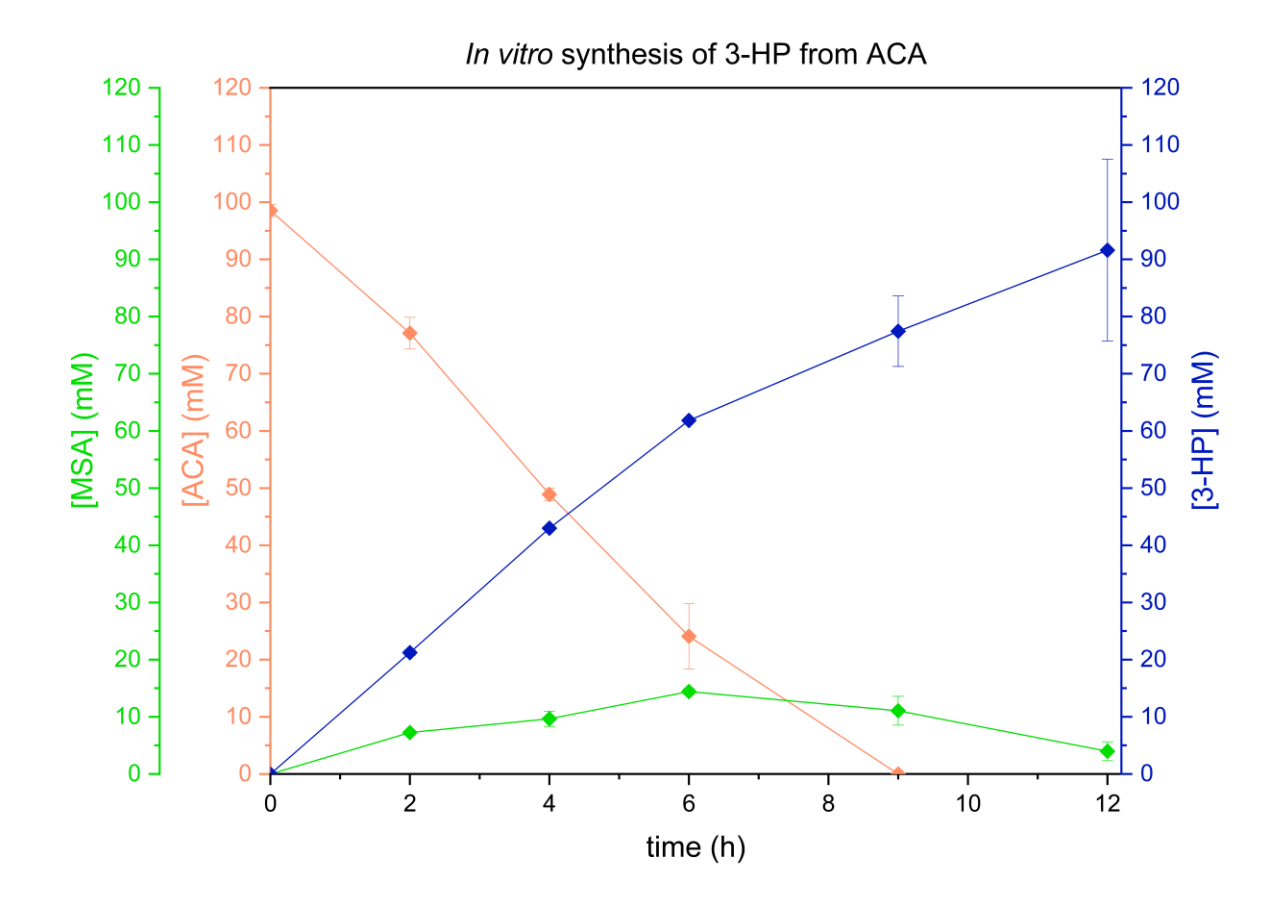


Figure 3.29. In vitro synthesis of 3-HP **10** from 100 mM ACA **6**. Conversion of ACA to 3-HP was carried out using 0.01 eq NAD(H) relative to ACA. ACA (orange), MSA **9** (green), and 3-HP (blue) were quantified by ¹H NMR. The average of duplicate reactions is plotted.

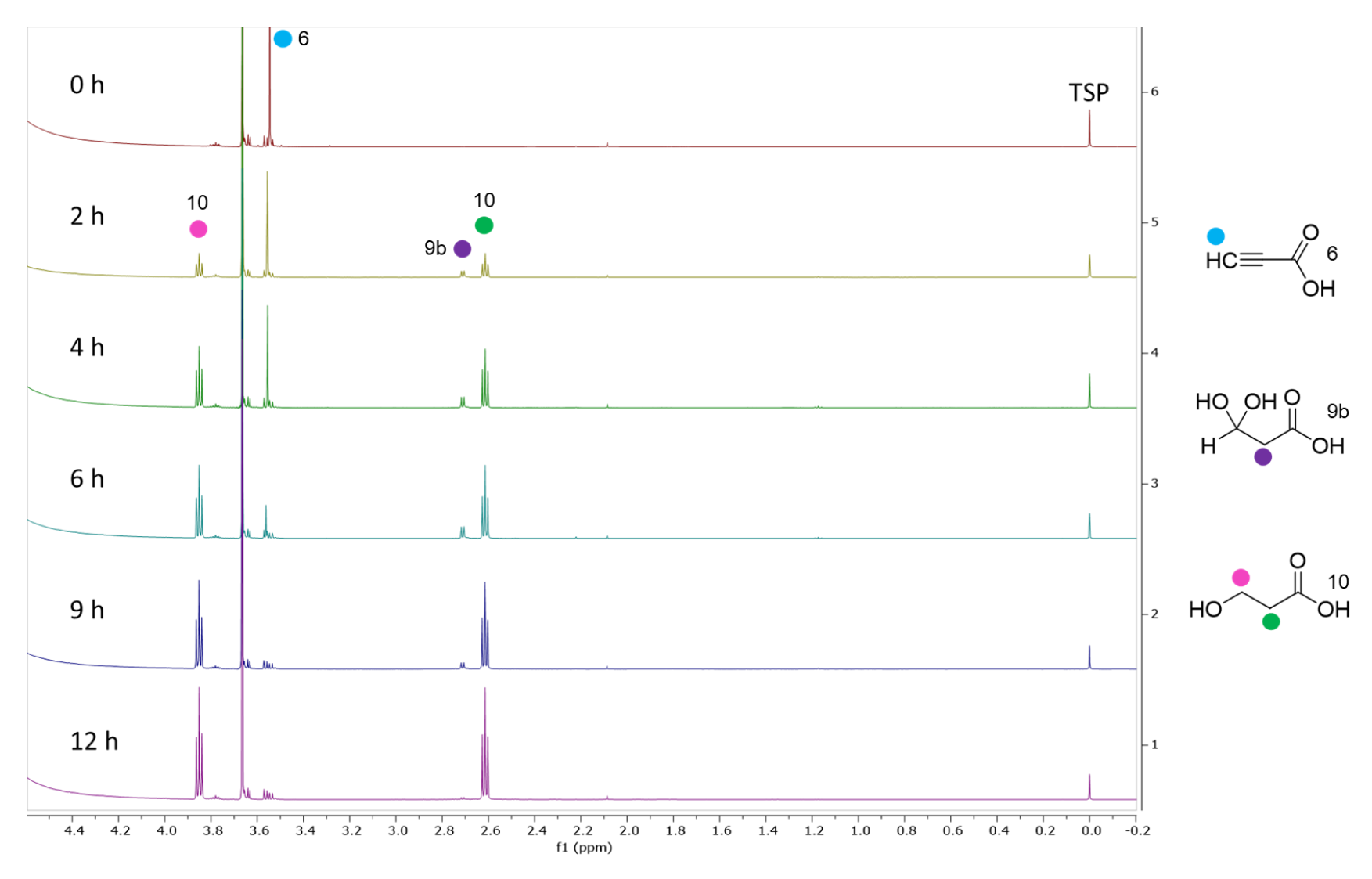


Figure 3.30. ¹H NMR spectra for the one-step quantitative conversion of 100 mM ACA **6** to 3-HP **10** containing 0.01 eq NAD⁺ and 33 U SH.

3.4.4 Kinetics of PTDH with NAD+ and NADP+

Figure 3.31. Enzymatic conversion of ACA **6** to 3-HP **10** using Cg10062(E114N), MmsB, and PTDH.

In the 3-HP 10 synthesis developed by Amaya Mathes Hewage, MSA 9 was reduced to 3-HP 10 by NADPH-dependent YdfG, and PTDH was coupled for cofactor recycling. 29,30 This biocatalytic pathway required NADPH which as of February 2023, is 1064% more expensive than NADH.43 The engineered PTDH that was used is capable of using NADP+ and NAD+, which would allow MmsB and PTDH to be coupled for NADH/ NAD+ recycling in the conversion of MSA 9 to 3-HP 10 (Figure 3.31). The kinetic parameters of PTDH were compared for NAD+ versus NADP+ and were measured by monitoring the reduction of NAD⁺ or NADP⁺ at 340 nm (ε = 6220 M⁻¹ cm⁻¹ 1). Assays (final volume 1 mL) contained PTDH, sodium phosphite and either NAD+ (25- 2500 μM) or NADP⁺ (25- 2500 μM) in 100 mM potassium phosphate pH 8. The assays were initiated by adding sodium phosphite, and A₃₄₀ was recorded. These experiments were conducted with the assistance of Esther Lee, an undergraduate researcher working in the lab. For NAD⁺ a K_m of 2360 \pm 279 μ M and a k_{cat} of 7.4 \pm 0.5 s⁻¹ were observed (Figure 3.32). For NADP+ a K_m of 1400 \pm 310 μ M and a k_{cat} of 0.7 \pm 0.1 s⁻¹ were observed (Figure 3.33). This suggests that PTDH has stronger binding affinity for NADP+, but a higher turnover with NAD+. Overall, PTDH has a better k_{cat}/K_m with NAD+ as substrate compared to NADP+ at 3.13 x 10³ M⁻¹s⁻¹ and 0.48 x 10³ M⁻¹s⁻¹ respectively. The included literature values are for PTDH variant A176R without the 12X mutations for thermostability. These values also show a higher turnover number and catalytic efficiency for PTDH with NAD+ as substrate (Table 3.6).

Table 3.6. Michaelis Menten kinetic values for PTDH (12X-A176R) with NAD⁺ and NADP⁺. Literature values are included for PTDH variant A176R.³⁴

Substrate	$K_m(\mu M)$	<i>k</i> _{cat} (s ⁻¹)	$k_{cat}/K_m \times 10^3 (\text{M}^{-1} \text{s}^{-1})$
NAD+	2360 ± 279	7.4 ± 0.5	3.1
NADP+	1400 ± 310	0.7 ± 0.1	0.5
NAD+ 34	60 ± 7	4.2 ± 0.01	70.0
NADP+ 34	77 ± 8	2.2 ± 0.01	28.6

Figure 3.32. Michaelis Menten kinetic plot for PTDH with NAD+.

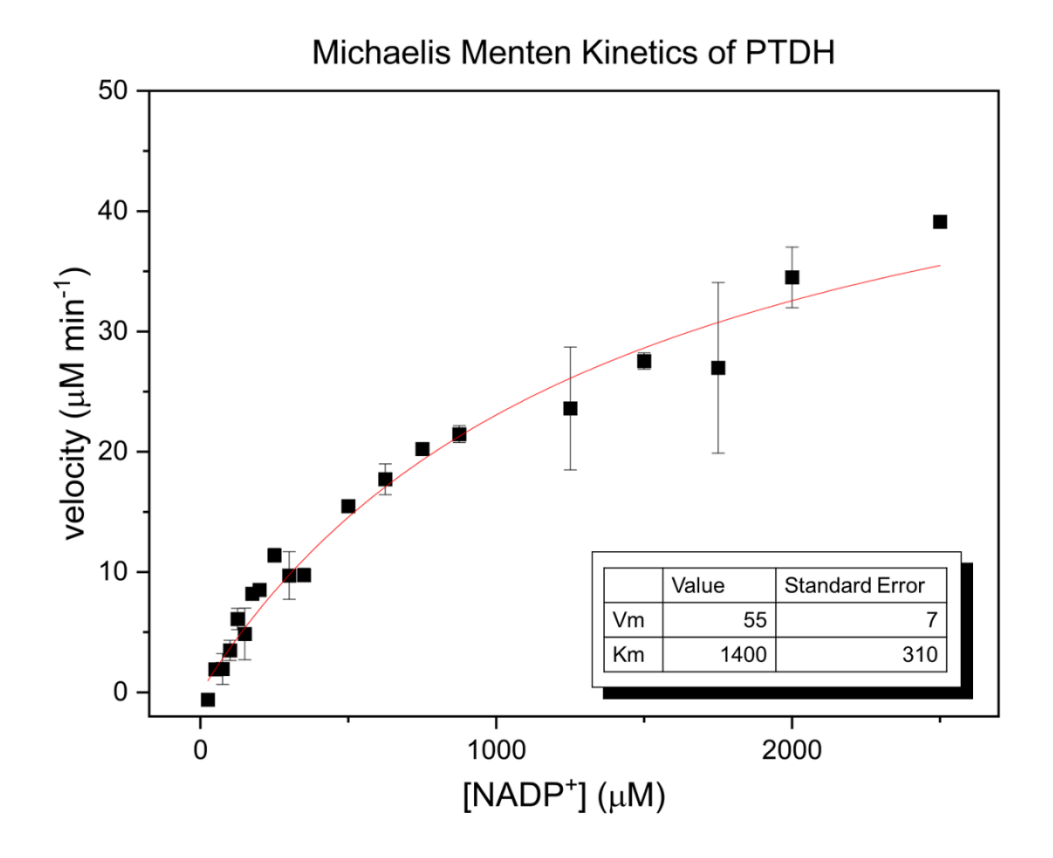


Figure 3.33. Michaelis Menten kinetic plot for PTDH with NADP⁺.

3.4.5 Production of 3-HP Using Cg10062(E114N), MmsB, and PTDH

Table 3.7. Reaction components in the conversion of ACA 6 to 3-HP 10.

						0.001 eq	0.01 eq	0.1 eq
Figure	[ACA] (mM)	Cg10062 (E114N) U	MmsB U	PTDH U	[Phosphite] (mM)	[NAD+] (mM)	[NAD+] (mM)	[NAD+] (mM)
3.34	100	3	6	6	100	-	0.25	2.5
3.41	100	3	6	6	100	0.025	0.25	2.5
3.43	100	3	6	6	100	0.025	0.25	2.5

ACA 6 can also be converted to 3-HP 10 using Cg10062(E114N), MmsB, and PTDH (Figure 3.31). ¹H NMR and HPLC were used as alternate quantification methods. All stock solutions were prepared in 100 mM potassium phosphate pH 8 regardless of quantification

method. Reactions quantified by NMR were carried out on a 4 mL scale. Each reaction was run in a stoppered pear-shaped flask with gentle stirring. For 1H NMR analysis, an aliquot (490 µL) of the reaction was removed via pipette at timed intervals and combined with 100 µL of D₂O containing 10 mM TSP and 10 µL concentrated H₂SO₄. Duplicate reactions run at two varying NAD⁺ equivalents of 0.1 eq NAD⁺ and 0.01 eq NAD⁺, with 100 mM ACA 6, 100 mM sodium phosphite, Cg10062(E114N) (3 U), MmsB (6 U) and PTDH (6 U) resulted in quantitative conversion (Figure 3.34) (Table 3.7). NMR analysis however, resulted in a mass balance greater than 100 mM (Figures 3.35 & 3.36). Compared to the reactions using SH to recycle cofactor, much less PTDH was needed in comparison to SH since it does not rely on hydrogen solubility. Interestingly, the reaction with 0.1 eq NAD⁺ resulted in slower conversion to product than the reaction containing 0.01 eq NAD⁺. Prior studies done by Amaya Mathes Hewage show that Cg10062(E114N) is inhibited by NADPH,²⁹ suggesting that NADH may also inhibit Cg10062(E114N).

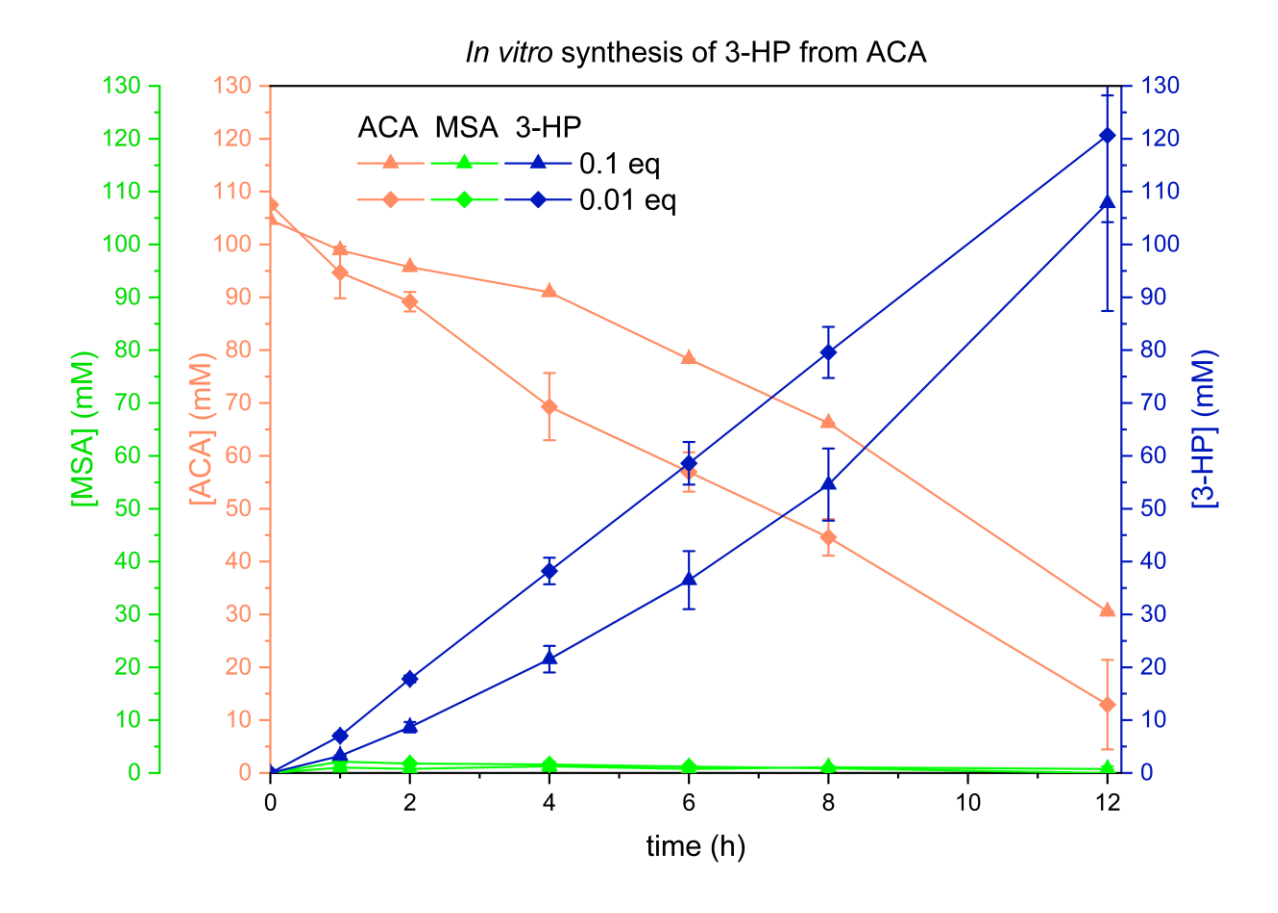


Figure 3.34. In vitro synthesis of 3-HP **10** from 100 mM ACA **6**. Conversion of ACA to 3-HP was carried out using 0.1 eq and 0.01 eq NAD(H) relative to ACA. ACA (orange), MSA **9** (green), and 3-HP (blue) were quantified by ¹H NMR.

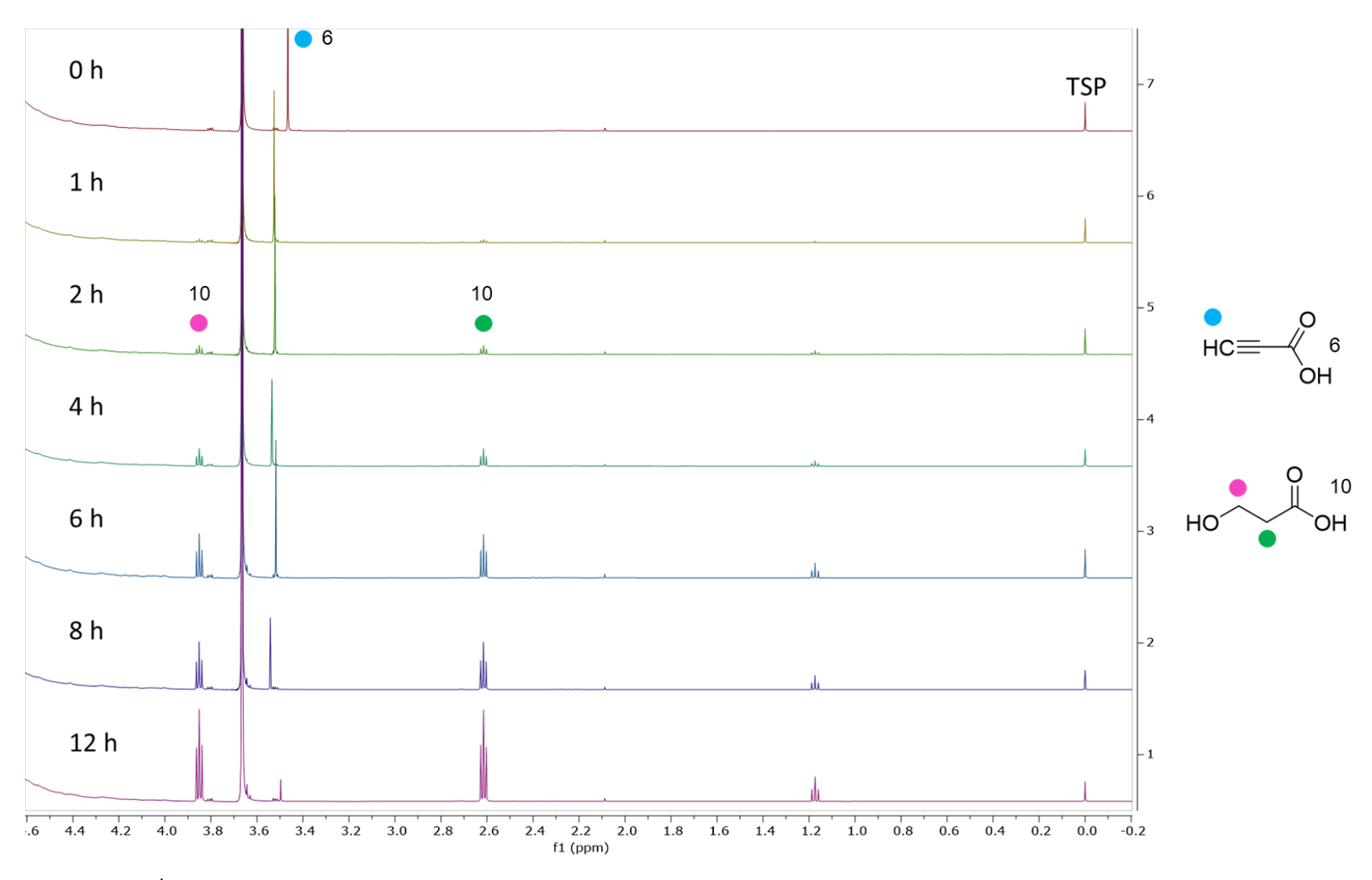


Figure 3.35. ¹H NMR spectra for the one-step quantitative conversion of 100 mM ACA **6** to 3-HP **10** containing 0.1 eq NAD⁺ and 6 U PTDH.

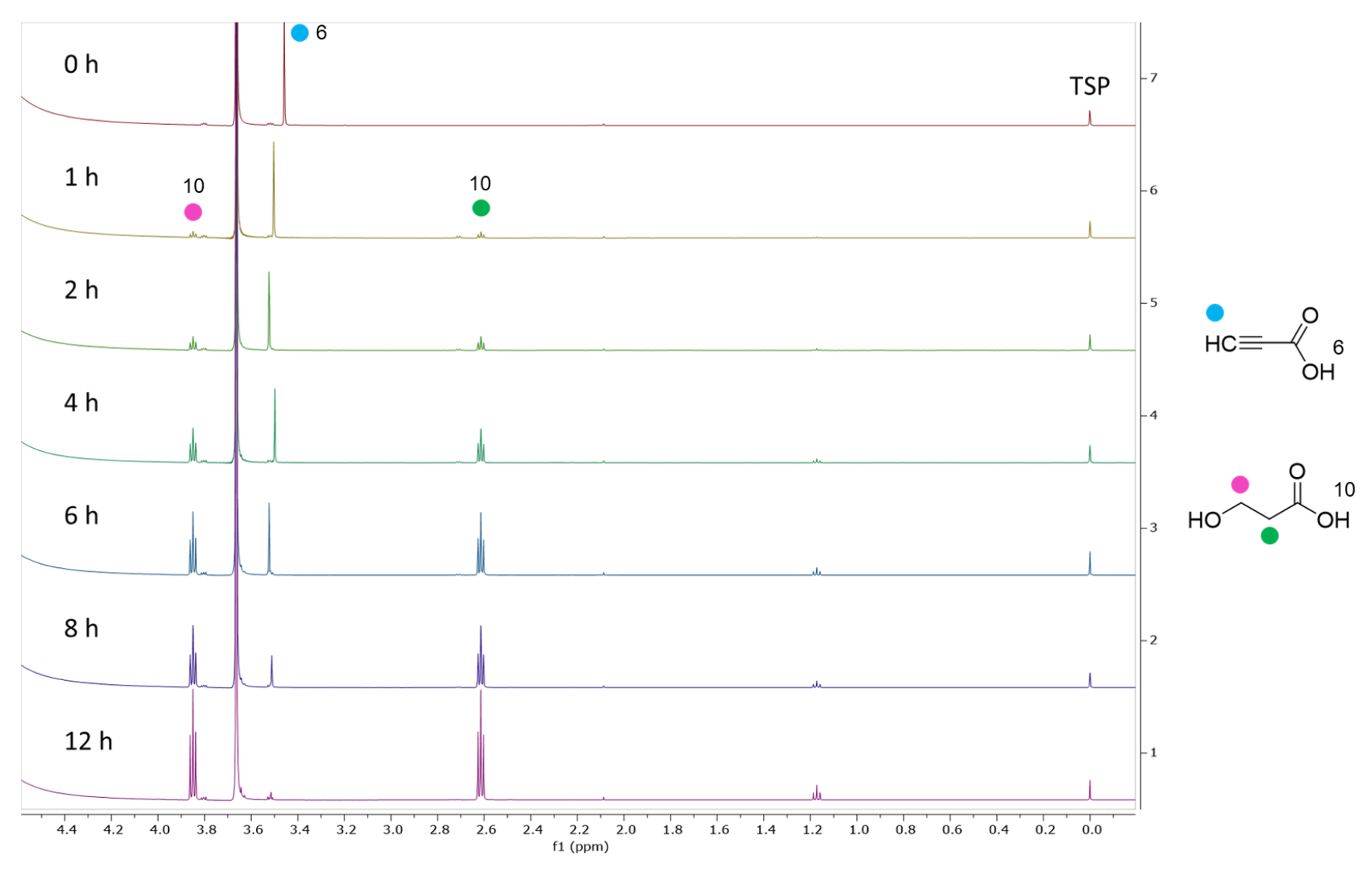


Figure 3.36. ¹H NMR spectra for the one-step quantitative conversion of 100 mM ACA **6** to 3-HP **10** containing 0.01 eq NAD⁺ and 6 U PTDH.

Since hydrogen was not limiting in these reactions, MSA 9 did not accumulate and analysis by HPLC was also possible. Calibration curves for ACA 6 and 3-HP 10 were created using 0.1 mM, 1 mM, 5 mM, 10 mM, and 20 mM standards that were acidified and diluted in 100 mM potassium phosphate buffer. Two curves for each set of standards were created using UV and RID detection (Figures 3.37 - 3.40). The samples with a concentration of 0.1 mM resulted in peaks that were too small for accurate RID detection. Reactions monitored by HPLC were carried out on a 1 mL scale containing NAD+ equivalents of 0.1, 0.01, and 0.001 eq NAD+, with 100 mM ACA 6, 100 mM sodium phosphite, Cq10062(E114N) (3 U), MmsB (6 U) and PTDH (6 U). Duplicates of each reaction were run in Eppendorf tubes with gentle mixing on a rocking platform. For HPLC analysis, samples (100 µL) were removed at timed intervals, quenched with 5 µL concentrated sulfuric acid, and diluted with 395 µL 0.01 N sulfuric acid. UV (Figures 3.41 & 3.42) and RID (Figures 3.43 & 3.44) detection were compared among HPLC samples. Reactions resulted in full conversion at 9 h and are reported as relative concentration. For each reaction, the concentration of ACA 6 and 3-HP 10 are relative to the concentration of ACA 6 at t = 0 and are reported as percentages. As was also seen in reactions analyzed by NMR, the reaction containing the highest concentration of NAD+ resulted in the slowest conversion of ACA 6 to 3-HP **10**. UV and RID detection are comparable.

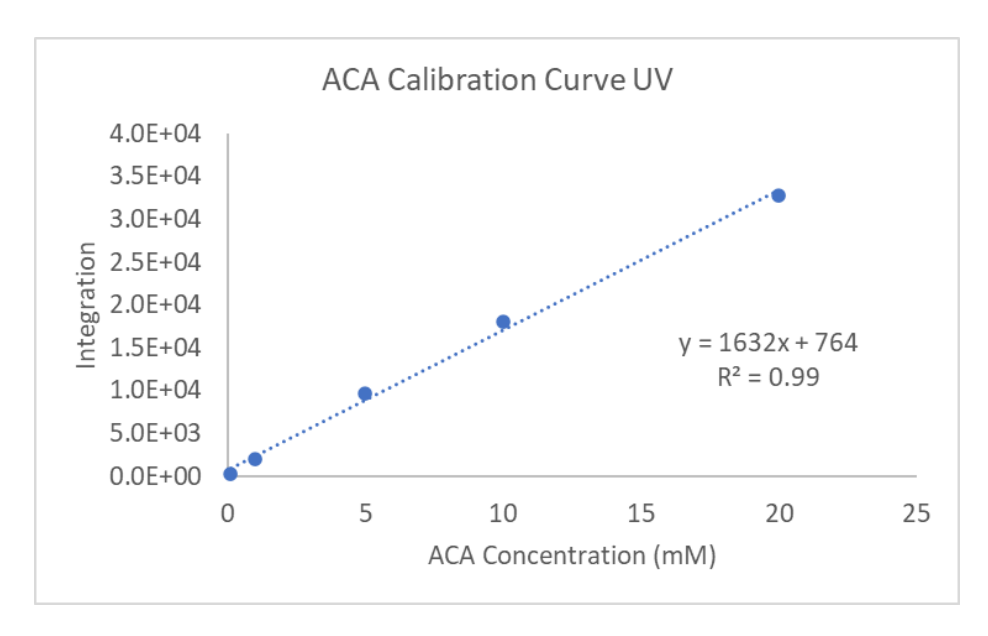


Figure 3.37. ACA 6 HPLC calibration curve with UV detection.

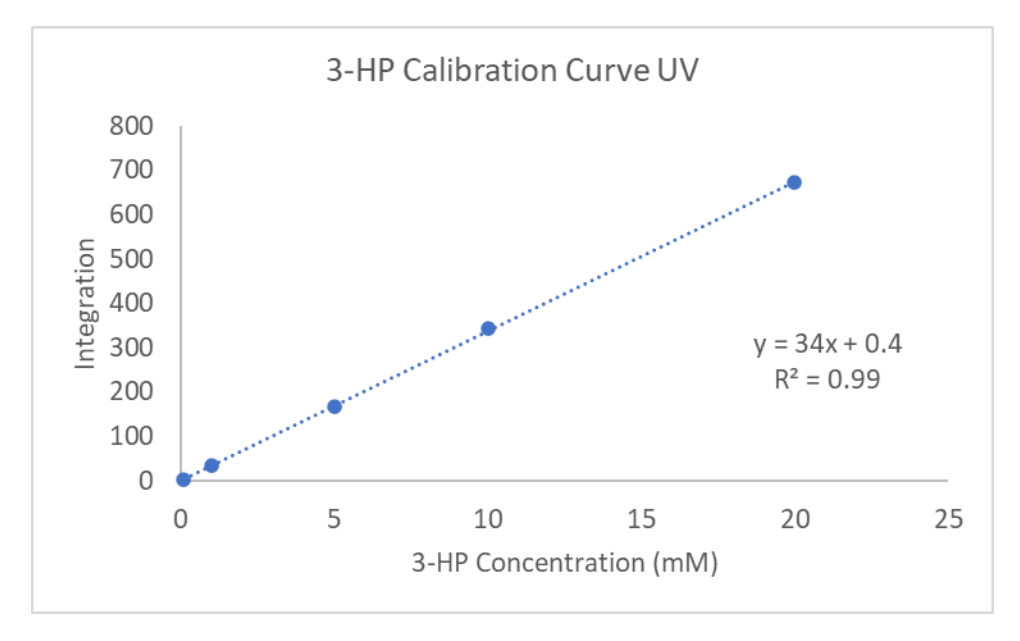


Figure 3.38. 3-HP 10 HPLC calibration curve with UV detection.

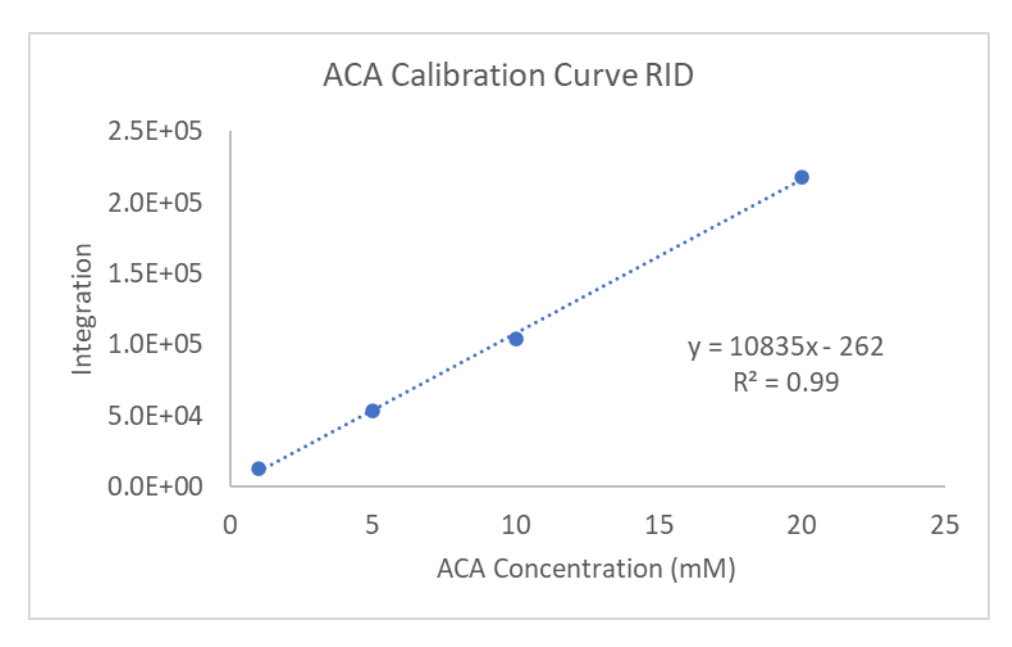


Figure 3.39. ACA 6 HPLC calibration curve with RID detection.

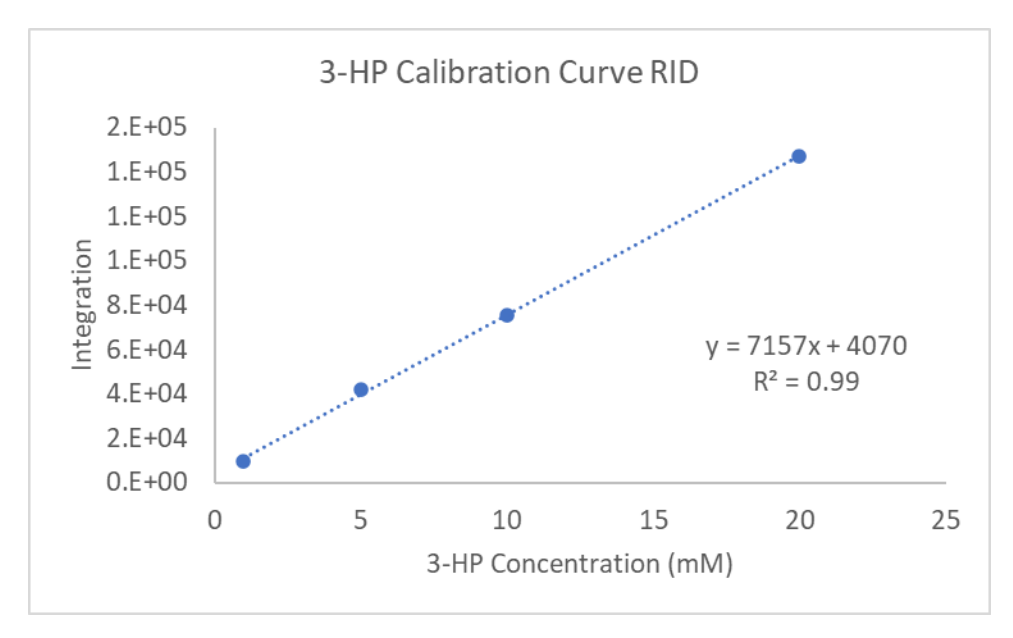


Figure 3.40. 3-HP 10 HPLC calibration curve with RID detection.

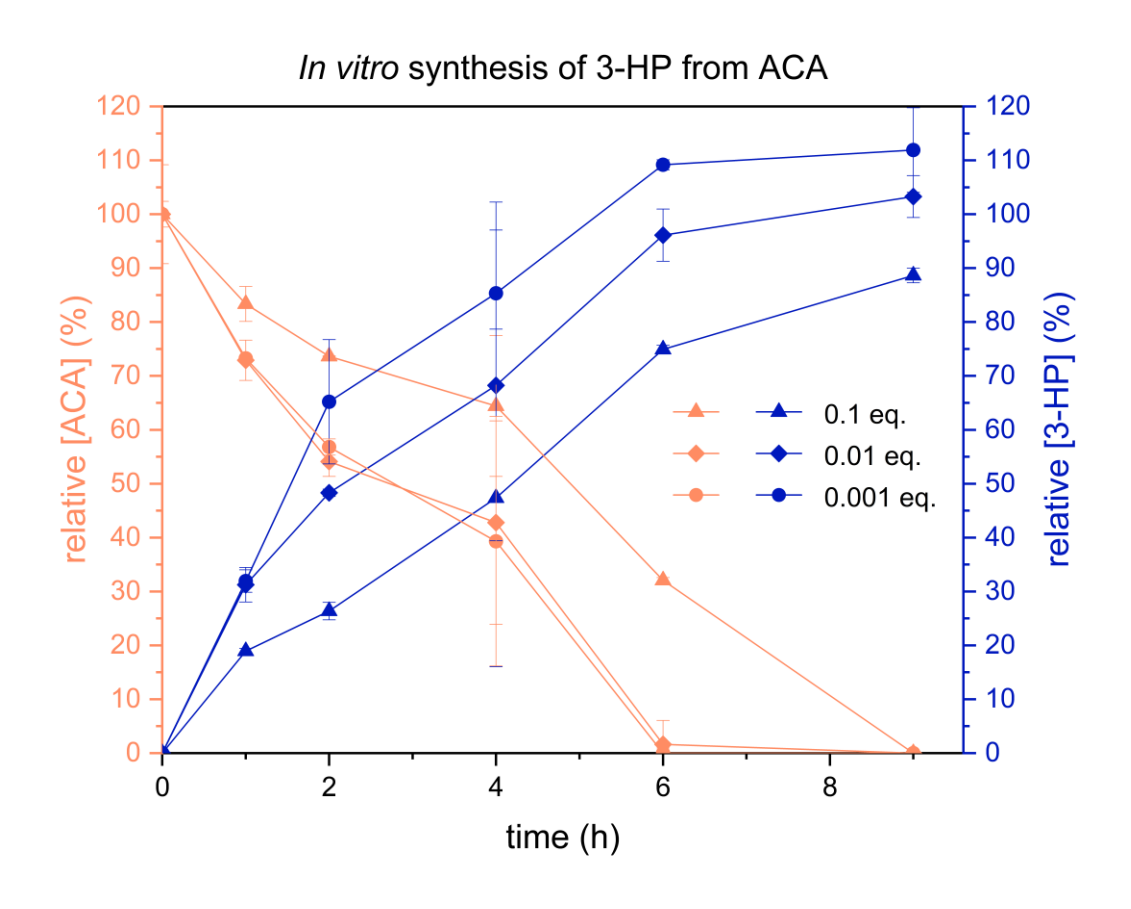


Figure 3.41. In vitro synthesis of 3-HP **10** from 100 mM ACA **6**. Conversion of ACA to 3-HP was carried out using 0.1 eq, 0.01 eq, and 0.001 eq NAD(H) relative to ACA. ACA (orange) and 3-HP (blue) were quantified by HPLC with UV detection.

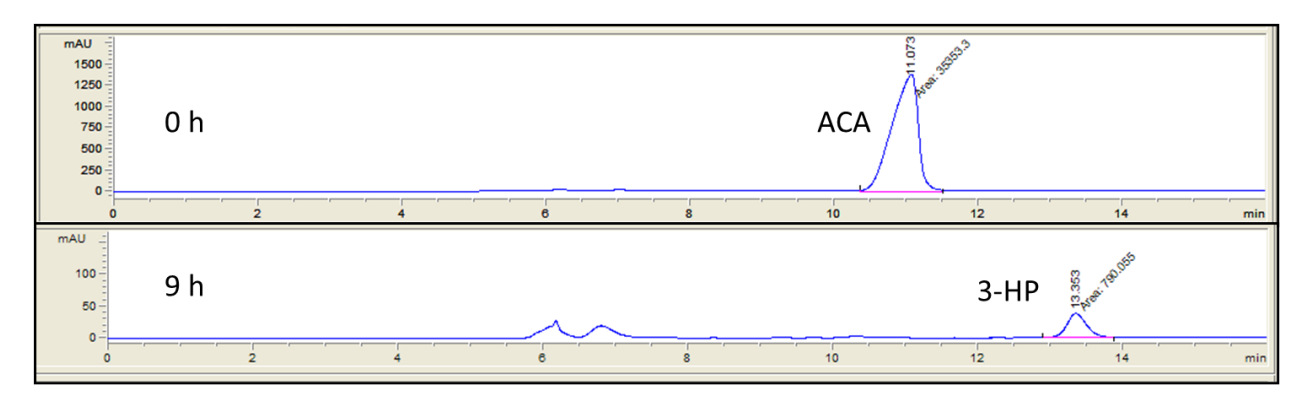


Figure 3.42. 0 hour and 9 hour HPLC-UV traces from the conversion of ACA 6 to 3-HP 10.

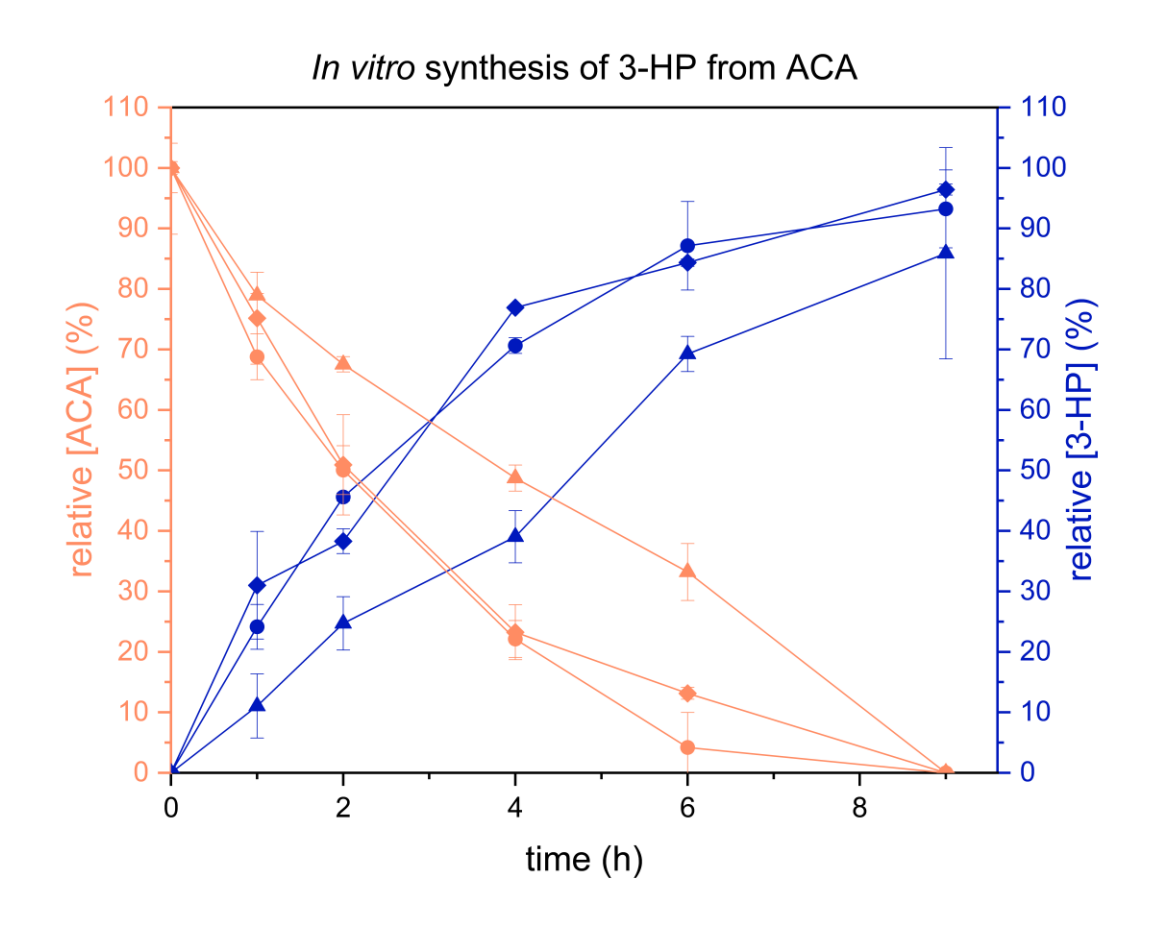


Figure 3.43. In vitro synthesis of 3-HP **10** from 100 mM ACA **6**. Conversion of ACA to 3-HP was carried out using 0.1 eq, 0.01 eq, and 0.001 eq NAD(H) relative to ACA. ACA (orange) and 3-HP (blue) were quantified by HPLC with RID detection.

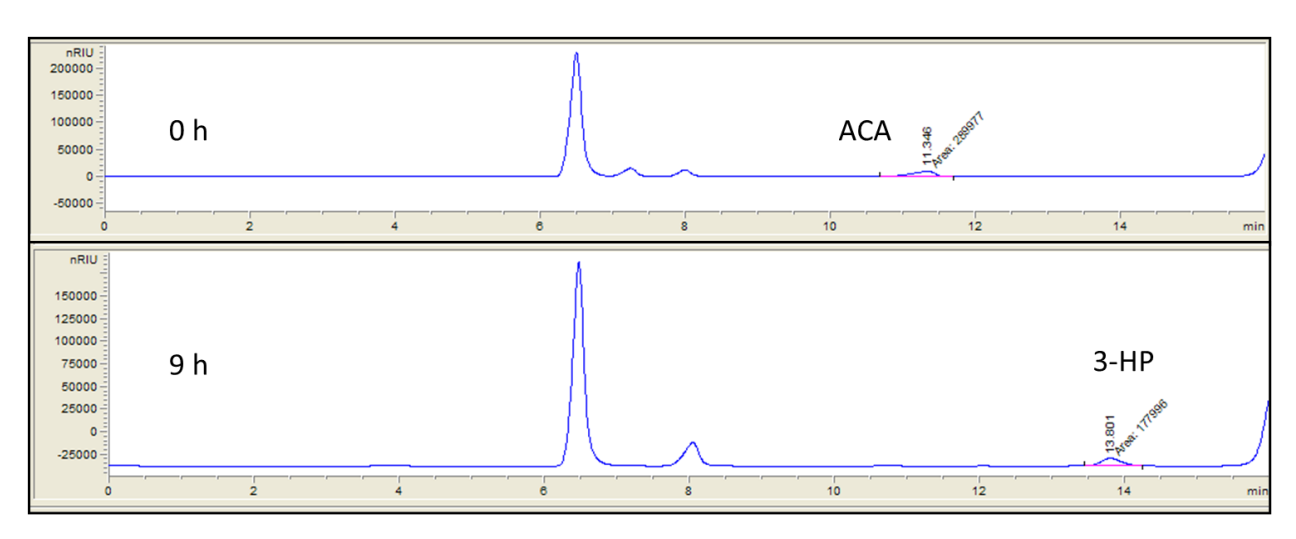


Figure 3.44. 0 hour and 9 hour HPLC-RID traces from the conversion of ACA 6 to 3-HP 10.

3.5 Conclusion

3-Hydroxypropionic acid 10 is an important building block with great potential to be transformed into a multitude of other important chemicals including acrylonitrile 18, acrylic acid 19, and acrylamide 20. Methane and carbon dioxide have been proposed as alternate starting materials for the synthesis of 3-HP 10 as current production mostly relies on glucose 1 and glycerol 29. Variant Cg10062(E114N) hydrates ACA 6 to produce MSA 9 as its sole product. MSA 9 can be reduced to 3-HP 10 using NADH-dependent MmsB. Cofactor can be recycled using SH or PTDH. Each method results in complete or nearly complete conversion of ACA 6 to 3-HP 10. Reactions can be monitored using ¹H NMR or HPLC analysis. As suggested in Chapter 2 for future work, these enzymatic conversions can also be transitioned to a continuous flow system. Preliminary work done involves the immobilization of Cq10062(E114N), MmsB, PTDH, and NADH onto porous glass that was activated with aminopropyltrimethoxysilane and functionalized with polyethylene glycol containing epoxy termini. 44,45 Further studies can assess other immobilization material including commercially-made ECR8285 resin containing epoxy functional groups.⁴⁶ Overall, this synthesis provides a method for producing 3-hydroxypropionic acid 10 from methane and carbon dioxide using ACA 6 as a bridge. The use of enzymes allows for easier downstream processing in comparison to fermentation. This system has great potential for further development as work on identifying superior Cg10062 variants with hydratase-only activity is already underway.

REFERENCES

- (1) Werpy, T.; Petersen, G. *Top Value Added Chemicals from Biomass: Volume I -- Results of Screening for Potential Candidates from Sugars and Synthesis Gas*; DOE/GO-102004-1992, 15008859; 2004.
- (2) Jiang, X.; Meng, X.; Xian, M. Biosynthetic Pathways for 3-Hydroxypropionic Acid Production. *Appl. Microbiol. Biotechnol.* **2009**, *82* (6), 995–1003.
- (3) Zabed, H. M.; Akter, S.; Rupani, P. F.; Akor, J.; Zhang, Y.; Zhao, M.; Zhang, C.; Ragauskas, A. J.; Qi, X. Biocatalytic Gateway to Convert Glycerol into 3-Hydroxypropionic Acid in Waste-Based Biorefineries: Fundamentals, Limitations, and Potential Research Strategies. *Biotechnol. Adv.* **2023**, *62*, 108075.
- (4) Dishisha, T.; Pyo, S.-H.; Hatti-Kaul, R. Bio-Based 3-Hydroxypropionic- and Acrylicacid Production from Biodiesel Glycerol via Integrated Microbial and Chemicalcatalysis. *Microb. Cell Fact.* **2015**, *14* (1), 200.
- (5) Cargill gives biobased acrylic acid one more go. Chemical & Engineering News. https://cen.acs.org/business/biobased-chemicals/Cargill-gives-biobased-acrylic-acid/98/i20 (accessed 2023-03-02).
- (6) Ohara, T.; Sato, T.; Shimizu, N.; Prescher, G.; Schwind, H.; Weiberg, O.; Marten, K.; Greim, H.; Shaffer, T. D.; Nandi, P. Acrylic Acid and Derivatives. In *Ullmann's Encyclopedia of Industrial Chemistry*; John Wiley & Sons, Ltd, 2020; pp 1–21.
- (7) Humans, I. W. G. on the E. of C. R. to. *Propylene*; International Agency for Research on Cancer, 1994.
- (8) Endo, M. Carbon Fiber. In *High-Performance and Specialty Fibers: Concepts, Technology and Modern Applications of Man-Made Fibers for the Future*; The Society of Fiber Science and Techno, J., Ed.; Springer Japan: Tokyo, 2016; pp 327–342.
- (9) Karp, E. M.; Eaton, T. R.; Sànchez i Nogué, V.; Vorotnikov, V.; Biddy, M. J.; Tan, E. C. D.; Brandner, D. G.; Cywar, R. M.; Liu, R.; Manker, L. P.; Michener, W. E.; Gilhespy, M.; Skoufa, Z.; Watson, M. J.; Fruchey, O. S.; Vardon, D. R.; Gill, R. T.; Bratis, A. D.; Beckham, G. T. Renewable Acrylonitrile Production. *Science* **2017**, *358* (6368), 1307–1310.
- (10) NREL Shifts Carbon Fiber Research into Second Gear. https://www.nrel.gov/news/features/2018/nrel-shifts-carbon-fiber-research-into-second-gear.html (accessed 2023-03-02).
- (11) Zhao, P.; Tian, P. Biosynthesis Pathways and Strategies for Improving 3-Hydroxypropionic Acid Production in Bacteria. *World J. Microbiol. Biotechnol.* **2021**, *37* (7), 117.
- (12) Kumar, V.; Ashok, S.; Park, S. Recent Advances in Biological Production of 3-Hydroxypropionic Acid. *Biotechnol. Adv.* **2013**, *31* (6), 945–961.
- (13) Matsakas, L.; Hrůzová, K.; Rova, U.; Christakopoulos, P. Biological Production of 3-Hydroxypropionic Acid: An Update on the Current Status. *Fermentation.* **2018**, *4* (1), 13.

- (14) Searchinger, T.; Heimlich, R. Avoiding Bioenergy Competition for Food Crops and Land. **2015**.
- (15) Cheng, Z.; Jiang, J.; Wu, H.; Li, Z.; Ye, Q. Enhanced Production of 3-Hydroxypropionic Acid from Glucose via Malonyl-CoA Pathway by Engineered Escherichia Coli. *Bioresour. Technol.* **2016**, *200*, 897–904.
- (16) Liu, C.; Wang, Q.; Xian, M.; Ding, Y.; Zhao, G. Dissection of Malonyl-Coenzyme A Reductase of Chloroflexus Aurantiacus Results in Enzyme Activity Improvement. *PLOS ONE.* **2013**, *8* (9), e75554.
- (17) Ganesh, I.; Ravikumar, S.; Hong, S. H. Metabolically Engineered Escherichia Coli as a Tool for the Production of Bioenergy and Biochemicals from Glycerol. *Biotechnol. Bioprocess Eng.* **2012**, *17* (4), 671–678.
- (18) Gholami, Z.; Abdullah, A. Z.; Lee, K.-T. Dealing with the Surplus of Glycerol Production from Biodiesel Industry through Catalytic Upgrading to Polyglycerols and Other Value-Added Products. *Renew. Sustainable Energy Rev.* **2014**, *39*, 327–341.
- (19) Jers, C.; Kalantari, A.; Garg, A.; Mijakovic, I. Production of 3-Hydroxypropanoic Acid From Glycerol by Metabolically Engineered Bacteria. *Front. Bioeng. Biotechnol.* **2019**, *7*, 124.
- (20) Zhu, J.-G.; Ji, X.-J.; Huang, H.; Du, J.; Li, S.; Ding, Y.-Y. Production of 3-Hydroxypropionic Acid by Recombinant Klebsiella Pneumoniae Based on Aeration and ORP Controlled Strategy. *Korean J. Chem. Eng.* **2009**, *26* (6), 1679–1685.
- (21) Vidra, A.; Németh, Á. Bio-Based 3-Hydroxypropionic Acid: A Review. *Period. Polytech. Chem. Eng.* **2018**, *62* (2), 156–166.
- (22) Nguyen-Vo, T. P.; Liang, Y.; Sankaranarayanan, M.; Seol, E.; Chun, A. Y.; Ashok, S.; Chauhan, A. S.; Kim, J. R.; Park, S. Development of 3-Hydroxypropionic-Acid-Tolerant Strain of Escherichia Coli W and Role of Minor Global Regulator YieP. *Metab. Eng.* **2019**, *53*, 48–58.
- (23) Nguyen-Vo, T. P.; Ryu, H.; Sauer, M.; Park, S. Improvement of 3-Hydroxypropionic Acid Tolerance in Klebsiella Pneumoniae by Novel Transporter YohJK. *Bioresour. Technol.* **2022**, *346*, 126613.
- (24) Wang, Y.; Ling, C.; Chen, Y.; Jiang, X.; Chen, G.-Q. Microbial Engineering for Easy Downstream Processing. *Biotechnol. Adv.* **2019**, *37* (6), 107365.
- (25) Abraham, T.; Allen, E.; Bohnert, E.; Frank, C.; Hahn, J.; Tsobanakis, P. Recovery of 3-Hydroxypropionic Acid, September 18, 2014. https://patentscope.wipo.int/search/en/detail.jsf?docId=WO2014144400 (accessed 2023-04-06).
- (26) Mathes Hewage, A.; Nayebi Gavgani, H.; Chi, D.; Qiu, B.; Geiger, J. H.; Draths, K. Cg10062 Catalysis Forges a Link between Acetylenecarboxylic Acid and Bacterial Metabolism. *Biochemistry.* **2021**, *60* (51), 3879–3886.

- (27) Poelarends, G. J.; Serrano, H.; Person, M. D.; Johnson, W. H.; Whitman, C. P. Characterization of Cg10062 from Corynebacterium Glutamicum: Implications for the Evolution of Cis-3-Chloroacrylic Acid Dehalogenase Activity in the Tautomerase Superfamily. *Biochemistry.* **2008**, *47* (31), 8139–8147.
- (28) Huddleston, J. P.; Johnson, W. H.; Schroeder, G. K.; Whitman, C. P. Reactions of Cg10062, a Cis-3-Chloroacrylic Acid Dehalogenase Homologue, with Acetylene and Allene Substrates: Evidence for a Hydration-Dependent Decarboxylation. *Biochemistry.* **2015**, *54* (19), 3009–3023.
- (29) Mathes Hewage, A. N. S. Synthesis of 3-Hydroxypropionic Acid from Acetylenecarboxylic Acid. Ph.D., Michigan State University, United States -- Michigan, 2022. https://www.proquest.com/docview/2708763781/Record/AD2D32FF46F34D5FPQ/3?parentSes sionId=kAaf93v32P8wvoRrdRMiOxMigM3OjWnU%2Fhm%2BkmpDadM%3D (accessed 2023-02-22).
- (30) Draths, K. F.; Geiger, J. H.; Hewage, A. N. S. M.; Gavgani, H. N. Synthesis of 3-Hydroxypropionic Acid via Hydration of Acetylenecarboxylic Acid. WO2022226190A1, October 27, 2022. https://patents.google.com/patent/WO2022226190A1/en?oq=WO2022226190A1 (accessed 2023-02-27).
- (31) Chowdhury, E. K.; Nagata, S.; Misono, H. 3-Hydroxyisobutyrate Dehydrogenase from Pseudomonas Putida E23: Purification and Characterization. *Biosci. Biotechnol. Biochem.* **1996**, *60* (12), 2043–2047.
- (32) Chowdhury, E.; Akaishi, Y.; Nagata, S.; Misono, H. Cloning and Overexpression of the 3-Hydroxyisobutyrate Dehydrogenase Gene from Pseudomonas Putida E23. *Biosci. Biotechnol. Biochem.* **2003**.
- (33) Lauterbach, L.; Lenz, O. Catalytic Production of Hydrogen Peroxide and Water by Oxygen-Tolerant [NiFe]-Hydrogenase during H2 Cycling in the Presence of O2. *JACS.* **2013**, *135* (47), 17897–17905.
- (34) Woodyer, R.; van der Donk, W. A.; Zhao, H. Relaxing the Nicotinamide Cofactor Specificity of Phosphite Dehydrogenase by Rational Design. *Biochemistry.* **2003**, *42* (40), 11604–11614.
- (35) Zou, Y.; Zhang, H.; Brunzelle, J. S.; Johannes, T. W.; Woodyer, R.; Hung, J. E.; Nair, N.; van der Donk, W. A.; Zhao, H.; Nair, S. K. Crystal Structures of Phosphite Dehydrogenase Provide Insights into Nicotinamide Cofactor Regeneration. *Biochemistry.* **2012**, *51* (21), 4263–4270.
- (36) Johannes, T. W.; Woodyer, R. D.; Zhao, H. Directed Evolution of a Thermostable Phosphite Dehydrogenase for NAD(P)H Regeneration. *Appl. Environ. Microbiol.* **2005**, *71* (10), 5728–5734.
- (37) Johannes, T. W.; Woodyer, R. D.; Zhao, H. Efficient Regeneration of NADPH Using an Engineered Phosphite Dehydrogenase. *Biotechnol. Bioeng.* **2007**, *96* (1), 18–26.

- (38) Lenz, O.; Lauterbach, L.; Frielingsdorf, S. Chapter Five O2-Tolerant [NiFe]-Hydrogenases of Ralstonia Eutropha H16: Physiology, Molecular Biology, Purification, and Biochemical Analysis. In *Methods in Enzymology*; Armstrong, F., Ed.; Enzymes of Energy Technology; Academic Press, 2018; Vol. 613, pp 117–151.
- (39) Lauterbach, L.; Lenz, O.; Vincent, K. A. H2-Driven Cofactor Regeneration with NAD(P)+-Reducing Hydrogenases. *FEBS J.* **2013**, *280* (13), 3058–3068.
- (40) Lees, G. J.; Jago, G. R. Role of Acetaldehyde in Metabolism: A Review 1. Enzymes Catalyzing Reactions Involving Acetaldehyde. *J. Dairy Sci.* **1978**, *61* (9), 1205–1215.
- (41) Kaye, G. W. C.; Laby, T. H. *Tables of Physical and Chemical Constants and Some Mathematical Functions*, 15th ed.; Longman: London, 1986.
- (42) Keefe, R. G.; Axley, M. J.; Harabin, A. L. Kinetic Mechanism Studies of the Soluble Hydrogenase from Alcaligenes Eutrophus H16. *Arch. Biochem. Biophys.* **1995**, *317* (2), 449–456.
- (43) NADPH | Sigma-Aldrich. https://www.sigmaaldrich.com/US/en/search/nadph?focus=products&page=1&perpage=30&sort =relevance&term=nadph&type=product (accessed 2023-02-27).
- (44) El-Zahab, B.; Jia, H.; Wang, P. Enabling Multienzyme Biocatalysis Using Nanoporous Materials. *Biotechnol. Bioeng.* **2004**, *87* (2), 178–183.
- (45) Buthe, A.; Wu, S.; Wang, P. Nanoporous Silica Glass for the Immobilization of Interactive Enzyme Systems. In *Enzyme Stabilization and Immobilization: Methods and Protocols*; Minteer, S. D., Ed.; Methods in Molecular Biology; Humana Press: Totowa, NJ, 2011; pp 37–48.
- (46) Mattey, A. P.; Sangster, J. J.; Ramsden, J. I.; Baldwin, C.; Birmingham, W. R.; Heath, R. S.; Angelastro, A.; Turner, N. J.; Cosgrove, S. C.; Flitsch, S. L. Natural Heterogeneous Catalysis with Immobilised Oxidase Biocatalysts. *RSC Adv.* **2020**, *10* (33), 19501–19505.

Chapter Four: Experimental

Portions reprinted with permission from:

Kwiatkowski, K.; Nguyen, V.; Draths, K.; Stereospecific Synthesis of Lactic Acid from Methane and Carbon Dioxide. Manuscript in preparation.

Hewage, A. M.; Kwiatkowski, K.; Silva, K. L. S.; Sreedhar, D.; Lee, E.; Nayebi, H.; Geiger, J. H.; Draths, K.; An Original Biosynthetic Route to 3-Hydroxypropionic Acid. Manuscript in preparation.

4.1 General

4.1.1 Materials

Media components and buffer salts were purchased from Thermo Fisher Scientific, MilliporeSigma, Becton, and Dickinson and Company. Acetylenecarboxylic acid 6 and 3hydroxypropionic acid 10 were purchased from MilliporeSigma. Ruthenium trichloride was purchased from Pressure Chemical. Copper sulfate pentahydrate was purchased from Columbus Chemical Industries. Copper triflate was purchased from Strem Chemicals. Mercuric acetate was purchased from J.T. Baker Chemical Company and silver nitrate was purchased from Spectrum Quality Products, Inc. The ruthenium standard used for ICP-OES was purchased from GFS Chemicals. Isopropyl-β-D-1-thiogalactopyranoside (IPTG) was purchased from Gold Biotechnology. QIAprep Spin Miniprep and Midiprep kits were purchased from Qiagen. Wizard Genomic DNA Purification Kit was purchased from Promega. Precision Plus Protein Electrophoresis Standards, Mini-PROTEAN TGX Precast 4-20% polyacrylamide gels, and Quick Start Bradford 1x dye reagent were purchased from Bio-Rad. Restriction enzymes, T4 DNA ligase, Q5 High-Fidelity DNA Polymerase, and purified Bovine Serum Albumin (B9001S) were purchased from New England Biolabs. HisTrap FF 5 mL pre-packed columns were purchased from Cytiva. Amicon Ultra-15 10K and 30K centrifugal filter units, 0.22 µm and 0.45 µm syringe filters, and mini EDTA-free protease inhibitor cocktail tablets were purchased from MilliporeSigma.

Zymo Research Corporation DNA Clean and Concentrator, Zymoclean Gel DNA Recovery kit, UltraPure agarose and Strep-Tactin Sepharose resin (50% suspension) were purchased from Thermo Fisher. dNTPs were purchased from Promega. Oligonucleotides were purchased from Integrated DNA Technologies. Alcohol dehydrogenase [1.1.1.1] from *Saccharomyces cerevisiae* (A7011) was purchased from MilliporeSigma. NADH, NAD+, L-lactate dehydrogenase (L-LDH) [1.1.1.27] from rabbit muscle (427217-M), and D-lactate dehydrogenase from *Lactobacillus leichmannii* (D-LDH) (L3888) were purchased from Roche. Soluble hydrogenase (SH) was obtained from the Lenz group at the Technical University of Berlin and isolated from *Ralstonia eutropha* strain Hf210/pGE771. Double deionized water was used for all experiments.

4.1.2 Instrumentation

NMR spectra were obtained on a 500 MHz Varian NMR spectrometer. UV-vis assays were performed on a Shimadzu UV-2600 spectrophotometer equipped with a TCC-100 Shimadzu temperature-controlled cell holder. HPLC spectra were obtained on an Agilent 1100 series equipped with UV and RID detection and an HPX 87-H column. His_{*}-tagged proteins were purified on an ÄKTA Start FPLC equipped with a HisTrap FF 5 mL nickel affinity column. Optical density (OD) and protein concentration were measured using a Thermo Scientific NanoDrop One^c. PCR amplification was performed in a Bio-Rad DNA Engine Peltier Thermal Cycler. A Sorvall RC 6+ centrifuge was used with either a Fiberlite F12-6x500LEX or a Fiberlite F21-8x50y fixed angle rotor.

4.1.3 Culture Media and Stock Solutions

Deionized water was used to prepare all culture media following standard protocols. ¹ The media was sterilized by autoclaving using the liquid cycle at 121 °C for 25 min. LB medium (1 L) was prepared by adding Bacto tryptone (10 g), Difco yeast extract (5 g) and NaCl (10 g) to water and then sterilized. ² 2XYeast-tryptone (2XYT) media (1 L) contained Bacto tryptone (16 g), Difco

yeast extract (10 g) and NaCl (5 g) and was sterilized by autoclaving. SOB medium (1 L) was prepared by adding Bacto tryptone (20 g), Difco yeast extract (5 g), NaCl (0.5 g), 250 mM KCl (10 mL) to water. The pH was adjusted to 7.0 by addition of 10 N NaOH before sterilization by autoclaving. Immediately prior to use, sterile 2 M MgCl₂ (5 mL) was added. SOC medium (1 L) was prepared by addition of 1 M D-glucose (20 mL) to sterile SOB medium (1 L). MgCl₂ 2 M and 1 M glucose stocks were prepared separately using deionized water and sterilized by autoclaving. FGN_{mod} medium (1 L) contained 10x H16 buffer (100 mL) and water (850 mL) and was sterilized by autoclaving. Immediately prior to use, sterile 20% (w/v) NH₄Cl (10 mL), 20% (w/v) MgSO₄ · 7 H₂O (1 mL), 1% (w/v) CaCl₂ · H₂O (1 mL), 0.5% (w/v) FeCl₃ · 6 H₂O (in 0.1 N HCl) (2 mL), 1 mM NiCl₂ (1 mL), 40% (w/v) fructose (1.25 mL), 40% (w/v) glycerol (10 mL), trace element solution SL6 (1 mL), and 40 mM ZnCl₂ (25 mL) were added. FN/Tc medium (1 L) contained 10x H16 buffer (100 mL) and water (850 mL) and was sterilized by autoclaving. Immediately prior to use, sterile 20% (w/v) NH₄Cl (10 mL), 20% (w/v) MgSO₄ · 7 H₂O (1 mL), 1% (w/v) CaCl₂ · H₂O (1 mL), 0.5% (w/v) FeCl₃ · 6 H₂O (in 0.1 N HCl) (1 mL), 1 mM NiCl₂ (1 mL), 40% (w/v) fructose (1.25 mL), and tetracycline (1.2 mL, 12.5 mg mL⁻¹) were added. 10x H16 buffer (1 L) contained Na₂HPO₄ · 12 H₂O (90 g) and KH₂PO₄ (15 g). The pH was adjusted to pH 7 and the solution was sterilized by autoclaving. Trace element solution SL6 (50 mL) contained MnCl₂ · 4 H₂O (25 mg), H₃BO₃ (15 mg), CoCl₂ (5 mg), ZnSO₄ · 7 H₂O (5 mg), 10 mM Na₂MoO₄ · 2 H₂O (620 μL), 10 mM NiCl₂ (420 μ L), and 10 mM CuCl₂ · 2 H₂O (295 μ L). Stock solutions of 20% (w/v) NH₄Cl, 20% (w/v) MgSO₄ · 7 H₂O, 1% (w/v) CaCl₂ · H₂O, 1 mM NiCl₂, and 40% (w/v) glycerol were prepared separately using deionized water and sterilized by autoclaving. Stock solutions of 40% (w/v) fructose, 0.5% (w/v) FeCl₃ · 6 H₂O (in 0.1 N HCl), trace element solution SL6 (1 mL), and 40 mM ZnCl₂ were prepared separately using deionized water and sterilized using 0.22 µm syringe filters. Tetracycline (12.5 mg mL⁻¹) was prepared in a 50:50 deionized water: ethanol solution. Stock solutions of ampicillin (50 mg mL⁻¹) and isopropyl β-D-1-thiogalactopyranoside (IPTG, 1 M) were prepared using deionized water and sterilized by passage through a 0.22 µm syringe filter. Antibiotics were added to media when appropriate to the final concentrations of 50 μ g mL⁻¹ ampicillin (Ap) and 15 μ g mL⁻¹ tetracycline (Tc). Solid media was prepared by adding Bacto Agar to a final concentration of 1.5% (w/v). Lyophilized powder of D-LDH (1 mg) was diluted in 50 mM Tris-HCl (500 μ L), pH 8, aliquoted (50 μ L), and stored at – 20 °C. For long term storage of all strains, an overnight culture in appropriate media was grown and added (750 μ L) to sterile 80% glycerol (250 μ L) in a cryovial. Prepared vials were left at room temperature for up to an hour with occasional gentle mixing. The vials were then flash frozen in liquid nitrogen and stored at - 80 °C.

4.1.4 Preparation and Transformation of Electrocompetent E. coli

To prepare electrocompetent cells, a standard protocol adapted from Sambrook and Russell was followed. Using a freshly streaked plate (<5 days old), a single bacterial colony was inoculated into a 5 mL LB culture and incubated overnight with shaking (37 °C, 200 rpm). A 2 mL aliquot of the overnight culture was used to inoculate 100 mL of sterile 2xYT media in a 500 mL baffled shake flask and incubated at 37 °C until an exponential phase OD₆₀₀ of 0.5-0.7 was reached. The culture was centrifuged using a Fiberlite F12-6x500LEX fixed angle rotor (6,100 x g, 5 min, 4 °C) to pellet cells. The cells were gently resuspended in 100 mL cold, sterile deionized water to remove residual salts from the culture media. The resuspension was centrifuged (6,100 x g, 5 min, 4 °C) and the supernatant was carefully decanted. The cells were washed with another 100 mL of cold, sterile deionized water and pelleted as above. Cold, sterile 10% aqueous (v/v) glycerol (100 mL) was used to resuspend the cell pellet and it was centrifuged at 6,100 x g, 5 min, 4 °C. The supernatant was carefully discarded, and the cell pellet was resuspended in 0.5 mL 10% (v/v) aqueous glycerol. Aliquots (50 μ L) were prepared in sterile microcentrifuge tubes on ice and flash-frozen in liquid nitrogen for storage at - 80 °C.

For the transformation of electrocompetent *E. coli* cells, plasmid DNA (1 μ L of 1-10 ng μ L⁻¹ in sterile deionized water) was combined with 50 μ L of electrocompetent cells thawed on ice. The sample was mixed by pipetting and transferred to a cold, sterile Gene Pulser electroporation

cuvette (0.2 cm electrode gap). A Bio-Rad Gene Pulser II electroporation system was used (2.5 kV, 25 μ F and 2000 Ω), which resulted in a time constant of 5.16–5.25 ms. The cuvette was quickly removed from the electroporator and placed on ice. SOC media (1 mL) was added to the sample, and the cells were allowed to recover at 37 °C with shaking (1 h, 200 rpm). The culture was centrifuged at 13,000 rpm in a microcentrifuge to pellet cells, and 800 μ L of the supernatant was decanted. The cell pellet was resuspended in the remaining media and 20 μ L and 80 μ L aliquots were plated onto LB solid media containing the appropriate antibiotic. The plates were incubated at 37 °C overnight.

4.1.5 Preparation and Transformation of Chemical Competent E. coli

To prepare chemical competent cells, a standard protocol adapted from Sambrook and Russell was followed. Using a freshly streaked plate (<5 days old), a single bacterial colony was inoculated into 5 mL LB and incubated overnight with shaking (37 °C, 200 rpm). A 1 mL aliquot of the overnight culture was used to inoculate 100 mL of sterile LB media in a 500 mL baffled shake flask and incubated at 37 °C until an exponential phase (OD_{600} of 0.5-0.7) was reached. The cells were transferred to a sterile centrifuge bottle, incubated on ice for 5 minutes, collected by centrifugation (2,700 x g, 5 min, 4 °C), and gently resuspended in 100 mL 0.9% NaCl. The cells were pelleted by centrifugation (2,700 x g, 5 min, 4 °C) and the sample was carefully decanted to remove the supernatant. While on ice, the cells were gently resuspended in 50 mL of 100 mM CaCl₂, left on ice for 30 minutes to 1 hour, and centrifuged (2,700 x g, 5 min, 4 °C). The supernatant was discarded, and the cell pellet was resuspended in 4 mL of 100 mM CaCl₂ in 15% (w/v) glycerol solution. Aliquots (100 μ L) were prepared in sterile microcentrifuge tubes on ice and flash-frozen in liquid nitrogen for storage at -80 °C.

For the transformation of chemical competent *E. coli* cells, plasmid DNA (1 μ L of 10-100 ng μ L⁻¹ in sterile deionized water) or purified, de-salted ligation or PCR products were combined with 100 μ L of chemical competent cells thawed on ice. The tube was gently tapped to mix, and

the sample was placed on ice for 30 minutes. Heat-shock was carried out using a 42 °C (\pm 2 °C) water bath for exactly 60 seconds. The tube was immediately placed on ice for 2 minutes, and 0.5 mL pre-warmed (37 °C) LB media was added. The recovery culture was incubated at 37 °C for 1 hour without shaking. The culture was centrifuged at 5,000 rpm in a microcentrifuge to pellet cells, and 500 μ L of the supernatant was discarded. The cell pellet was resuspended in the remaining media and 20 μ L and 80 μ L aliquots were plated onto LB solid media containing the appropriate antibiotic. The plates were incubated at 37 °C overnight.

4.1.6 Isolation of Plasmid DNA

For small-scale and large-scale plasmid purification, Qiagen Plasmid Miniprep and Midiprep Kits were used, respectively. When using a Miniprep Kit, a 5 mL LB culture containing the appropriate antibiotic was inoculated using a single colony from a freshly transformed plate. The culture was grown overnight at 37 °C with shaking (200 rpm). Cells were pelleted at 13,000 rpm using a microcentrifuge (1 min). When using a Midiprep Kit, a 100 mL LB culture containing the appropriate antibiotic was inoculated using a single colony from a freshly transformed plate. The culture was grown overnight at 37 °C with shaking (200 rpm). Cells were pelleted by centrifugation (6,100 x g, 10 min, 4 °C). Purification of plasmid was carried out following the instructions provided by Qiagen. For Miniprep purification, DNA was eluted from the column using 50 µL of deionized water. For Midiprep purification, the plasmid was dissolved in 100-200 µL of deionized water. Purified plasmids were stored at 4 °C.

4.1.7 Restriction Digestion of DNA

Restriction digestion of plasmid DNA was used to confirm the identity of a purified plasmid or for restriction enzyme cloning. A typical digest (20 μ L) included the components listed in Table 4.1. To achieve a final volume of 20 μ L, the volume of deionized water was adjusted accordingly. Samples were incubated at 37 °C for 1-2 h and quenched with 2.2 μ L 10X Endostop (50% glycerol

(w/v), 1.1 M EDTA (pH 8), 1% SDS, 0.1% bromophenol blue, 0.1% xylene cyanol). The digested DNA was visualized on a 0.7% agarose gel (see DNA Gel Electrophoresis section).

Table 4.1. Components of a standard restriction digest

Component	Volume (µL)	Final Concentration	
Plasmid DNA	varies	500-600 ng	
10X Buffer*	2	1X	
Restriction enzyme	1	10 U	
Deionized water	up to 20 μL	-	

^{*}The appropriate buffer is provided by NEB with the restriction enzyme.

4.1.8 DNA Gel Electrophoresis

DNA was visualized using agarose gel electrophoresis. TAE buffer (1X) contains 0.5% tris(hydroxymethyl)aminomethane, 0.1% acetic acid, and 0.03% ethylenediaminetetraacetic acid in water (pH 8). To make one 2.5" x 4" gel, 50 mL 1x TAE buffer and 0.35 g UltraPure agarose were combined in an Erlenmeyer flask and microwaved until the mixture came to a boil. Ethidium bromide (2.5 μ L) was added. After cooling to approximately 60 °C, the solution was poured into a gel mold and left to solidify. The gel was placed in an electrophoresis gel box and submerged in 1x TAE buffer. A DNA size marker stock was prepared with 20 μ L of 1 kb size marker (0.5 μ g μ L⁻¹), 20 μ L purple loading dye with no SDS, and 80 μ L sterile dd H₂O. Samples (15-25 μ L) and DNA size marker (1 kb, 8-10 μ L, 0.7-0.8 μ g) were loaded into the wells via pipette. When running a DNA sample from a PCR, 5 μ L of PCR product was combined with 10 μ L water and 3 μ L NEB 6X SDS Purple Loading Dye. The gel was run at 98 V until the loading dye was 1-2 inches from the bottom of the gel (~1 hr) and was imaged using an Axygen imaging system.

4.1.9 Protein Expression

All protein expression, with the exception of soluble hydrogenase, relied on a T7-expression system. The desired plasmid, created from a pET-21a(+) vector, was transformed into $E.\ coli$ BL21(DE3). A single colony was inoculated into 25 mL of LB media containing ampicillin. The culture was grown overnight at 37 °C with shaking (12-15 h, 200 rpm). The overnight culture was used to inoculate 1 L of LB media containing ampicillin to an OD₆₀₀ of 0.05 and was incubated at 37 °C with shaking (200 rpm). The OD₆₀₀ was monitored until it reached 0.5-0.7. Isopropyl β -D-1-thiogalactopyranoside (IPTG, 1 M) was added to a final concentration of 1 mM to induce expression of the desired protein. The culture was grown at 30 °C for 8-10 hours with shaking (200 rpm). The cells were pelleted via centrifugation (17,000 x g, 10 min, 4 °C) and supernatant was decanted. Cell pellets were stored at -20 °C.

4.1.10 Protein Purification

All proteins, with the exception of soluble hydrogenase, contained a C-terminal His₆-tag to allow for nickel affinity purification. Thawed cell pellets were gently resuspended in lysis buffer (20 mM sodium phosphate, pH 7.4, 20 mM imidazole), using 2 mL of buffer per gram of cell weight. The resuspended cells were passed twice through a chilled SLM Aminco French Pressure cell at 124 MPa into a chilled centrifuge tube. Cell debris was pelleted via centrifugation using a Fiberlite F21-8x50y fixed angle rotor (47,500 x g, 4 °C, 30 min). The cell lysate was decanted from the insoluble cellular debris and filtered through a 0.45 µm syringe filter. The proteins were purified on an ÄKTA Start FPLC equipped with a HisTrap FF 5 mL nickel affinity column. Binding buffer (20 mM sodium phosphate, pH 7.4, and 500 mM NaCl) and elution buffer (20 mM sodium phosphate, pH 7.4, 500 mM sodium chloride and 500 mM imidazole) were prepared in advance and were mixed in a ratio of 96:4 respectively in all steps except elution. Using a flow rate of 4 mL min⁻¹, 5 column volumes of buffer was used to equilibrate the column. Crude protein was

applied to the column at a flow rate of 1 mL min⁻¹, and 15 column volumes of buffer (4 mL min⁻¹), was used to elute unbound proteins. Bound protein was eluted from the column using 20 column volumes and an imidazole gradient ramping from 20 mM to 500 mM (4 mL min⁻¹). After use, the column was washed and stored in 20% ethanol. Purified protein was added to an Amicon Ultra-15 10K filter and centrifuged (6,600 x g, 4 °C, 30 min), and the flow-through was discarded. To exchange the buffer, 100 mM potassium phosphate, pH 8.0, containing 20% ethylene glycol was added to the concentrated protein until the top compartment was filled (15 mL). Protein was concentrated again by centrifugation (6,600 x g, 4 °C, 30 min). The buffer exchange process was repeated one additional time (final volume ~ 2 mL). Purified protein was stored at -20 °C.

4.1.11 Protein Quantification

The concentration of protein in crude lysate was measured using a Bradford Assay. Bradford reagent was diluted 1:5 with water. Diluted Bradford reagent (1 mL) was mixed with crude lysate (20 µL) and allowed to stand at room temperature for five minutes. Absorbance was measured at 595 nm. If absorbance exceeded a value of 1, the assay was repeated with lysate diluted with water (for example, 1:5 or 1:10, as appropriate). The protein concentration was calculated using a standard curve created using bovine serum albumin (Figure 4.1).

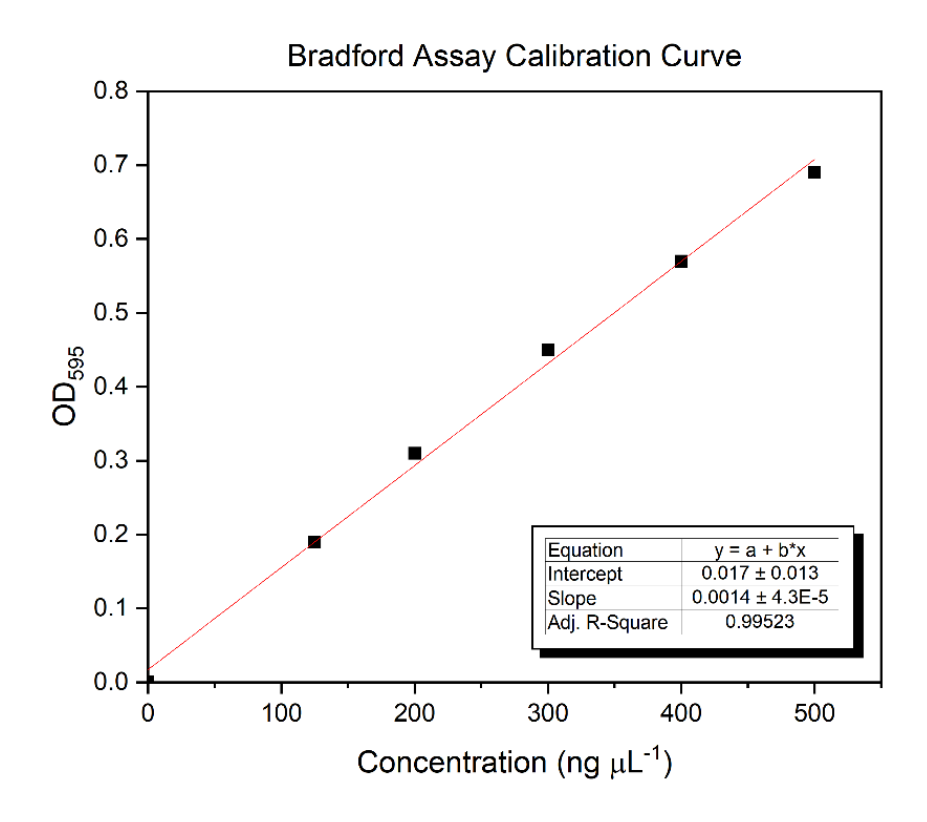


Figure 4.1. Standard curve for a Bradford Assay created using bovine serum albumin standard.

The concentration of purified protein was determined by first denaturing it with guanidine hydrochloride. Purified protein (10 μ L) was added to 6 M guanidine hydrochloride (990 μ L), and the solution was thoroughly mixed. Absorbance was measured at 280 nm, and the molar extinction coefficient and molecular weight including the His₆-tag were used to calculate a concentration (Table 4.2).

Table 4.2. Molecular weight and extinction coefficients for His₆-tagged proteins.

Enzyme	MW (Da)	ε ₂₈₀ (M ⁻¹ cm ⁻¹)
Cg10062(E114N)	18998	30440
MSAD	16464	8250
MmsB	31386	17780
PTDH	36568	26600

4.2 Chapter Two: Stereospecific Synthesis of Lactic Acid from Methane and Carbon Dioxide

4.2.1 Vacuum Distillation of ACA and pyruvic acid

Commercial supplies of ACA 6 was distilled prior to use. All glassware was dried at 100 °C for a minimum of 0.5 h and cooled to room temperature prior to use. A distillation apparatus including a short path condenser equipped with three receiving flasks was assembled. All joints were greased to ensure a proper seal. The neck of the boiling flask was wrapped with glass wool and foil. A column containing Drierite desiccant was inserted between the distillation apparatus and the vacuum pump, and the receiving flasks were maintained at -78 °C. Temperature was monitored using an overhead thermometer in the neck of the short-path condenser, and ACA 6 was collected at 55-60°C and about 12 psi vacuum pressure. Distilled ACA 6 was stored under nitrogen and exposure to air was minimized thereafter.

Pyruvic acid **8** was distilled prior to use following the same protocol described above for ACA **6**. Pyruvic acid **8** was collected at 65°C, and about 12 psi vacuum pressure. Distilled pyruvic acid **8** was stored under nitrogen and exposure to air was minimized thereafter.

4.2.2 Standard Hydration Reaction

Water (20 mL, 1.1 mol) and RuCl₃ trihydrate (12 mg, 46 µmol) were added to a flask equipped with a condenser and stir bar. ACA **6** (310 µL, 5.00 mmol) was added to the flask, which was blanketed with nitrogen and allowed to stir at 100 °C for 11-12 hours. All variations of substrate, solvent, scale, temperature, and catalyst were modified relative to these standard conditions.

4.2.3 Calculating Concentrations via NMR

Reaction progress and product concentrations were determined based on integration ratios obtained by 1 H NMR. The sodium salt of 3-(trimethylsilyl)propionic-2,2,3,3- d_4 acid (TSP) served as a standard. At timed intervals, an aliquot (100 µL) of the reaction was removed via syringe and combined with 600 µL of D₂O containing 10 mM TSP. A 10 s relaxation delay and 64 scans were used. Representative spectra from reaction initiation and termination are included (Figure 4.2). The resonance at δ 3.36 (s, 1H) corresponds to ACA 6. Resonances at δ 2.39 (s, 3H) and δ 1.56 (s, 3H), respectively, correspond to pyruvic acid 8a and its hydrate 8b. Resonances at δ 2.24 (d, 3H) and δ 1.32 (d, 3H), respectively, correspond to acetaldehyde 11a and its hydrate 11b. The resonance at δ 2.08 (s, 3H) corresponds to acetic acid 14. Product concentrations were calculated using the formula in Figure 4.2C. To determine the percent yield for each product, the concentration of product was divided by the known concentration of ACA 6 (or ADCA 7 when applicable) added to initiate the reaction. At a minimum, reactions were run in duplicate, and average product concentrations are reported.

To assess the reproducibility of NMR measurements, 100 μ L of a completed hydration reaction was combined with 600 μ L of D₂O containing 10 mM TSP. The sample was run three times with 64 scans and a 10 s relaxation delay. The pyruvic acid **8a** peak at δ 2.39 was integrated relative to the TSP peak, and pyruvic acid **8a** concentrations were compared for the three spectra.

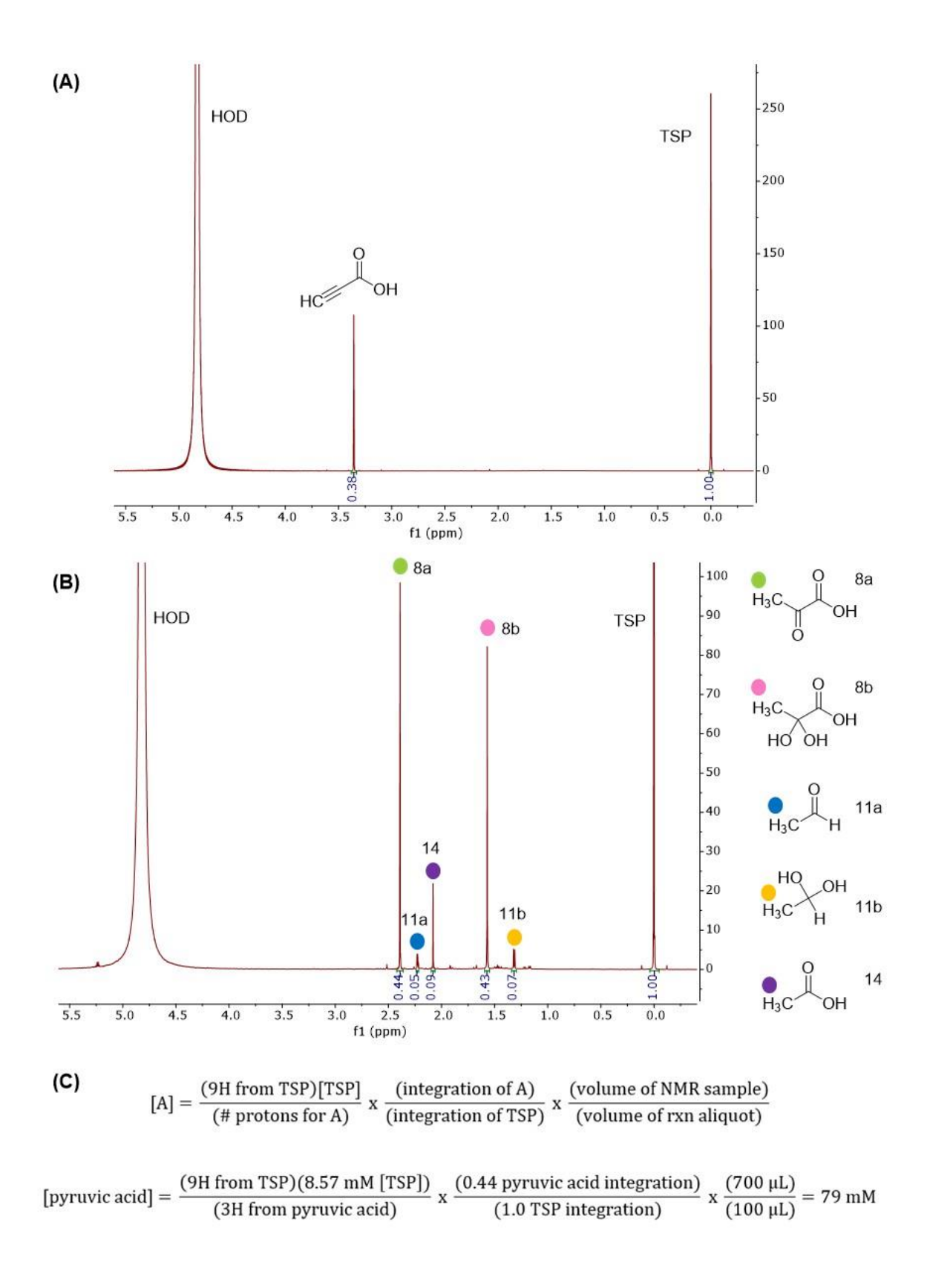


Figure 4.2. NMR spectra of RuCl₃-catalyzed hydration of ACA **6** at A) t = 0 h and B) t = 12 h. C) Sample calculation of pyruvic acid **8a** concentration from the spectrum provided in B).

4.2.4 Extraction Methods for Ruthenium Removal

In a standard liquid-liquid extraction, pyruvic acid **8** was extracted using diethyl ether. A 2X scale-up of a "standard" hydration reaction (40 mL) was mixed with 145 mL diethyl ether in a separatory funnel. After separation of the layers, the diethyl ether was collected. This process was repeated two additional times. The organic layers were combined, washed with brine, and sodium sulfate was added to dry any residual water. After sitting overnight, the sodium sulfate was filtered off and the diethyl ether was removed *in vacuo*.

For a continuous liquid-liquid extraction, methyl *tert*-butyl ether (MTBE) was first distilled over sodium. A 2X scale-up of a "standard" hydration reaction (40 mL) was mixed with 70 mL of MTBE and added to the continuous extractor equipped with a stir bar. MTBE (120 mL) was added to a flask connected to the side arm and heated to maintain a constant reflux. The top of the extractor and the side arm were wrapped with glass wool and foil. After approximately 3 h of extraction, the MTBE in the flask was exchanged with fresh solvent, and the sample was extracted for an additional 3 h. This process was repeated one additional time. The three organic fractions were combined and dried with sodium sulfate overnight. The sodium sulfate was removed via gravity filtration and the MTBE was removed *in vacuo*.

Dowex 50WX8 hydrogen form resin was defined prior to use. The Dowex resin was combined with water. After the resin settled, the water layer was decanted. This process was repeated five additional times. Two Dowex columns were prepared (5 mL and 15 mL). The columns were eluted with five column volumes (CV) of 2M HCl followed by water until the flow-through was neutral to pH paper. Duplicate hydration reactions run at "standard" conditions were added to each column. The columns were rinsed with 10 CV of water, and the eluent was collected as a single batch. Pyruvic acid 8 was extracted from the aqueous column flow-through using the standard liquid-liquid extraction method described above.

4.2.5 ICP-OES

Inductively coupled plasma- optical emission spectrometry (ICP-OES) was used to compare the removal of ruthenium from hydration reactions using liquid-liquid extraction and Dowex 50WX8 resin. Ruthenium standards were prepared using a 1,000 ppm ruthenium standard (in 20% HCl). To protect the instrument, the standard (15 mL) was digested in 3:1 HCl:HNO₃ (v/v). This standard was used to prepare ruthenium standards at concentrations of 0.08, 0.4, 2.0, and 10 ppm. These standards (100 mL) were diluted in water, and nitric acid was added (2 mL), resulting in a 2% nitric acid matrix. Three samples of hydration reaction, one purified with a standard diethyl ether extraction versus two reactions purified by Dowex columns followed by diethyl ether extraction were prepared for ICP-OES analysis. The samples were diluted to 1 L in a 2% nitric acid matrix to digest any organics and filtered with a 0.45 µm syringe filter. The standards were first run to create a calibration curve. Samples were analyzed at ruthenium wavelengths of 240.272, 245.554, 245.657, and 267.876 nm. The samples were then run including a blank and a standard to serve as a check sample.

4.2.6 Expression of SH

Soluble hydrogenase is expressed from *Ralstonia eutropha* Hf210/pGE771, which was obtained from the Lenz group. A single colony of *R. eutropha* Hf210/pGE771 from an FN/Tc plate (grown at 30 °C) was inoculated into 50 mL of FGN_{mod} media. The culture was grown at 30 °C with shaking (120 rpm) until it reached late stationary phase (~48 h). The entire pre-culture was used to inoculate 1L of FGN_{mod} media and was incubated at 30 °C with shaking (120 rpm). After 4 days, an additional 1 mL of 1 mM NiCl₂ was added. The OD₄₃₆ was monitored until it reached 10-12 (7-10 days). The cells were pelleted via centrifugation (11,000 x *g*, 20 min, 4 °C) and the supernatant was decanted. Cell pellets were flash frozen in liquid nitrogen and stored at -80 °C.

4.2.7 Purification of SH

The protocol for purification of soluble hydrogenase (SH) was adapted from the Lenz group.3 The following buffers were prepared: buffer SH-A: 50 mM KH₂PO₄, pH 7.0, containing 5% glycerol and 5 mM NAD+, and an EDTA-free protease inhibitor cocktail tablet; buffer SH-B: 50 mM KH₂PO₄, pH 7.0, containing 5% glycerol and 5 mM NAD⁺; buffer SH-C: 50 mM KH₂PO₄, pH 7.0, containing 5% glycerol; and buffer SH-D: 50 mM KH₂PO₄, pH 7.1, containing 5% glycerol, 5 mM desthiobiotin. Buffer SH-A was bubbled with argon for 10 minutes immediately prior to use. The frozen cell pellet (~ 5 g) was suspended in buffer SH-A using 2 mL buffer per gram of cell weight, and the suspension was bubbled with argon for 2 minutes prior to use. The cell suspension was passed twice through a chilled French press cell at 124 MPa into an argon-flushed centrifuge tube. Cellular debris was separated from cell lysate by centrifugation (47,500 x g, 4 °C, 1 h), and the resulting soluble lysate was filtered through a 0.45 µm syringe filter. SH was purified via column chromatography using strep-Tactin Sepharose resin (1 mL bed volume per 5 mL lysate). The column was eluted with ~ 2 CV of buffer SH-B, prior to addition of lysate. The column was washed with 3 CV of buffer SH-B followed by 7 CV of buffer SH-C, and the combined wash fractions were set aside for later analysis by SDS-PAGE. Strep-tagged SH was eluted with 4 CV buffer SH-D and the eluent was collected. The column was regenerated with 5 CV of 0.5 M NaOH, and washed with a minimum of 5 CV buffer SH-C prior to storage. The buffer in eluent containing SH was exchanged with buffer SH-C using an Amicon Ultra-15 30 kDa exclusion centrifugal concentrator (final volume ~ 1 mL). Protein concentration was measured using the Bradford method. An average of 234 U of purified SH was obtained per purification. Purified SH was stored at -80 °C.

4.2.8 Calculation of Enzyme Specific Activity

The following equation was used to calculate specific activity of enzymes when the rate was determined using a UV-Vis assay. When calculating the specific activity of soluble

hydrogenase, an extinction coefficient of 3480 M⁻¹ cm⁻¹ was used, and an extinction coefficient of 6220 M⁻¹ cm⁻¹ was used for all other enzymes.⁴

$$\begin{split} \text{specific activity} \left(\frac{U}{mg} \right) &= \text{Rate} \, \left(\frac{m\text{AU}}{\text{min}} \right) \times \frac{\text{AU}}{1000 \, \text{mAU}} \times \frac{\text{mol cm}}{\epsilon \, \text{L}} \times \frac{1}{\text{b cm}} \times \frac{\text{mL}}{\text{x mg}} \times \frac{\text{z mL}}{\text{y ml}} \times \frac{10^6 \, \mu \text{mol}}{1 \, \text{mol}} \times \frac{1 \, \text{L}}{1000 \, \text{ml}} \\ \epsilon &= \text{extinction coefficient} \, (\text{L mol}^{-1} \, \text{cm}^{-1}) \\ b &= \text{path length (cm)} \\ x &= [\text{enzyme stock}] \, (\text{mg mL}^{-1}) \\ y &= \text{volume of enzyme stock used (mL)} \\ z &= \text{final assay volume (mL)} \end{split}$$

4.2.9 Enzyme Assays

Figure 4.3. L-LDH or D-LDH activity was monitored following the oxidation of NADH at 340 nm.

Lactate dehydrogenase activity was measured by monitoring the decrease in absorbance at 340 nm (Figure 4.3), corresponding to the consumption of NADH (ϵ = 6220 M⁻¹ cm⁻¹). Measurements were made at 30 °C. Assays (final volume 1 mL) contained NADH (10 μ L of 10 mM stock, 100 nmol), L-LDH (10 μ L of 3.5 μ M stock, ~0.05 U) or D-LDH (10 μ L of 0.5 mg/mL, 0.03 U), and pyruvate **8** (10 μ L of 5 mM stock, 50 nmol) in 50 mM Tris-HCl (pH 8 at 30°C). The reaction was initiated by addition of pyruvate **8** and A₃₄₀ was recorded at 1 s intervals. To determine their impact on LDH activity, 2 mM stock concentrations of acetaldehyde **11**, acetic acid **14**, and RuCl₃ were prepared and added individually to the standard LDH assay to final concentrations of 5 μ M, 50 μ M, and 500 μ M. Assays were performed in triplicate and average values are reported.

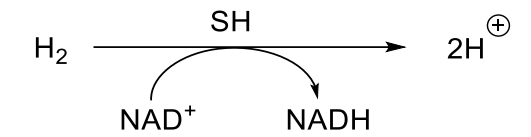


Figure 4.4. SH activity was monitored following the reduction of NAD+ at 365 nm.

Soluble hydrogenase activity was measured by monitoring the increase in absorbance at 365 nm (Figure 4.4), corresponding to production of NADH (ϵ = 3480 M⁻¹ cm⁻¹).^{3,5} Measurements were made at 30 °C. Assays (final volume 2 mL) contained NAD+ (20 µL of 100 mM stock, 2 µmol) and soluble hydrogenase (SH) (10 µL of 0.2-1 mg/mL stock (varied), ~0.2 U) in 50 mM Tris-HCl (pH 8 at 30°C). The cuvette containing buffer and NAD+ was sealed and saturated with hydrogen by bubbling for 2 minutes followed by incubation with a hydrogen balloon for 2 minutes at 30 °C. The reaction was initiated by addition of SH via syringe and A₃₆₅ was recorded at 0.1 s intervals. To determine their impact on SH activity, 2 mM stock concentrations of acetaldehyde 11, acetic acid 14, and RuCl₃ were prepared and added individually to the standard SH assay to final concentrations of 5 µM, 50 µM, and 500 µM. Assays were performed in triplicate and average values are reported.

4.2.10 Production of Lactic Acid

Reactions (final volume 4 mL) were run in 50 mM Tris-HCl (pH 8 at 30 °C). Pyruvic acid **8** (concentration determined via NMR) was added as part of a crude reaction mixture produced from the hydration of ACA **6** in water (stored at -20 °C). Stock solutions of NAD+, LDH, and SH were prepared in 50 mM Tris-HCl (pH 8 at 30 °C), and appropriate volumes were added to achieve the designated concentrations and units (Table 4.3). Reaction flasks were sealed with septa and placed in a 30 °C water bath. Hydrogen was bubbled in using a needle, with a second needle used to relieve pressure. Reaction progress and product concentrations were determined by NMR. At timed intervals, an aliquot (490 μ L) of the reaction was removed via pipette and combined with 100 μ L of D₂O containing 10 mM TSP and 10 μ L concentrated H₂SO₄. The resonance at δ

1.42 (d, 3H) corresponds to lactic acid **2**. The resonances at δ 2.47 (s, 3H) and δ 1.58 (s, 3H) correspond to pyruvic acid **8a** and its hydrate **8b** respectively, and the resonance at δ 2.09 (s, 3H) corresponds to acetic acid **14**.

Table 4.3. Lactate dehydrogenase-catalyzed conversion of pyruvate 8 to lactate 2a-b.

Entry [[pyruvate]	D-LDH	L-LDH	SH	[NAD+]
	(mM)	U	U	U	(mM)
1	12	-	0.4	2.6	1
2	12	-	0.4	2.6	0.1
3	12	0.2	-	5.3	1
4	12	0.2	-	5.3	0.1
5	12	-	2.4	23.5	0.01
6	12	-	2.4	23.5	0.001

4.3 Chapter Three: The Enzymatic Production of 3-Hydroxypropionic Acid from Acetylenecarboxylic Acid

4.3.1 Bacterial Strains, Genes, Plasmids, and Primers

Table 4.4. Primers used for the construction and sequencing of MmsB plasmid pKK1.1025.

Primer	Sequence
KK035 MmsB fwd	GGAGTACCATATGCGTATCGCATTCATCG
KK036 MmsB rev	CACCTCTTCTCGAGATCCTTCTTGCGATAACCCTC
KK037 Seq fwd	ACCATCGACCCGCAGAC
KK038 Seq rev	TGTTGATGATGCCGGCCAG

Table 4.5. Bacterial strains and plasmids used in chapter 3.

Strain/Plasmid	Genotype/Description	Reference/ Source
E. coli DH5α	F^- φ80 Iac ZΔM15 Δ(Iac ZYA- arg F)U169 rec A1 end A1 hsd R17(r_K^- , m_K^+) pho A sup E44 λ^- thi-1 gyr A96 rel A1	Invitrogen
E. coli BL21(DE3)	F^- omp T hsd S_B (r_B^- , m_B^-) gal dcm (DE3)	Invitrogen
Pseudomonas putida KT2440	rmo⁻ mod⁺	ATCC 47054
pET-21a(+)	Ap ^R , <i>lacl, P</i> ₇₇ pMB1 replicon	Invitrogen
pAS1.046	<i>Рт</i> сg10062 in pET-21a(+)	Sirinimal
pAS2.100	cg10062(E114N) in pAS1.046	Sirinimal
pKK1.1025	<i>P</i> _∞ mmsB in pET-21a(+)	this study

4.3.2 Isolation of Genomic DNA

Genomic DNA was isolated using a Wizard Genomic DNA Purification Kit. A single colony of *Pseudomonas putida* KT2440 was inoculated into 5 mL LB and grown overnight at 37 °C with shaking (200 rpm). The cells were pelleted using a microcentrifuge (14,000 x g, 1 min). DNA isolation was carried out following the instructions for gram negative bacteria provided by Promega.

4.3.3 PCR Amplification of MmsB from P. putida

The PCR amplification of MmsB from P. putida KT2440 contained the components listed in Table 4.6 with a final volume of 50 μ L. The conditions for thermocycling are summarized in Table 4.7. Once the amplification process was complete, 10 μ L of 6X loading dye containing SDS was added to quench the reaction and allow visualization before running on a 0.7% agarose gel.

Table 4.6. Components of the PCR reaction for the Amplification of MmsB from *P. putida*.

Component	Volume (μL)	Final Concentration
5X Q5 reaction buffer	10	1X
10 mM dNTPs	1	200 μΜ
10 μM KK035 forward primer	2.5	0.5 μΜ
10 μM KK036 reverse primer	2.5	0.5 μΜ
P. putida genomic DNA	1	7.7 ng
Q5 High-Fidelity DNA polymerase	0.5	0.02 U μL ⁻¹
5X Q5 High GC Enhancer	10	1X
Nuclease-free water	22.5	-

Table 4.7. Thermocycling conditions for the PCR reaction in the Amplification of MmsB from *P. putida.*

Step	Temperature (°C)	Time
Initial Denaturation	98	2 min
	98	10 sec
30 cycles	71	30 sec
	72	26 sec (30 sec kb ⁻¹)
Final Extension	72	4 min
Hold	4	-

^{*}Annealing temperature was determined using NEBasechanger.

4.3.4 Creation of pKK1.1025

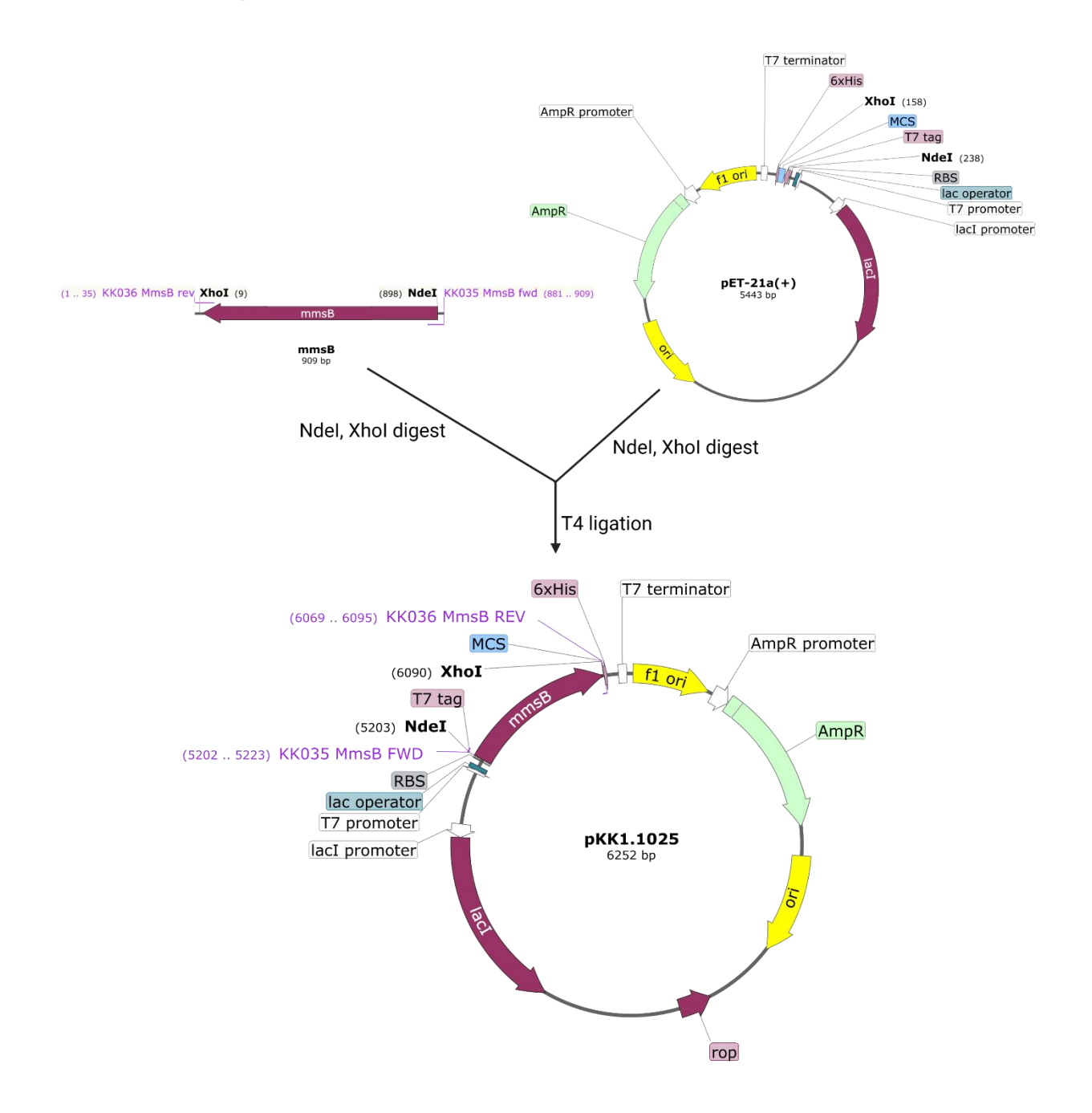


Figure 4.5. Creation of plasmid pKK1.1025 using restriction enzyme cloning.

Plasmid pKK1.1025 was created using restriction enzyme cloning(Figure 4.5). The gene for MmsB and pET-21a(+) vector were digested with Ndel and Xhol using the restriction digest protocol described above. The unwanted digested fragments were removed from the MmsB fragment using Zymo Clean and Concentrator, following the protocol supplied by the

manufacturer. The digested pET21-a(+) was visualized using agarose gel electrophoresis. The band was excised from the gel and DNA was recovered using Zymoclean Gel DNA Recovery kit, following the protocol supplied by the manufacturer. The DNA was eluted from the column using 12 µL DD water. The pET21a(+) and MmsB fragments were ligated using T4 ligation. The reaction components are summarized in Table 4.8, using a ratio of 1:3 vector: insert. The reaction and control were left at room temperature for two hours, and then warmed to 65 °C for 20 minutes to quench. The ligated plasmid, pKK1.1025 was transformed into chemical competent *E. coli* DH5α. To ensure pKK1.1025 had the proper sequence, it was sent for Sanger sequencing to the Michigan State University Research Technology Support Facility (MSU RTSF) Genomics Core using T7 forward and reverse primers supplied by the genomics core as well as KK037 seq fwd and KK038 seq rev (Table 4.4). The sequencing data was aligned to a reference sequence using SnapGene.

Table 4.8. Components of the T4 ligation of MmsB and pET-21a(+).

Component	Reaction Volume (μL)	Control Volume (µL)		
pET-21a(+)	5	5		
MmsB	7	0		
T4 ligase	1	1		
T4 buffer	2	2		
DD water	5	12		

4.3.5 Enzyme Assays

Figure 4.6. The activity of Cg10062(E114N) is measured by coupling MSAD and ADH which allows the oxidation of NADH to be monitored at 340 nm.

Cg10062(E114N) activity was measured using a coupled enzyme assay (Figure 4.6) where ACA **6** was hydrated using Cg10062(E114N) to form malonic semialdehyde **9**. This was then decarboxylated using malonic semialdehyde decarboxylase (MSAD) to form acetaldehyde **11**. The reduction of acetaldehyde **11** by NADH-dependent alcohol dehydrogenase (ADH) was monitored by following the oxidation of NADH at 340 nm (ϵ = 6220 M⁻¹ cm⁻¹). All coupling enzymes were added in excess to allow measurement of Cg10062(E114N) activity. Assays (final volume 1 mL) contained Cg10062(E114N) (10 µL of 2 mg mL⁻¹ stock, ~ 0.09 U), MSAD (40 µL of 4 mg mL⁻¹ stock, ~ 6 U), ADH (40 µL of 1 mg mL⁻¹ stock, ~ 12 U), NADH (20 µL of 5 mg mL⁻¹ stock, 150 nmol), and ACA **6** (50 µL of 100 mM stock, 250 nmol) in 100 mM potassium phosphate, pH 8. The reaction was initiated by addition of ACA **6** and A₃₄₀ was recorded at 0.1 s intervals.

Figure 4.7. The hydration of ACA **6** by Cg10062(E114N) was coupled to the reduction of MSA **9** to 3-HP **10** by MmsB. Enzyme activity was followed by the loss of absorbance at 340 nm due to NADH oxidation.

The specific activity of MmsB was measured (Figure 4.7) by generating MSA $\bf 9$ in situ from the Cg10062(E114N)-catalyzed hydration of ACA $\bf 6$. The reduction of MSA $\bf 9$ by NADH-dependent MmsB was monitored by following the oxidation of NADH at 340 nm (ϵ = 6220 M⁻¹ cm⁻¹). Assays

(final volume 1 mL) contained Cg10062(E114N) (0.8 U), MmsB (10 μ L of 0.1 mg mL⁻¹ stock, 0.2 U), NADH (20 μ L of a 5 mg mL⁻¹ stock, 150 nmol), and ACA **6** (50 μ L of 100 mM stock, 250 nmol) in 100 mM potassium phosphate, pH 8. ACA **6** and Cg10062(E114N) were mixed in buffer and left to sit 15 min before MmsB and NADH were added.

Figure 4.8. PTDH activity was monitored following the reduction of NADP+ at 340 nm.

The specific activity of PTDH was measured (Figure 4.8) by monitoring the reduction of NAD⁺ at 340 nm (ϵ = 6220 M⁻¹ cm⁻¹). Assays (final volume 1 mL) contained PTDH (10 μ L of a 1 mg mL⁻¹ stock, 0.01 U), NAD⁺ (10 μ L of a 10 mg mL⁻¹ stock, 150 nmol) and sodium phosphite (10 μ L of a 1 M stock, 10 μ mol) in 100 mM potassium phosphate, pH 8. The assays were initiated with the addition of sodium phosphite and A₃₄₀ was recorded at 0.1 s intervals.

4.3.6 Kinetics of MmsB

The kinetic parameters of MmsB were characterized using the coupled enzyme assay show in Figure 4.7. All assays were carried out in triplicate at 25 °C in 100 mM potassium phosphate, pH 8, with a final volume of 1 mL. All stock solutions for the assays were prepared in 100 mM potassium phosphate, pH 8. The kinetic parameters of MmsB were measured by generating MSA **9** *in situ* from the Cg10062(E114N)-catalyzed hydration of ACA **6**. The assays contained Cg10062(E114N) (0.8 U), MmsB (10 μ L of 0.1 mg mL⁻¹ stock, 0.2 U) and NADH (20 μ L of a 5 mg mL⁻¹ stock, 150 nmol). ACA **6** (50 – 10,000 μ M) and Cg10062(E114N) were mixed in buffer and left to sit 15 min before MmsB and NADH were added. A K_m of 2220 \pm 192 μ M and a K_{cat} of 101 \pm 5 s⁻¹ were observed.

4.3.7 PTDH Kinetics

The kinetic parameters of PTDH were compared for NAD+ versus NADP+ and were measured by monitoring the reduction of NAD+ at 340 nm (ε = 6220 M⁻¹ cm⁻¹). Assays (final volume 1 mL) contained PTDH (10 µL of a 1 mg mL⁻¹ stock, 0.01 U), sodium phosphite (10 µL of a 1 M stock, 10 µmol) and either NAD+ (25- 2500 µM) or NADP+ (25- 2500 µM) in 100 mM potassium phosphate, pH 8. The assays were initiated with the addition of sodium phosphite and A₃₄₀ was recorded at 0.1 s intervals. These experiments were conducted with the assistance of Esther Lee, an undergraduate researcher in the lab. For NAD+ a K_m of 2360 ± 279 µM and a K_{cat} of 7.4 ± 0.5 s⁻¹ were observed. For NADP+ a K_m of 1400 ± 310 µM and a K_{cat} of 0.7 ± 0.1 s⁻¹ were observed.

4.3.8 Buffer Dependence Assays

The pH dependence of Cg10062(E114N) and MmsB was measured using four different buffer systems: 100 mM potassium phosphate, 50 mM Tris-HCl, 50 mM bis-tris propane and 50 mM HEPES buffers for pH 6.5–8.0, 7.0–9.0, 7.0–9.0 and 7.0–8.0, respectively. The pH dependance of SH was measured in a subset of these buffers including 100 mM potassium phosphate, 50 mM bis-tris propane and 50 mM HEPES buffers for pH 7.0-8.0. Each respective assay was carried out as described above.

4.3.9 Production of 3-HP

Reactions (final volume 4 mL) were run in 100 mM potassium phosphate, pH 8. Stock solutions of ACA 6, NADH, Cg10062(E114N), MmsB, and SH were prepared in 100 mM potassium phosphate, pH 8, and appropriate volumes were added to achieve the designated concentrations and units (Table 4.9). All reactions were gently stirred and run in either two-steps or one-step. In a two-step reaction, all of the components were added besides MmsB. Once ACA 6 was converted to malonic semialdehyde 9, MmsB was added, reaction flasks were sealed with septa, and hydrogen was bubbled in using a needle, with a second needle used to relieve

pressure. In a one-step reaction, all of the reaction components were added at initiation, flasks were sealed with septa, and hydrogen was supplied to the headspace. Reaction progress and product concentrations were determined by NMR. At timed intervals, an aliquot (490 μ L) of the reaction was removed via pipette and combined with 100 μ L of D₂O containing 10 mM TSP and 10 μ L concentrated H₂SO₄. The resonance at δ 3.55 (s, 1H) corresponds to ACA 6. The resonances at δ 3.85 (d, 2H) and δ 2.62 (d, 2H) correspond to 3-hydroxypropionic acid 10, and the resonance at δ 2.71 (d, 2H) corresponds to the hydrate of malonic semialdehyde 9.

Table 4.9. Reaction components in the conversion of ACA 6 to 3-HP 10.

					0.01 eq	0.1 eq
Reaction	[ACA] (mM)	Cg10062 (E114N) U	MmsB U	SH U	[NAD+] (mM)	[NAD ⁺] (mM)
One-step	25	3.1	0.7	9.8	0.25	2.5
Two-step	100	3	12	22	0.25	-
Two-step	100	3	12	33	0.25	-

In 3-HP **10** production reactions using MmsB and PTDH, they were run using two methods depending on the method of quantification. For reactions monitored by NMR, reactions (final volume 4 mL) were run in 100 mM potassium phosphate, pH 8, with gentle stirring. Stock solutions of ACA **6**, NADH, Cg10062(E114N), MmsB, PTDH, and phosphite were prepared in 100 mM potassium phosphate, pH 8, and appropriate volumes were added to achieve the designated concentrations and units (Table 4.10). Reactions were initiated with the addition of ACA **6** and the flasks were sealed with septa. Reaction progress and product concentrations were determined by NMR. At timed intervals, an aliquot (490 μ L) of the reaction was removed via pipette and combined with 100 μ L of D₂O containing 10 mM TSP and 10 μ L concentrated H₂SO₄.

Reactions monitored by HPLC were carried out on a 1 mL scale in 100 mM potassium phosphate, pH 8. Stock solutions of ACA 6, NADH, Cg10062(E114N), MmsB, PTDH, and phosphite were prepared in 100 mM potassium phosphate, pH 8, and appropriate volumes were added to achieve the designated concentrations and units (Table 4.10). Reactions were prepared in Eppendorf tubes and mixed by gently rocking. For HPLC analysis, samples (100 µL) were pulled at timed intervals, quenched with 5 µL concentrated sulfuric acid, and diluted with 395 µL 0.01 N sulfuric acid. Samples were filtered using 0.45 µm syringe filters. An HPX-87H HPLC column was used with a 0.01 N sulfuric acid mobile phase and a 0.6 mL min⁻¹ flow rate. UV and RID detection were used.

Table 4.10. Reaction components in the conversion of ACA 6 to 3-HP 10.

					-	0.001 eq	0.01 eq	0.1 eq
Reaction	[ACA] (mM)	Cg10062 (E114N) U	MmsB U	PTDH U	[Phosphite] (mM)	[NAD+] (mM)	[NAD+] (mM)	[NAD+] (mM)
NMR	100	3	6	6	100	-	0.25	2.5
HPLC	100	3	6	6	100	0.025	0.25	2.5

REFERENCES

- (1) Sambrook, J.; Russell, D. W. Molecular Cloning: A Laboratory Manual; CSHL Press, 2001.
- (2) Miller, J. H. *Experiments in Molecular Genetics*.; Cold Spring Harbor Laboratory: Cold Spring Harbor, N. Y, 1972.
- (3) Lenz, O.; Lauterbach, L.; Frielingsdorf, S. Chapter Five O₂-Tolerant [NiFe]-Hydrogenases of Ralstonia Eutropha H16: Physiology, Molecular Biology, Purification, and Biochemical Analysis. In *Methods in Enzymology*; Armstrong, F., Ed.; Enzymes of Energy Technology; Academic Press, 2018; Vol. 613, pp 117–151.
- (4) Haid, E.; Lehmann, P.; Ziegenhorn, J. The Molar Absorption Coefficients of SS-Nicotinamide-Adenine Dinucleotide. In *Quality Control in Clinical Chemistry*; De Gruyter, 2014; pp 235–240.
- (5) Lauterbach, L.; Lenz, O. Catalytic Production of Hydrogen Peroxide and Water by Oxygen-Tolerant [NiFe]-Hydrogenase during H2 Cycling in the Presence of O2. *JACS.* **2013**, *135* (47), 17897–17905. https://doi.org/10.1021/ja408420d.